

# Master thesis

## Hydrodynamics at a large river confluence of the Sava and Danube Rivers in Belgrade



**UNIVERSITY OF TWENTE.**



Feite Harmannij

2 November 2018

HYDRODYNAMIC AT A LARGE RIVER CONFLUENCE OF THE SAVA AND DANUBE  
RIVERS IN BELGRADE

STUDENT Feite Harmannij  
STUDENT NUMBER S1479814  
CONTACT feiteharmannij@gmail.com

GRADUATION COMMITTEE

*University of Twente* Dr.ir. B. Vermeulen  
Dr.ir. D. Augustijn  
Dr.ir. E. Horstman

*University of Belgrade* Dr. Dejana Đorđević

*Master thesis*  
*University of Twente*  
*Water Engineering and*  
*Management*  
*2 November 2018*

## Abstract

This study focuses on the hydrodynamics of the Danube and Sava rivers confluence. It concerns a confluence with a low width to depth ratio ( $\sim 20$ ) for its scale and within the confluence there is a large bed discordancy, meaning a bed level difference between the tributary channel and the main channel. Previously a PhD research has been done on the confluence in which the confluence has been analyzed numerically using a SSIIM2 model and in which Acoustic Doppler current Profiler (ADCP) measurements have been done. The conventional way of processing the ADCP data is by transforming the four radial velocities as measured by the four beams of the ADCP into a velocity vector containing the streamwise, cross-stream and vertical velocity. However, caused by among others the bed discordancy, the flow in the confluence is thought to be inhomogeneous. Therefore, a newly proposed method on processing ADCP data has been used in this study. This method predefines a mesh onto a transect of a river and combines the radial velocities that are measured within this mesh into a vector containing the streamwise, cross-stream and vertical velocity. This method depends less on the assumption of homogeneity within the flow. With these two processing methods and the numerical model the flow structure and bed shear stress within the confluence have been investigated, which should give a better understanding of the hydrodynamics of the Sava and Danube Rivers confluence.

Firstly, it has been investigated to what extent the two methods could give different results for this confluence by investigating to which extent the assumption of homogeneous flow is reduced by the new method. Secondly, for the new and conventional method it has been determined how much data is needed to capture the turbulence in the data. This is done for different mesh cell widths to determine the mesh cell width that is required to capture the turbulence. Next the resulting secondary flow patterns from the new and conventional method were compared and differences were analyzed. These secondary flow patterns have afterwards been compared to the patterns that resulted from the numerical simulation, which were performed for the same conditions as the observed in the ADCP measurements. Also, the bed shear stress from the numerical simulations have been compared to estimates based on the ADCP data. Lastly, the observed flow structures have been compared to other studies on confluences.

It has been found that, based on the accuracy of the data and on the used mesh cell width of ten meters, the new method does not outperform the conventional method. The same result has been found when comparing the two methods on the secondary flow field they produce, and the average flow velocities over the transect. The lack of differences between the methods seems to be caused by the location where the measurements have been collected. These measurements were collected downstream of the confluence where less inhomogeneity of the flow is expected. The flow field that resulted from the two methods is a large helical cell produced by the bend in the confluence, with a small counter rotating cell in the transects of ADCP measurements nearest to the confluence. This cell that is attributed to the curvature of the channel had a larger size in the ADCP data compared to the similar cell that was visible in the output of the numerical model. The numerical model also showed streamwise velocity values which remained more constant when moving to the bed, compared to the streamwise velocities derived from ADCP data. This could implicate an underestimation of the roughness of the bed in the numerical bed. This is also indicated by the bed shear stresses, which show lower values for the numerical model compared to the estimation based on the ADCP data.

The absence of clear back-to-back helical cells is also seen for other large-scale confluences, however these confluences mostly possess much larger width to depth ratios ( $>100$ ). Since this ratio is much smaller for the Danube River and Sava River confluence, the large-scale effects are thought not to

cause the absence of helical cells. Based on other research on confluences the large bed discordancy in this case seems to be the reason of the absence of the back-to-back helical cells which is typical for confluences.

## Samenvatting

Deze studie focust op de hydrodynamica van de confluente van de Donau en de Sava in Belgrado. Het gaat om een confluente met een lage breedte tot diepte verhouding ( $<20$ ) voor de schaal van de confluente en er is een groot verschil tussen de bodemhoogten tussen de twee instromende rivieren. De confluente is bestudeerd binnen een doctoraal onderzoek waarvoor Acoustic Doppler Current Profiler (ADCP) metingen zijn verricht en waarin een numeriek model voor de confluente is ontwikkeld. De conventionele manier van ADCP-data verwerken is het transformeren van de vier metingen die door de ADCP simultaan worden gedaan tot een snelheidsvector met de stroomsgewijze richting, de dwarsstroomse richting en de verticale snelheid. Echter, voor deze methode wordt aangenomen dat de stroom homogeen is in het horizontale vlak tussen de metingen. Daarom is er een nieuwe methode ontwikkeld om ADCP-data te verwerken. Deze methode definieert een raster, waarbinnen in elke cel de ADCP-metingen worden verzameld. Uit al deze metingen wordt dan een snelheidsvector bepaald met dezelfde componenten als voor de conventionele methode. Door de cellen in het raster kleiner te houden, in vergelijking tot de grootte van het vlak waarbinnen de ADCP simultaan meet, is deze methode minder afhankelijk van de horizontale homogeniteit in de stroming. Door deze twee methoden toe te passen en de resultaten van het numerieke model te gebruiken, wordt de stroming structuur en de bodem schuifspanning binnen de confluente bekeken. Dit moet meer inzicht geven in de hydrodynamica van de confluente.

Eerst is bekeken tot op welke hoogte de twee methoden van het verwerken van ADCP-data verschillende resultaten zouden kunnen opleveren, door het bekijken in hoeverre beide methoden afhankelijke zijn van de horizontale homogeniteit in de stroming. Hierna is bekeken hoeveel data beide methoden omgaan met turbulentie in de stroming. Daarna is de gekeken naar de secundaire stromingsstructuur die volgt uit de nieuwe en conventionele methoden en het verschil hiertussen is bekeken. These structuren zijn daarna weer vergeleken met de structuren die uit het model resulteren, waarbij het model is doorgerekend voor dezelfde omstandigheden als geobserveerd tijdens de ADCP-metingen. Ook de bodem schuifspanning die volgt uit de numerieke simulaties is vergeleken met schattingen die zijn gedaan op basis van de ADCP-data. Als laatste zijn de observaties vergeleken met studies van andere confluenties.

Hieruit is gebleken dat, gebaseerd op de accuraatheid van de data en de gebruikte breedte van de rastercellen, de nieuwe methode geen betere resultaten zou geven vergeleken met de conventionele methode. Hetzelfde resultaat is gevonden in de daadwerkelijke vergelijking tussen de twee methoden, waarbij het secundaire stromingspatroon en de gemiddelde snelheid over de doorsneden van de rivier geen verschillen vertoonden tussen de methoden. Het ontbreken van deze verschillen lijkt te zijn veroorzaakt door de gebruikte raster cel breedte, maar ook door de locatie waar de metingen verricht zijn. Deze metingen zijn namelijk benedenstrooms van de confluente gedaan, waar verwacht wordt dat de stroming homogener is dan dicht bij de confluente zelf. De stromingspatronen die resulteerde lieten een grote secundaire cel zien over de volledige breedte van de dwarsdoorsnede van rivier, waarbij in doorsneden dicht bij de confluente een stuk kleinere cel te zien was die de andere kant op draait. De grote cel wordt toegeschreven aan de bocht die aanwezig is in benedenstroomse gedeelte van de confluente en is ook zichtbaar in de resultaten van het numerieke model. In dit geval is deze echter kleiner vergeleken met wat er in de data te zien is. Ook was te zien dat de stroomgewijze snelheden uit het model constanter bleven in de buurt van de bodem vergeleken met wat de ADCP-data liet zien, waar de snelheden in de buurt van de bodem snel richting 0 gaan. Dit zou kunnen betekenen dat het model de ruwheid van de rivier onderschat, wat bevestigd wordt door de lagere waarden voor de bodemschuifspanning die uit het model komen in vergelijking met de schatting op basis van de ADCP-data.

Het ontbreken van een duidelijk stromingsprofiel waar bij er twee secundaire cellen die tegen elkaar instromen aanwezig zijn over de volledige breedte van de rivier is iets wat ook in andere studies over confluenties van deze grootte is waargenomen. Echter, deze confluenties hebben over het algemeen een veel grotere breedte tot diepte verhouding ( $<100$ ) in vergelijking met de confluente die hier bestudeerd is. Daardoor is in dit geval de afwezigheid van het genoemde stromingsprofiel toegeschreven aan het verschil in de bodemhoogte tussen rivieren.

## Preface

This document is the result of a process that started almost a year ago, when I found an assignment about rivers in Serbia. It caught my attention and it managed to hold that up to this day. In this thesis I had the chance to study an incredibly interesting location where two large rivers meet each other. It also gave me the opportunity to travel towards this location and to get to know more about the project. With it I also learned a lot about the culture of Serbia and Belgrade in particular.

For this I need to thank my supervisor from the university in Belgrade: Dejana Đorđević. Both the discussions about project and the feedback you gave me were important for the thesis. And I want to thank you for making me feel really welcome in Belgrade and all the things you taught me about the city and its history. The second person I want to thank from Serbia is Nikola Rosić, who was a nice roommate and taught me a lot about the Serbian culture and cuisine.

The persons who I also made an invaluable contribution to this work, are my supervisors from the University of Twente. First of all, Bart Vermeulen, who was my daily supervisor. I really want to thank you for how helped to me start this project and all the things you taught me about ADCP's and all the ideas you gave on what to investigate at the confluence. Secondly, I want to thank Denie Augustijn for all the elaborate feedback, on the content of the research, but especially your remarks on how to write the thesis down has made this document a lot better. Thirdly I want to thank Erik Horstman to step in at the last moment and still be able to give helpful feedback on the, among others, technical details.

Furthermore, I would like to thank my family and friends for their support during the thesis. And I want to thank all the people from the afstudeerkamer for the nice atmosphere and conversations.

# Contents

Abstract.....	2
Samenvatting.....	4
Preface.....	6
1. Introduction.....	9
1.1. Location.....	9
1.2. Confluences.....	11
1.2.1. Confluences and meanders.....	12
1.3. ADCP measurements.....	12
1.3.1. What is an ADCP?.....	13
1.3.2. Conventional method.....	14
1.3.3. New method.....	15
1.4. Numerical model.....	16
1.4.1. Bed shear stress.....	16
1.5. Research objective and questions.....	16
1.6. Research scope.....	17
1.7. Report outline.....	17
2. Methods.....	18
2.1. Data.....	18
2.1.1. Description.....	18
2.1.2. Data processing.....	18
2.2. Gap between GPS and ADCP measurements.....	20
2.3. Required repeated transects.....	22
2.4. Comparing the two methods.....	22
2.5. Bed shear stress estimation.....	22
2.5.1. Fitting a logarithmic profile.....	22
2.5.2. Fitting a scaled logarithmic profile.....	23
2.5.3. Reach-average bed shear stress.....	24
2.6. Comparison of the ADCP data with the numerical model results.....	24
3. Results.....	26
3.1. Gap between GPS and ADCP measurements.....	26
3.2. Required repeated transects.....	28
3.3. Comparison between the methods.....	30
3.3.1. Magnitudes.....	30
3.3.2. Flow structure.....	35
3.4. Comparison with the model.....	36

3.4.1.	Flow structures .....	36
3.4.2.	Velocity magnitudes.....	38
3.5.	Bed shear stress .....	41
4.	Discussion.....	45
4.1.	Comparison of the methods .....	45
4.2.	Comparison of the ADCP data and numerical model .....	47
4.3.	Bed shear stress estimations .....	48
4.4.	Flow structures .....	50
4.5.	Data set .....	52
4.6.	Bed load transport .....	53
5.	Conclusions .....	54
5.1.	Recommendations .....	55
	References .....	56
	Appendix A Secondary velocity structures in the five transects.....	60
A.1.	Secondary flow structures obtained by the conventional method.....	60
A.2.	Secondary flow structures obtained by the new method.....	62
	Appendix B bed shear stress distributions.....	65
	Appendix C Distribution of the $R^2$ values .....	67
C.1.	Distributions of the $R^2$ values based on the fits of the logarithmic profile .....	67
C.2.	Distributions of the $R^2$ values based on the fits of the scaled logarithmic profile .....	69

## 1. Introduction

Confluences are common points within all fluvial networks. Confluences represent locations of complex three-dimensional flow, caused by the convergence of the multiple channels. This convergence and resulting complex flow have its impact on the morphology of confluences. Scours and bars are commonly present around confluence, which can impact for example the possibility of shipping routes around a confluence. The evolution of the morphology can impact the decision making on the development around the confluence as well. Due to an evolving bathymetry the discharge capacity of the channel can change. This must be considered when developing the land around a confluence. An example of a confluence where a lot of development take place around a confluence, is the location that is assessed in this study. This is the confluence of the Sava River and Danube river, which is located in the urban area of the capital of Serbia: Belgrade.

The last detailed hydraulic and hydrological study of the Danube and Sava rivers confluence dates to the sixties of the previous century. With the emergence of new technologies new plans arose some ten years ago to do a new study on the confluence, which should aid in the analysis of different development strategies of the City of Belgrade. The analysis was started by using an Acoustic Doppler Current Profiler (ADCP), which is a device which, in this case, is fixed to a boat and obtains flow velocities throughout the water column by sending out sound signals. In section 1.3 this will be explained in more detail. The ADCP measurements were carried out at 18 October 2007. Apart from these ADCP measurements, the confluence has been simulated numerically as well.

Both these parts of the analysis were done as part of a PhD dissertation (Djordjevic, 2010). However, shortly after the field campaign the City council decided to abandon the project. However, the data and dissertation got renewed interest when the idea arose for the research described within this report. This idea arose after a new method had been developed to process ADCP data (Vermeulen *et al.*, 2014). This new method is developed such that it should capture the flow in a better way at places where the flow is inhomogeneous, for example at locations with large bed gradients. Since these types of gradients are present within the Danube and Save confluence, this provided a good starting point to investigate how the new method performed on the data set. With this also the interest on the confluence itself was fueled, so also the desire was there again to investigate the flow structure and to see how this compared to other confluences that are described in the literature.

### 1.1. Location

The location around which this study is centered, is the large confluence of the Danube River and Sava River. The average discharge of the Sava River is just upstream of the confluence is approximately  $1600 \text{ m}^3/\text{s}$  and the average discharge of the Danube River at Belgrade, upstream of the confluence, is around  $4000 \text{ m}^3/\text{s}$ . This confluence is atypical, since the Danube River, coming from the northwest (see Figure 1), first bifurcates into two branches which flow around the Great War Island. This causes the rivers to merge together in two parts. First, there is a confluence of the secondary branch of the Danube River and the Sava River, which flows in from the south in Figure 1. Secondly, there is a confluence about a kilometer downstream of the first one, where the main branch of the Danube River meets the joint flow of the first confluence. An overview of the channels is given in Figure 1, together with the transects along which the ADCP measurements are done. This first confluence, consisting of the secondary branch of the Danube River with the main channel of the Sava River, will be the focus of this study.

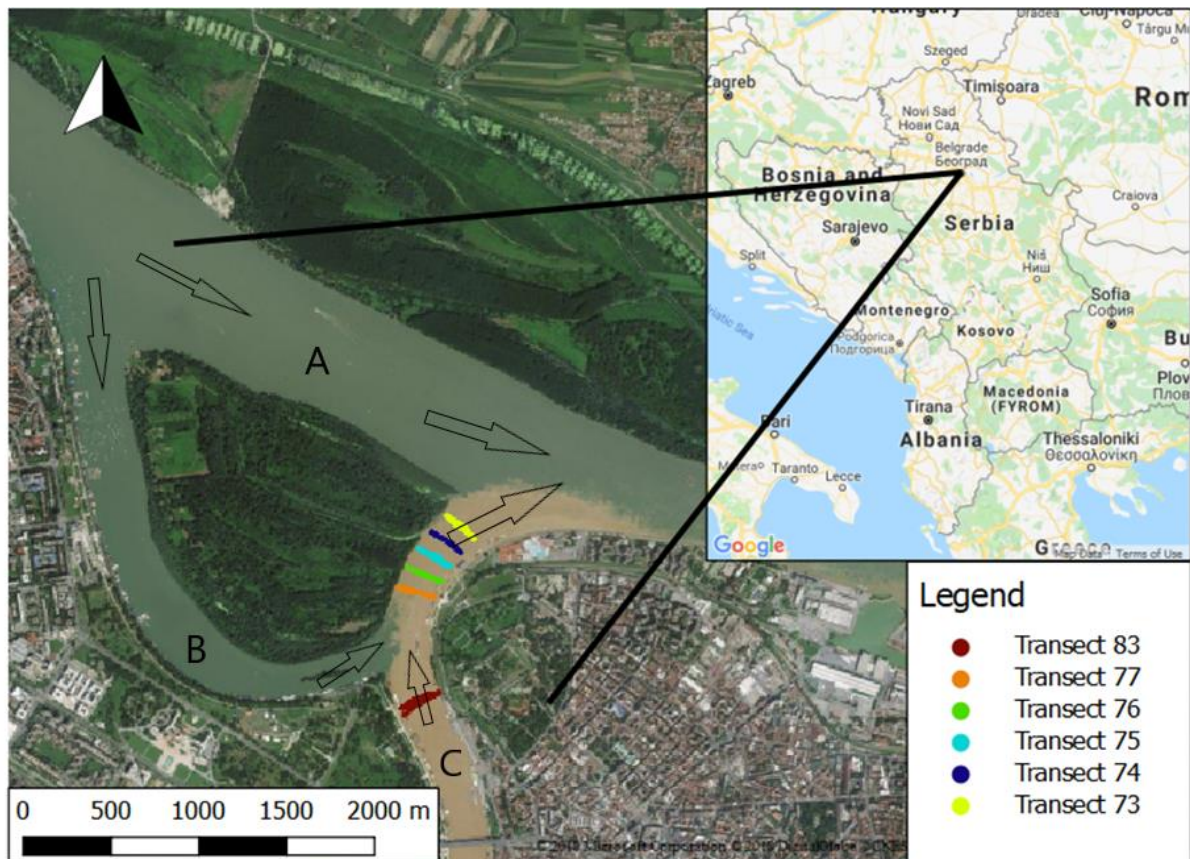


Figure 1 Overview of the Sava River and Danube River confluence and the locations of the transects where ADCP measurements were done 18 October 2007. Here (A) is the main channel of the Danube, (B) is the side channel of the Danube and (C) is the Sava River, the arrows indicate the flow direction.

This confluence is smaller compared to the confluence of the Sava River with the main channel of the Danube River. The combined discharge downstream of the confluence is, approximately around 2000 m<sup>3</sup>/s on average although there are large deviations of this number (Djordjevic *et al.*, 2006). The discharge ratios between the secondary channel of the Danube River and the Sava River range between 0.5 and 6 where the main Sava River has the largest discharge the most times. This is also visible from Figure 1, where the different flows are clearly distinguishable by the difference in sediment concentration. Despite it only being a picture of a single moment, for the upstream confluence it is visible that the flow within the confluence seems to be dominated by the flow of the Sava River. The width of the branches are 290 meter for the Sava River (both downstream and upstream of the confluence) and 275 meter for the side branch of the Danube River (Djordjevic *et al.*, 2006). The reason why the discharges of the Sava River are much larger, for a similar width compared to the tributary channel of the Danube River, can be found in the difference in depth, which is one of the distinct features of this confluence.

The difference in bed elevations between the Sava River and the side branch of the Danube River, is about 10 meters (Djordjevic *et al.*, 2006). Where the Sava River is deeper compared to the side branch of the Danube River. A second distinct feature of the confluence is the scour hole that is positioned downstream of the confluence. Here the depth of the channel, as shown by the ADCP measurements, increased from 12 meter at the position of transect 83 towards 20 meters at transect 73. Both these features have a clear impact on how the flow in the confluence behaves.

## 1.2. Confluences

Confluences are studied extensively within the literature. Most of this research is based on experiments in laboratories and a few small-scale confluences. Especially locations like the Kaskaskia River and Copper Slough confluence are studied thoroughly (Rhoads *et al.*, 2001, 2009; Constantinescu *et al.*, 2011) and forms the basis for the current knowledge. Based on laboratory experiments Best (1987) defines six different areas within a confluence (see Figure 2).

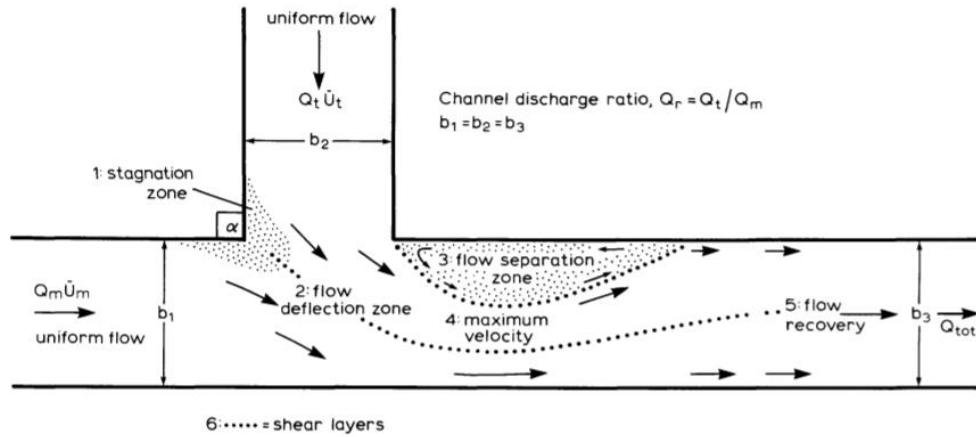


Figure 2 Characteristic flow zones within an open channel confluence (Best, 1987)

In laboratory and small confluence studies it has been found that the secondary flow structure usually consists out of two back-to-back helical cells formed by the vertical and cross-stream velocity, that rotate in the opposite direction of each other. These cells are a results from the collision of the flows, which continue along the same channel afterwards (Bradbrook *et al.*, 2000). This is visualized in Figure 3. An important parameter herein is the discharge ratio, which is defined as:

$$D_r = \frac{Q_{mr}}{Q_t} \quad (1)$$

Where  $D_r$  is the discharge ratio,  $Q_{mr}$  is the discharge of the main river and  $Q_t$  is the discharge of the of the side channel, which is also called the tributary channel. For completeness the densities of the water bodies could be added to both sides, but it in most cases these are omitted.

This parameter has a large impact on where the two incoming flows mix (Rhoads *et al.*, 2009). This is visible in the back-to-back helical cells, in the sense that one helical cell will grow larger at the expense of the other when the discharge ratio moves further from 1. The bed step, frequently stated as bed discordancy within the literature, as observed in the Danube and Sava rivers confluence, is found to have an impact on the presence of the back-to-back cells as well. The bed discordancy in a confluence is mostly quantified as the ratio between the depth of the shallower channel compared to that of the deeper channel. Data from a small confluence with discordant beds in Canada showed the absence of these cells (De Serres *et al.*, 1999).

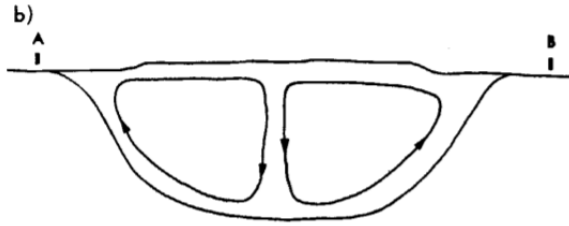


Figure 3 Back-to-back helical cells as found in a small-scale laboratory study of a symmetrical confluence when looking from the upstream direction (Ashmore, 1982)

### 1.2.1. Confluences and meanders

An important part of the confluence are the bends that are present within the confluence. From Figure 1 it is visible that the side channel of the Danube River (B), shows a large curvature. The Sava River (C) shows curvature to a lesser extent upstream of the confluence as well. Downstream of the confluence in the Sava channel a sharp bent is visible in the section where most of the ADCP data has been collected.

Research has been done on the influence of curvature upstream of a confluence. A distinction can be made between left bend meanders and right bend meanders, as visible in Figure 4. The confluence that is assessed here is a right bend confluence, with the strong curvature in the secondary channel of the Danube River. It has been found in a numerical study that the influence of this type of upstream meander is negligible (Djordjevic, 2013b). Therefore, it is expected that the influence of the bend in the secondary channel of the Danube River will also be negligible. Left bend meandering can magnify the 3D flow and interfere with the flow patterns of a confluence.

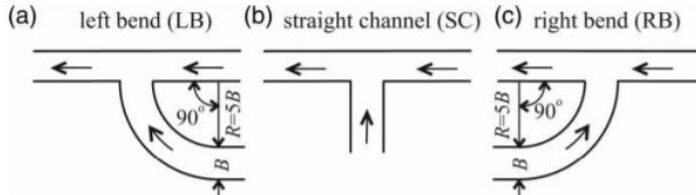


Figure 4 Distinction between meanders with a (a) left bend meander (b) straight channel and (c) a right bend meander upstream of the confluence (Djordjevic, 2013b)

These observations have later been confirmed by Riley *et al.* (2015). In study it was shown as well that high-angled bend can cause a significant impact on the flow. However, the bend in the Sava river has a low angle. Therefore, the impact of this curvature is expected to be limited.

The last curvature that is present within the confluence, is the curvature in the downstream part of the Sava river. Because of the sharpness of the bend and the ADCP measurements being done there, it can be expected that the influence of this bend is at least visible in the ADCP data.

### 1.3. ADCP measurements

For this study ADCP measurements were available. An ADCP is a device that measures, among others, the velocities in a flow by using sound signals. This data has been obtained over 5 transects in the downstream section of the confluence and one transect is measured in the upstream section of the confluence in the Sava River (see Figure 1). The measurements are so called moving-boat measurements, which implies that the device is mounted to a boat. This boat traverses the channel multiple times while the ADCP is sending out ultrasound pulses in a regular interval (every 0.92 seconds in this case). This will give four radial velocities for around 100.000 locations within a transect.

The reported conditions under which the measurements were performed are a discharge of 930 m<sup>3</sup>/s for the Sava River and 325 m<sup>3</sup>/s for the side branch of the Danube River (Djordjevic, 2010). These numbers are below average combined discharge of 2000 m<sup>3</sup>/s for the confluence and account for a discharge ratio of approximately 2.9.

### 1.3.1. What is an ADCP?

This section explains how an Acoustic Doppler Current Profiler ADCP device functions. The ADCP uses the doppler effect to estimate velocities within a water body. The doppler effect was first described in the 19<sup>th</sup> century by Christian Doppler (Doppler, 1842) with the hypothesis that the sound of an object coming at an observer has a higher frequency compared to the sound of an object moving away from an observer. This change in frequency can be described by the following relationship:

$$\Delta f = \frac{\Delta v}{c} f_0 \quad (2)$$

Where  $\Delta f$  is the change in frequency of a signal,  $\Delta v$  is the difference in velocity between receiver of the signal and the source of the signal and  $f_0$  is the frequency that would be observed when the receiver and source of the signal would have the same velocity in the same direction and  $c$  is the speed of sound. This principle can be used to calculate velocities of objects or, in this case, the velocity of a fluid (cf. Muste *et al.*, 2004; Dinehart *et al.*, 2005). However, the ADCP cannot calculate the velocity of the fluid directly. This is done by making use of the particles that are present within the fluid.

The ADCP sends out sound signals at a fixed frequency into the water body. This signal will be reflected by the particles within the fluid and by the bed of the channel. By comparing the frequency of the returning signal, the velocity of these particles can be determined. By assuming that these particles are small enough to adopt the same velocity as the fluid, the velocity of the fluid can be determined. There should be enough particles present in the water to reflect the signal of the ADCP as well (Teledyne RD Instruments, 2011). By assessing the backscatter signals from the beam, the velocities along the beam can be calculated.

The ADCP sends out ultrasound pulses along multiple beams, in this case 4 beams, of sound frequencies, which will give the velocity in the directions of these beams (Teledyne RD Instruments, 2011). This data can be used to calculate the velocity in three dimensions. This requires only three beams and therefore an error velocity can be calculated. This is done by the calculation of an extra vertical velocity, which in theory should give the same value as the vertical velocity that is determined using three beams. The difference between these vertical velocities is can give information about inhomogeneity in the velocity and can indicate possible errors in the equipment (Rennie, 2008).

However, the raw ADCP data of one transect does not give a clear insight in the different flow characteristics. This data consists out of radial velocities in the direction of the beams and are mostly inconsistent, due to the turbulence within the flow. This turbulence can interfere with the general flow pattern on a local scale, making the general patterns hard to see. Therefore, all the data of a cross-section will be combined, by projecting the measured data on a straight line between the two banks. Also, the individual measurements of the ADCP will be combined into meshes, which are predefined in size. This gives a better insight into the flow characteristics compared to the point measurements of the ADCP. Two methods will be used to process these measurements, one conventional method and a new method.

### 1.3.2. Conventional method

The conventional way to use the ADCP data is to take the measurements of the four beams of the ADCP and to combine these four measurements of radial velocities that are done simultaneously into an estimated velocity vector. This is done by the following transformation (Vermeulen *et al.*, 2015):

$$\begin{pmatrix} b_1 \\ \vdots \\ b_4 \end{pmatrix} = \begin{pmatrix} r_1^{\rightarrow T} \\ \vdots \\ r_4^{\rightarrow T} \end{pmatrix} \vec{u} \quad (3)$$

Here  $b_1$  to  $b_4$  are the four radial velocities as measured by the ADCP,  $\vec{u}$  is the velocity vector which consists of the streamwise ( $u$ ), cross-stream ( $v$ ) and vertical direction ( $w$ ) and  $r_1$  to  $r_4$  represent the direction of the four beams. The direction of the beams is affected by the tilting of the boat, caused by the roll, pitch and heading of the boat. These three concepts are illustrated in Figure 5. The values for the roll pitch and heading are also measured by the ADCP and can therefore be used to obtain the velocity vectors.

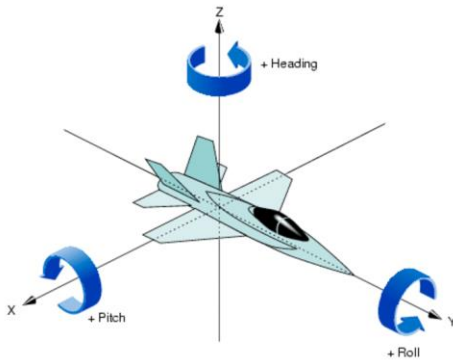


Figure 5 Illustration of the meaning of roll, pitch and heading for the context of an aircraft (Nikolaos *et al.*, 2010)

In this transformation from the radial velocities towards the velocity vectors with  $u$ ,  $v$  and  $w$  it is assumed that measurements at the same vertical location give the same velocities. I.e., the assumption is made that the flow in a horizontal layer of water is homogeneous (Parsons *et al.*, 2013). This assumption is illustrated in Figure 6, where the area in which the flow should be homogeneous is indicated by a circle. The transformation will be performed for all the ADCP measurements that are made by the ADCP, except for the areas which are filtered out beforehand. These areas are described in section 2.1. All these estimated velocity vectors with  $u$ ,  $v$  and  $w$  from this method are projected on a mesh to gain insight in the flow field of a certain transect. Within the mesh cells the outcomes of the conventional method are averaged. An example of a mesh on which these results will be projected is given in Figure 7.

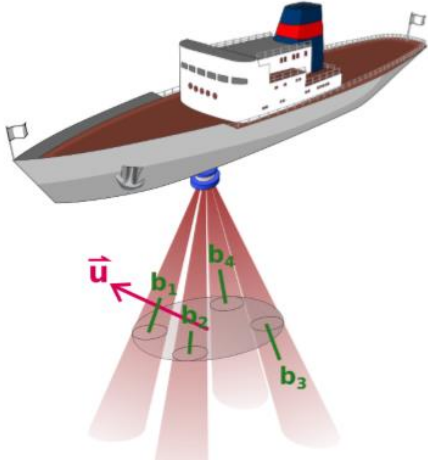


Figure 6 Illustration of the conventional method of combining ADCP data (Vermeulen, et al. 2015)

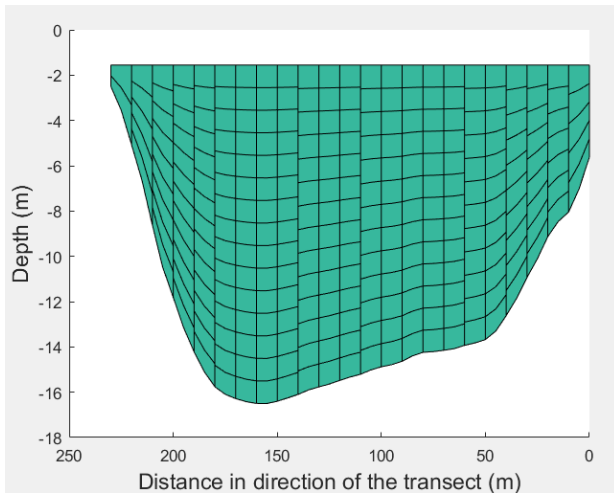


Figure 7 Example of a predefined mesh on which the new and conventional method project their results

### 1.3.3. New method

The new method starts by defining a mesh, similar to Figure 7, for a cross section. However, now the radial velocities will be projected on a mesh instead of the velocity vector with  $u$ ,  $v$  and  $w$  (Vermeulen *et al.*, 2014). These velocities will be transformed to the streamwise, cross-stream and vertical velocity in a similar way to the conventional method:

$$\begin{pmatrix} b_1 \\ \vdots \\ b_n \end{pmatrix} = \begin{pmatrix} r_1^{\rightarrow T} \\ \vdots \\ r_n^{\rightarrow T} \end{pmatrix} \vec{u} \quad (4)$$

Where  $n$  is the number of radial velocities in a mesh cell. This number can go up to a few hundred in most cells, therefore the number of solutions for  $\vec{u}$  is also large. To find the best solution, an error component can be added to eq. (4):

$$\begin{pmatrix} b_1 \\ \vdots \\ b_n \end{pmatrix} = \begin{pmatrix} r_1^{\rightarrow T} \\ \vdots \\ r_n^{\rightarrow T} \end{pmatrix} \vec{u} + \epsilon \quad (5)$$

Where  $\epsilon$  is the combined effect of all errors. By minimizing this  $\epsilon$ , a solution for  $\vec{u}$  is found. In this way a velocity vector can be obtained for all mesh cells.

This new method can reduce the horizontal distance between the radial velocities that are used to obtain the velocity vector with  $u$ ,  $v$  and  $w$ , because the width of a mesh cell can be smaller compared to the distance between the beams of an ADCP. This is illustrated in Figure 8 with the smaller circle around the measurements that are used to obtain a velocity vector with  $u$ ,  $v$  and  $w$ . Hereafter the method described here will be referred to as the new method.

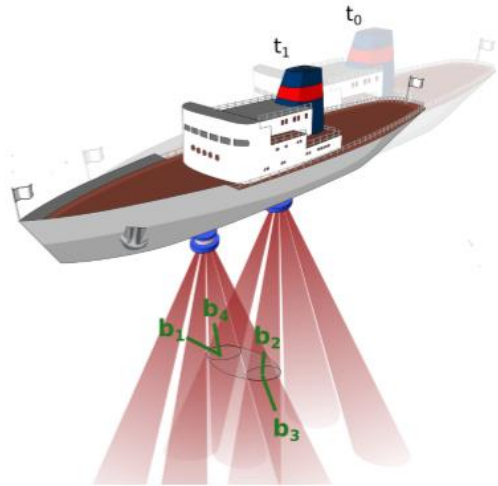


Figure 8 Illustration of the new method of combining ADCP data (Vermeulen, et al. 2015)

#### 1.4. Numerical model

Apart from the ADCP measurements, the confluence has been modelled numerically as well, using a SSIIMM2 model. This model solves the Reynolds Averaged Navier-Stokes equations combined with a  $\kappa - \epsilon$  turbulence model (Djordjevic *et al.*, 2006). The output of this model contains the three-dimensional flow structure, together with additional factors like the turbulence kinetic energy. The latter is subsequently used in the model to calculate the bed shear stress. The comparison between the results from this model and the ADCP can help in understanding the flow structure as visible in the ADCP data. By looking at the differences that occur between these two, causes for the difference can be found which can be related to mechanics that drive the flow within the confluence.

##### 1.4.1. Bed shear stress

The bed shear stress is one of the results of the model and an important variable in the relationship between the flow conditions and the sediment transport (Biron *et al.*, 2004). By making estimations of the bed shear stress based on the ADCP data, this gives another opportunity to compare the numerical model and the ADCP data.

#### 1.5. Research objective and questions

The aim of this study is to better understand the flow in the confluence of the Sava River and Danube River, by comparing two methods on that process the available ADCP data and using a numerical model. These results should give insight in how the flow structures look like in this confluence and how these structures compare to other confluences described in the literature.

To achieve this objective a main question and four sub questions have been formulated:

##### **Main question:**

*‘To what extent can different flow patterns be distinguished and understood by comparing the available ADCP data from the confluence of the secondary channel of the Danube River and the Sava River and a numerical model that uses the Reynolds Averaged Navier-Stokes equations?’*

### **Sub questions:**

1. *To what extent do the conventional method and new method of processing the ADCP data different results for the available data set?*
2. *What does the flow structure of the confluence look like according to the ADCP data?*
3. *How does the numerical model compare to the data obtained for the confluence, with respect to the secondary flow structure and bed shear stress?*
4. *How does the flow structure of the Sava River-Danube River confluence compare to other confluences?*

### 1.6. Research scope

Most of the six zones as given in Figure 2 are present at the junction itself. Because the ADCP data is gathered downstream of the confluence, these characteristics cannot be observed within the data. For this reason, this study focuses more on the characteristics that could be seen in the data. One of this are the velocity accelerations and decelerations around the maximum velocity, which has been labeled (4) in Figure 2. The other zone from Figure 2 that might be investigated from the data, is the flow deflection zone (2). This zone might be investigated by looking at the flow structure as shown by the ADCP and assessing how the flows merge together. Especially the secondary flow structure should provide insight on where and how the flows are deflected by each other.

### 1.7. Report outline

The second chapter of this report contains an explanation of the methods that are used within this study. This will include the processing that is done on the ADCP data and the ways in which the methods on processing the ADCP data and the numerical model are compared to each other.

Chapter 3 will present the results of these methods. Here the structures of the flow within the confluence will be shown, together with results of the SSIIM2 model and the bed shear stress estimations.

Chapter 4 and 5 are the discussion and the conclusions of the thesis, completed with some recommendations.

## 2. Methods

This chapter provides a description of the methods that have been applied within this study to come to the results. This starts with the processing that has been performed on the available ADCP data, after which the different ways are described in which the two processing methods of the ADCP data are compared to each other and to the results of the numerical model. Also, it will be described how the bed shear stresses have been obtained from the ADCP data.

### 2.1. Data

#### 2.1.1. Description

At six locations (see Figure 1) ADCP measurements have been taken on 18 October 2007. The ADCP was attached to the side of a boat, which repeatedly traversed the Sava River on all six transects. How much repeated transects have been made for each cross-section is different for the six locations. Because not all measurements were done with the same success as well, it differs per location how much usable data is available. However, for all the locations at least four usable repeated transects are available and for some transects up to six are available. The routes that have been navigated by the ship are visible

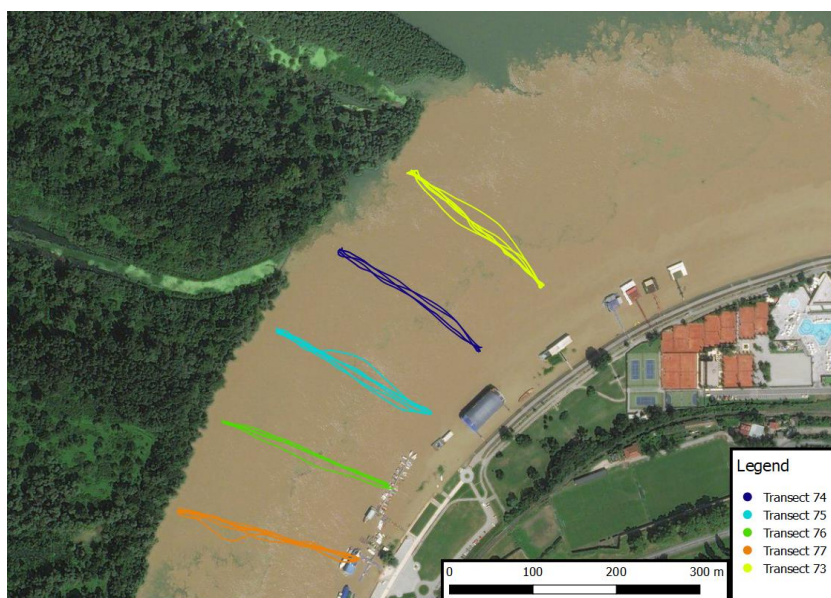


Figure 9 Detailed overview of the ship tracks of the five transects upstream of the confluence as measured by the ADCP

In this case the ADCP sent out ultrasound pulses with a frequency of 600 kHz every 0.92 seconds under an angle of 20 degrees. For every 0.5 meter towards the bed the averaged velocity of the particles for that 0.5 meter have been determined in the direction of the four beams. Due to the blanking distance of 0.25 meter and the depth of the ADCP in the water, the top of the first cell of 0.5 meter starts at 111 cm from the water surface. From there the ADCP has been set to measure 73 cells of 0.5 meter. Apart from the ADCP measurements, also GPS measurements were done to determine the position of the boat for each measurement. These measurements were done separately from the ADCP measurements, i.e. with another device that was not connected to the ADCP.

#### 2.1.2. Data processing

Several operations have been performed on the data before was used to analyze the flow. First, the transects are all checked on whether they contain the right data. Some transects were used to calibrate instruments and others had large sections of missing data. The data of these transects have been omitted from further analysis.

Before the conventional and new method can be applied on the data, a few other operations are performed. Most of these operations are done by an existing tool in MATLAB, which also applies the two methods themselves (Available on <https://sourceforge.net/projects/adcptools/>).

This tool first filters the measurements of the ADCP. Since 73 cells have been measured, results are available towards a depth of approximately 38 meters, keeping in mind that the first cell starts at a depth of 111 cm under the water surface. However, the maximum depth of the Sava river at the time of the measurement was less than 20 meters. This implies that a large part of the measurements is below the bed of the river and do not contain useful information. These measurements are recognized by the tool by assessing the intensity of the returning signal and filtered out of the data.

Also, velocities in the flow just above the bed will be filtered. This area is contaminated by the side lobe effect. Side lobes are unwanted signals that are sent out by the ADCP, that are also reflected by the flow but do not give sensible estimation of the flow. Normally these signals are suppressed by the ADCP by suppressing signals of a certain strength. However, the signals that are reflected by the bed are so much stronger compared to the reflection of the signal that these signals are not always suppressed. For signals that are sent out an angle of 20 degrees the bottom six percent of the flow can be contaminated by this effect (Teledyne RD Instruments, 2011). Therefore, the velocities in this region (see Figure 10) of the flow cannot be used and are removed from the data set as well.

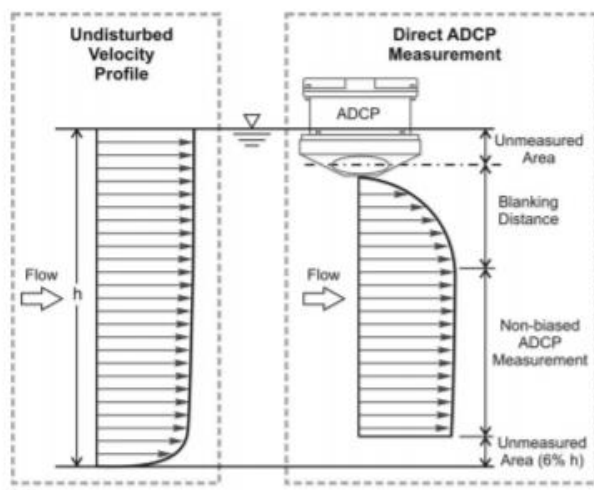


Figure 10 Velocity obtained by measuring the flow through an ADCP and the theoretical velocity profile (Muste et al., 2010)

Afterwards a mesh is constructed by the tool on which the remaining data is projected. Since the boat does not navigate on the exact same location for every repeated transect (see Figure 9), first a track must be defined on which the mesh is made. This track made by the tool by taking all the locations where the ADCP has sent out ultrasound pulses. From these points the line has been taken that explains the largest portion of the variance within the points, by calculating the eigenvalues.

Hereafter the plane that is formed will first be cut in vertical slices, based on a cell width that is given as input by the user. The next step is to divide these vertical slices into mesh cells that have an height that is closest to height that is requested by the user (Vermeulen et al., 2014). Since there is a given water depth, it is not possible to match the desired mesh cell height of the user and the height that is used in the mesh exactly.

After the mesh is constructed the new method and conventional method will be applied as described in section 1.3.

When the output of the tool was assessed roughly at first, it became clear that the vertical flow in the upper region was directed downward over the width of the transects. This indicates an error in the data, since the flow at the top of the channel is not expected to be pointed downwards over the width of a channel. This can be caused by a bias in the most upper measurements of the ADCP, as displayed in Figure 10. The velocities measured in this region under the ADCP tend to give lower velocities, until a depth of 1.5 times the diameter of the ADCP (Muste *et al.*, 2010). To overcome this bias in this study, the results of the first measurement, thus removing the top 50 centimeters of the measured flow, below the ADCP for each ping have been omitted for further analysis. In this study the exact diameter of the ADCP is not known, but it is approximately 25 centimeters (Teledyne RD Instruments, 2007). Thus, removing the upper cell should resolve this bias.

It also became apparent that some cells in the resulting mesh showed divergent values. After a more thorough analysis, it became clear that the estimate of the velocities within these cells was based on a small amount of ADCP measurements. This is probably the reason why the velocities showed a large deviation from the other estimated velocities. To overcome this, a minimum amount of measurements within a cell is imposed. This minimum amount of measurements is determined by calculating the average amount of measurements of the cells in the grid and then requiring each cell to have a certain percentage of this amount. Throughout the research a value of 1 percent is used, with value

## 2.2. Gap between GPS and ADCP measurements

Since the GPS was not an integrated part of the ADCP data, the two data sets needed to be coupled manually. This is done by matching the time observations, which were registered in both data sets. Because the measurements were not done integrated, these time observations did not match each other perfectly. Therefore, interpolation had to be applied to match the data series. This will induce some errors within the locations of the measurements.

However, after the integration of the GPS data within the system it became apparent that the time stamps of the ADCP and the GPS data do not seem to be in line with each other. When the locations determined by the GPS were compared with the locations obtained by bottom tracking, a shift of around 20 seconds became visible as can be seen in Figure 11. The bottom tracking is determined by a separate longer ultrasound pulse, which can calculate the velocity of the bed relative to the boat up to a few mm/s (Teledyne RD Instruments, 2011). By assuming that the bed is fixed, the resulting velocities can be attributed to the velocity of the boat. And with it the position of the boat can be determined, relative to its starting position. The downside of this method is that it does not consider the movement of the bed.

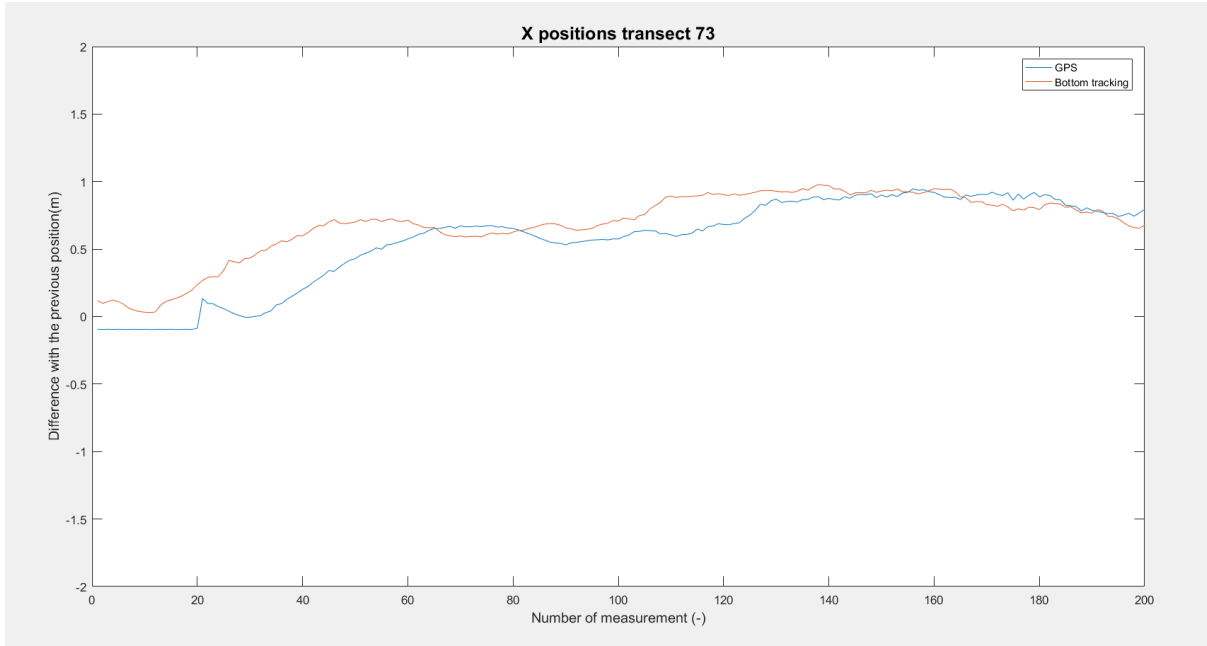


Figure 11 Distance from one x-coordinate to the subsequential one for the first 200 measurements of the ADCP in transect 73

Because the accuracy of the GPS data is important for the new method, the gap between GPS data and the bottom tracking will be minimized. Since the location obtained by the bottom tracking looks at the relative position, in contrast with the real coordinates coming from the GPS, also the relative position will be assessed in this adjustment. For both the location series, the distance between the individual measurements will be calculated, this will be done for the determined x and y coordinates. These x and y coordinates represent the longitudinal and latitudinal coordinates, respectively. Then, the difference between these distances of both the GPS data and the bottom-tracking will be calculated. The idea is that if this distance is minimized, that also the influence of the time shift will be minimized. The date attached to the GPS data will be shifted until a minimal difference is found between both the methods. So, for the x coordinate this can be summarized by the minimalization of the following expression:

$$\sum_{i=1}^{n-1} ((BTMx_{i+1} - BTMx_i) - (GPSx_{i+1} - GPSx_i)) \quad (6)$$

Where BTMx is the x coordinate obtained by the bottom-tracking method, GPSx the x coordinate obtained by the GPS and  $n$  the number of available data points for x. The same method has been applied for the y-coordinate.

The uncertainty will be assessed by comparing the magnitude of the inaccuracies induced by this time shift and the accuracy that is required for the new method to potentially give additional information on the flow. The first will be estimated by converting the obtained time shift to a distance. This can be obtained by estimating the velocity of the boat. The needed accuracy for the new method relates back to the point where the new method should get its advantage compared to the conventional method. This is caused by the smaller distance between the radial velocities that are combined into Cartesian velocities. Consequently, the distance between the radial velocities for the conventional method should be larger than the inaccuracies within the determination of the location of the radial velocities. This distance between the radial velocities will be determined based on the distance from the boat and the angle of the beams of the ADCP.

### 2.3. Required repeated transects

Only a finite amount of measurements has been carried out. This can cause there to be not enough data to average out the noise in the data, caused by turbulence or flow inhomogeneity. In the literature it is mentioned that at least enough transects should be taken to overcome the effect of irregularities in the flow (Muste *et al.*, 2004). However, the required amount of repeated transect is highly dependent of the flow characteristics.

A way to test for this is to use the standard deviation of the estimated velocities. This standard deviation will increase when more measurements are available, due to the noise in the data. When enough measurements are taken, however, the standard deviation should become stable, implying that enough data is taken to capture the variability within the flow. To see if this is the case, the average standard deviation over the grid is taken for an increasing amount of transects. This is done for a range of grid cell sizes and for both new and conventional methods, which will be compared to each other.

### 2.4. Comparing the two methods

To compare the two different methods, the velocities in the three directions have been plotted for both methods. Also, the difference between the two methods has been calculated for the three different velocity directions. This should give insight in where the differences between the two methods are most visible for the available data. Apart from looking directly at the three velocity components, also the flow field of the secondary velocities will be visualized. The secondary velocities are defined as the velocities that are not in the direction of the cross-sectional averaged flow. This should give insight in the flow patterns in the flow, like whether the back-to-back helical cells as mentioned in the introduction are present.

The largest differences in estimated velocities between the two methods are expected at the locations where the assumption of the homogeneous flow is the least valid. This can be caused by certain features in, of which in this case the bed discordancy is the most prominent. Other locations where this assumption might be invalid, are the locations where the channel depth is large. Here the distance between the different beams of the ADCP becomes larger, which requires the flow to be horizontal homogeneous over a larger distance to make the assumptions behind the conventional method valid. This difference in velocities can only be visible at depths where the distance between the beams of the ADCP is large enough.

### 2.5. Bed shear stress estimation

From the determined velocity fields, the bed shear stress will be estimated. There are multiple ways in which the bed shear stress can be estimated. These include: (1) fitting a logarithmic profile, (2) calculating a reach-averaged bed shear stress, (3) using a quadratic stress law and (4) using a turbulent kinetic energy approach (Biron *et al.*, 2004). Since the data is obtained from measurements from a moving boat measurements, turbulence is hard to estimate (Muste *et al.*, 2004). Furthermore, the third technique, which uses a drag coefficient to estimate the bed shear stress, is difficult to apply, because the drag coefficient is not a constant (Dietrich *et al.*, 1989). Because of this, the first two methods will be used in this study to estimate the bed shear stress. For the first method two approaches will be used: a logarithmic profile and a scaled logarithmic profile.

#### 2.5.1. Fitting a logarithmic profile

This method assumes that the stream wise flow velocity increases logarithmically with the depth from the bed towards the surface (von Karman, 1931). This assumption can be used to fit the available data to a logarithmic function described by Biron *et al.* (2004):

$$\frac{u}{u_*} = \frac{1}{\kappa} \ln\left(\frac{z}{z_0}\right) \quad (7)$$

Where  $u$  is the streamwise velocity,  $u_*$  the shear velocity,  $\kappa$  the von Karman constant,  $z$  the height above the bed and  $z_0$  the characteristic roughness length. In this study, this fit will be made using the verticals of the meshes that are the output of the ADCP processing methods (see e.g., Figure 7). All the mesh cells that are present within a vertical contain a value that can be used to fit the logarithmic function. By using this approach, an estimate can be made for the distribution of the bed shear stress in the cross-section. A disadvantage of this method is that there is a lot of uncertainty within the fit of this profile (Williams, 1995). For example, the lower half of the flow, which is claimed to give a better fit for the logarithmic profile compared to the whole depth of the flow (Nikora *et al.*, 1997). Therefore, the bottom six percent of the flow for which the ADCP does not give usable results might have a significant impact on the results.

In this study the part of the flow which is used for the fit is determined by the correlation coefficient  $R^2$ . Starting at the bed, first the two streamwise velocities of the mesh cells that are nearest to the bottom will be used to determine a best fit of those two points with a logarithmic profile. For this fit the correlation coefficient will be calculated. Then the same will be done for the first three streamwise velocities from the bottom. This will be repeated until the correlation coefficient will drop below a certain threshold. Then, the previous fit will be selected as the best fit for that vertical. The threshold for the correlation coefficient is set at 0.5. For the selected fit, the shear velocity and the characteristic roughness length can be determined from equation (7). These can be used within the bed shear stress estimation, using a reach averaged approach.

#### 2.5.2. Fitting a scaled logarithmic profile

A logarithmic profile can also be fitted by using a scaled representation of the velocity profile in the channel. This scaled profile is described by a slightly different equation for the flow and incorporates the vertically averaged streamwise velocity. The approach here is based on a description of the flow which also includes a dip correction factor (Sassi *et al.*, 2011):

$$u(\sigma, t) = \frac{u_*}{\kappa(\ln(\sigma) + 1 + \alpha + \alpha \ln(1 - \sigma))} + U \quad (8)$$

Where  $U$  is the vertically averaged velocity,  $\sigma$  the sigma coordinate, which described the vertical position of the velocity on a scale between zero at the bed and 1 at the surface, and  $\alpha$  the dip correction factor. The dip correction factor is related to the point of maximum velocity in the vertical. This can be positioned elsewhere in the vertical than the most upper part of the flow, as is assumed in conventional logarithmic description of the flow. For the given data set, no indication is found that the maximum velocity is located lower than the surface. By setting this factor to zero the equation reduces to:

$$u(\sigma, t) = \frac{u_*}{\kappa(\ln(\sigma) + 1)} + U \quad (9)$$

This function will be fitted to the complete vertical, in contrast to the approach in the previous section. For this approach the goodness of fit will be determined by the correlation factor  $R^2$  as well. These values will be compared afterwards, to get an idea if there is a difference in performance in the two methods. With the fits, the shear velocity and resulting bed shear stress can be determined. A downside of this method that it does not provide an estimate of the bed roughness.

### 2.5.3. Reach-average bed shear stress

A reach-averaged bed shear stress can be calculated by using the energy slope (Babaeyan-Koopaei *et al.*, 2002):

$$\bar{u}_* = \sqrt{gRS_f} \quad (10)$$

Where  $\bar{u}_*$  is the reach-average shear velocity over the cross-section,  $g$  the gravitational acceleration,  $S_f$  the energy slope and  $R$  the hydraulic radius. Here the water depth ( $H$ ) can be used instead of the hydraulic radius, since the channel can be considered as wide ( $R \approx H$ ). The energy slope will be calculated using the Manning equation (Manning, 1891):

$$\bar{u} = \frac{1}{n} R^{\frac{2}{3}} S_f^{\frac{1}{2}} \quad (11)$$

Where  $\bar{u}$  is the average velocity over the cross-section,  $n$  the manning coefficient,  $R$  the hydraulic radius and  $S_f$  the energy slope. The equation can be solved to obtain the energy slope, which can be used to calculate the shear velocity. In this study a local water depth and a local velocity have been used to consider the distribution of the bed shear stress in the cross-section (Babaeyan-Koopaei *et al.*, 2002). For the Manning coefficient a value  $0.035 \text{ s/m}^{1/3}$  has been used as representative value for a major stream (Chow, 1959).

This Manning value will be compared to the value that can be obtained by calculating the Manning coefficient using the Strickler relationship (Marriott *et al.*, 2010):

$$n = 0.038k_s^{\frac{1}{6}} \quad (12)$$

Herein is  $n$  the Manning coefficient and  $k_s$  is the equivalent roughness height of Nikuradse. The latter can be related to the characteristic roughness height ( $z_o$ ) by (Ribberink *et al.*, 2016):

$$z_o = 0.11 \left( \frac{\nu}{u_*} \right) + 0.03k_s \quad (13)$$

In which  $\nu$  is the kinematic viscosity and  $u_*$  the shear velocity. Both the Nikuradse roughness height and the shear velocity can be obtained from the method that is described in section 2.5.1. This will give an indication on the correctness of the used Manning coefficient.

## 2.6. Comparison of the ADCP data with the numerical model results

Apart from the data obtained by the ADCP, there are also results available from the numerical simulation of the confluence using a SSIIM2 model. These simulations were performed during the PhD dissertation which studied the confluence (Djordjevic, 2010) and were done for the same conditions as the ADCP measurements. Hence, the same discharges and bathymetry are used that resulted from the measurements with the ADCP. Since the simulations were executed externally, a limited set of results is available. The following three types of data from the results of the numerical simulation are used to make the comparison with the ADCP data:

Firstly, figures are available which indicate the secondary velocity structure with streamlines for the five transects. Since also streamlines are plotted for the velocities obtained by the ADCP data, qualitative comparison can be made between the flow structure as observed in the numerical simulations and in the flow structure that is observed in the ADCP data.

The second type of results from the model that are available are the information about the bed shear stress and the flow velocity near the bed. This information is available at the same locations as the

five transects downstream of the confluence. These results will be used to make a comparison of distribution of the bed shear stress over the channel width. Also, it will be used to identify the quantitative differences in the bed shear stress between the estimations using the ADCP data and the output of the numerical method.

Lastly the velocity magnitudes resulting from the numerical simulations are available from one transect. This concerns the middle transect (transect 75), for which the  $u$ ,  $v$  and  $w$  velocities are available for an irregular mesh. These results will be compared qualitatively to the velocity fields of the ADCP data.

### 3. Results

This chapter will deal with the results of the methods that are described in the previous chapter. First the ADCP data will be assessed on the inaccuracies caused by the way of positioning the measurements and the noise in the ADCP will be looked at. Afterwards the two methods of processing the ADCP data will be compared. Subsequently ADCP data will be compared to results of a numerical model. Lastly, the bed shears stress obtained in various ways will be compared to each other.

#### 3.1. Gap between GPS and ADCP measurements

First the time shifts that are performed on the ADCP data are treated. The final shifts are given in Table 1, which gives an idea of the uncertainty that is still present after the correction. This table gives the optimal times shift, which is defined as the time shift that gives the lowest difference between the distances calculated by the bottom-tracking and those of the GPS-coordinates, for both the x and y direction as well as the final applied time shift per transect. Herein there is a noticeable difference between the optimal time shift for the x (longitudinal) and y (latitudinal) direction. This difference gives an indication of the inaccuracy within the method that is used to shift the time of the GPS data. This difference is smaller than 0.3 seconds for all the transects. However, it would be logical if the error is systematic and the same for all transects, since the same device has been used to measure the time for every transect. If this is true, then all the time shifts should be combined to estimate the inaccuracy in the method. This results in a maximum difference of 0.5 seconds between the minimum and maximum time shifts of the ten time shifts that are found in Table 1. This seems to be a reasonable estimate of the inaccuracy induced by this correction on the data.

*Table 1 Final time shifts that have been applied on the transect to align the GPS coordinates with the ADCP measurements*

<b>Transect number</b>	<b>Optimal time shift in the X-direction (s)</b>	<b>Optimal time shift in the Y-direction(s)</b>	<b>Final time shift applied (s)</b>
<b>73</b>	17.2	17.1	17.15
<b>74</b>	17.1	17.3	17.2
<b>75</b>	17	17.3	17.15
<b>76</b>	16.8	17.1	16.95
<b>77</b>	17	16.8	16.9

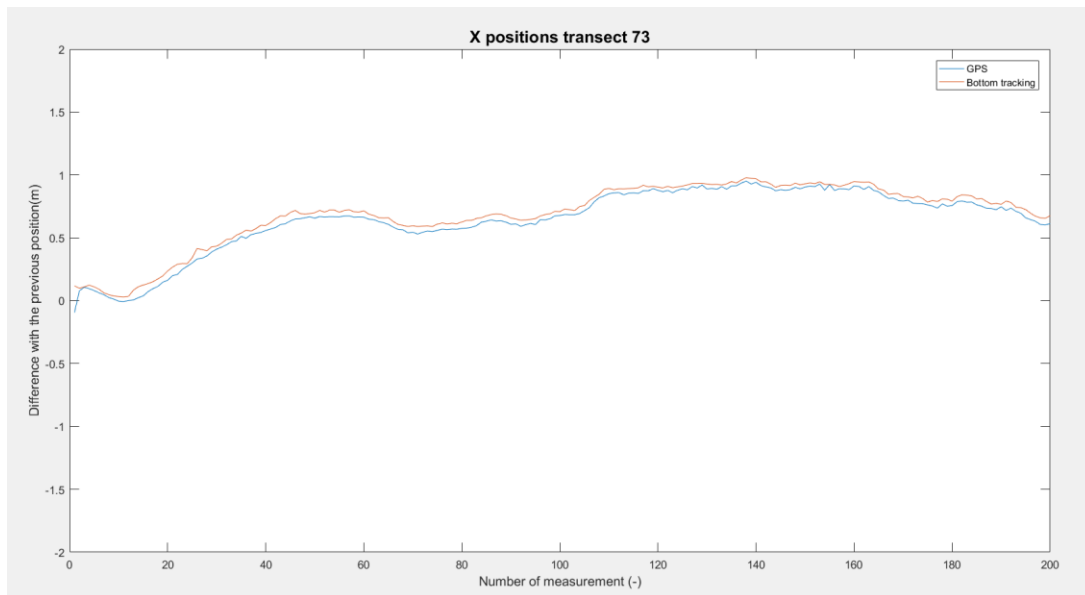


Figure 12 Distance between measurements for the GPS coordinates and the bottom tracking coordinates in the x-direction for transect 73

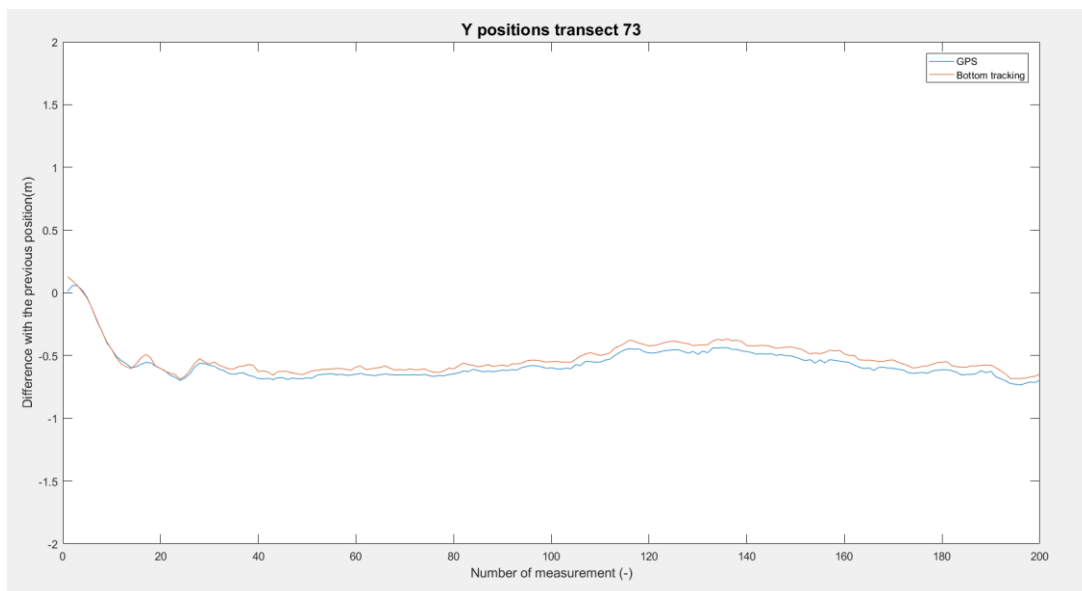


Figure 13 Distance between measurements for the GPS coordinates and the bottom tracking coordinates in the y-direction for transect 73

The result of this shift is indicated in Figure 12 and Figure 13 for the x and y coordinate, respectively, where the results of the first 200 measurements are given for transect 73. The figures give an indication of the similarity between the distances determined by the GPS-coordinates and those that are determined by the bottom-tracking method for the first 200 ADCP measurements. Here the shape of the lines is significantly more similar, compared to the lines in Figure 11. There is still a systematic difference between the lines, which indicates a moving bed. This could be further investigated by combing the difference of both the x and y- coordinate, but this is not done in detail within this study. This is explained in more detail within the discussion.

This inaccuracy in time will be converted towards a distance, to compare it with the distance between the radial velocities in the conventional method. The ADCP does send out a sound signal every 0.92 seconds. The distance that is covered between the measurements is not constant, as is indicated in

Figure 12 and Figure 13. For this distance the average of median values for the distance within the five transects has been taken, which resulted in a value of 0.93 meter. This results in a boat velocity of approximately 1 m/s. This implies an accuracy of around 0.5 meter, keeping in mind that the inaccuracy was 0.5 seconds. Additionally, the GPS device itself can also cause an error, which is also indicated in the results of the GPS measurements. The device indicated an additional inaccuracy of up to 6 centimeters, with outliers reaching up to 14 centimeters. Consequently, 56 centimeters is compared to the distance between the beams.

The angle of the beams, compared to the vertical plane, is 20 degrees. Since the beam on the opposite site points 20 degrees in the opposite direction, the distance will be calculated at which the distance between the beam and the vertical beneath the ADCP is 28 centimeters. This distance is 77 centimeters, which coincides with the upper 5-10 percent of the flow, depending on the position along the transect. Comparatively, the distance between the beams of the ADCP increase to around 10 meters at the bottom of the bed.

However, the difference between the GPS and ADCP measurements is not the only point that should be considered when expressing the accuracy of the new method. This new method uses all measurements within a cell, therefore also the width of the mesh cell can determine the accuracy of the new method. This width is 10 meters throughout this thesis, which is around the same as the distances between the beams of the ADCP near the bed. Therefore, both methods assume horizontal homogeneity over the same distance near the bed and the conventional methods depends less on this assumption near the upper part of the flow. This contrasts with what the new method is designed for, to rely less on this assumption.

### 3.2. Required repeated transects

The results are shown for two transects downstream of the confluence. Transect 73, which is the furthest from the confluence, and transect 77 which is the closest transect to the confluence (Figure 1). For the latter one, it is expected that more turbulence is present. Therefore, it is expected that more repeated transects are needed to stabilize the value of the standard deviation compared to transect 73.

Searching for differences along the channel, Figure 16 and Figure 14 can be compared. This shows clearly that the standard deviation is flattening earlier for transect 73. This is best visible for the smaller mesh cell widths, which can be explained by the lower number of measurements that are used for each mesh cell. So, an increase in repeated transects, and thus an increase in the amount of measurements per cell, has a larger impact here compared to meshes with larger cells. This effect is less visible when the results of the different transects are compared for the conventional method, which can be seen in Figure 17 and Figure 15. Here there seems to be hardly any difference between the two locations.

When the two methods are compared no distinct differences are noticeable. For example, comparing Figure 16 and Figure 17 shows the results for both methods calculated for transect 73. The standard deviation is converging to a stable around the same number of repeated transects for both methods. This does not confirm the results that were obtained by applying the method on an Indonesian river (Vermeulen *et al.*, 2014). Here the new method seemed to overcome the influence of the turbulence and flow inhomogeneity with less repeated transects, compared to the conventional method. This might be because the new method is less dependent on the flow homogeneity. For transect 77, visible in Figure 14 and Figure 15, the opposite seems to be true. Here the conventional method seems to converge to a stable value of the standard deviation earlier compared to the new method.

Another aspect in the comparison between both methods is that the new method shows a lot more variation in the evolution of the standard deviation compared to the conventional method. This is illustrated by the comparison between Figure 14 and Figure 15. Figure 15 shows an increase in standard deviation with an increase in repeated transects for all mesh cell widths and the corresponding lines do not cross each other. Figure 14 on the other hand shows multiple intersections of lines and even slightly decreasing values for the standard deviation with an increase in repeated transects. The same effects are visible by the comparison between Figure 16 and Figure 17.

A reason for the higher variation in the growth of the standard deviation for the new method might be the dependence of the new method on the quality of the data that indicates the position of the measurements. Since the GPS data for this case is not measured simultaneously with the ADCP measurements, but rather with an external device, some discrepancies can arise between the actual location of the measurements and the location that is determined from the external GPS measurements, as is assessed in the previous section. Since the new method is highly depended on the position measurements (GPS in this study), which are used to combine the beams to each other, the accuracy of the new method is reduced when the quality of this position measurements is less accurate. Therefore, inaccuracies in the GPS measurements themselves can influence the accuracy of the new method as well.

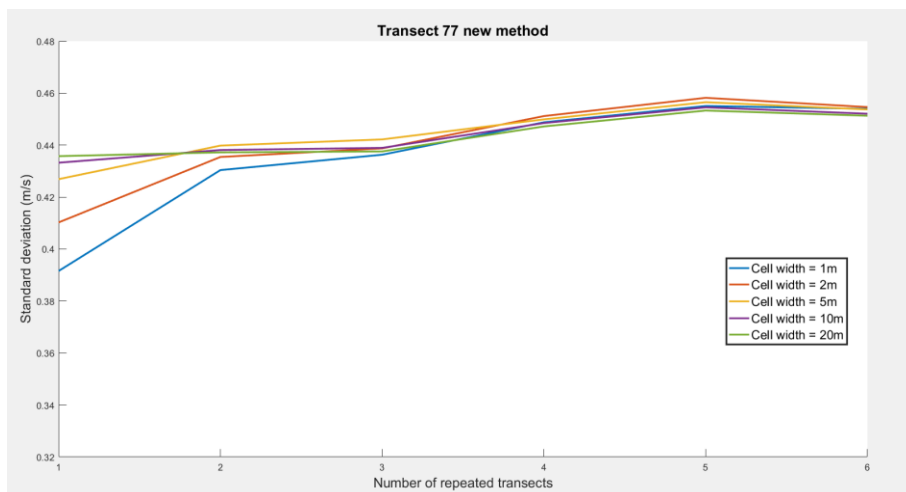


Figure 14 Standard deviation of the mesh for the new method depending on the grid size for transect 77

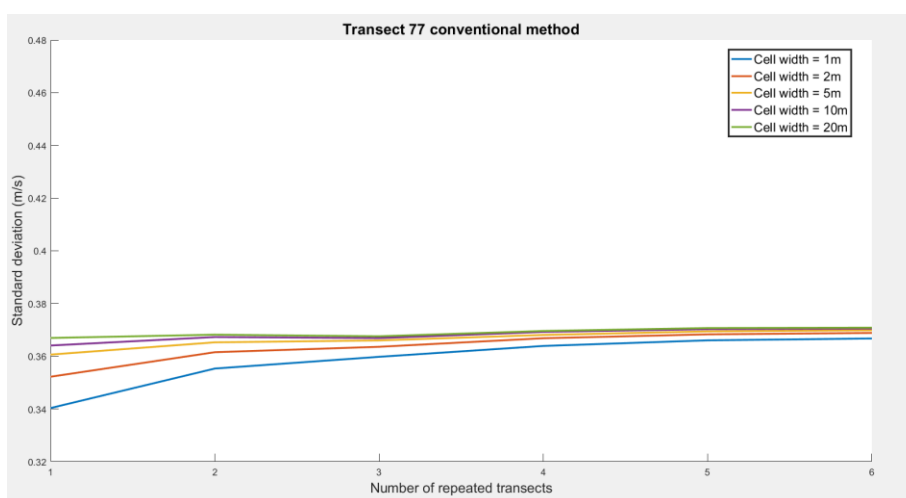


Figure 15 Standard deviation of the mesh for the conventional method depending on the grid size for transect 77

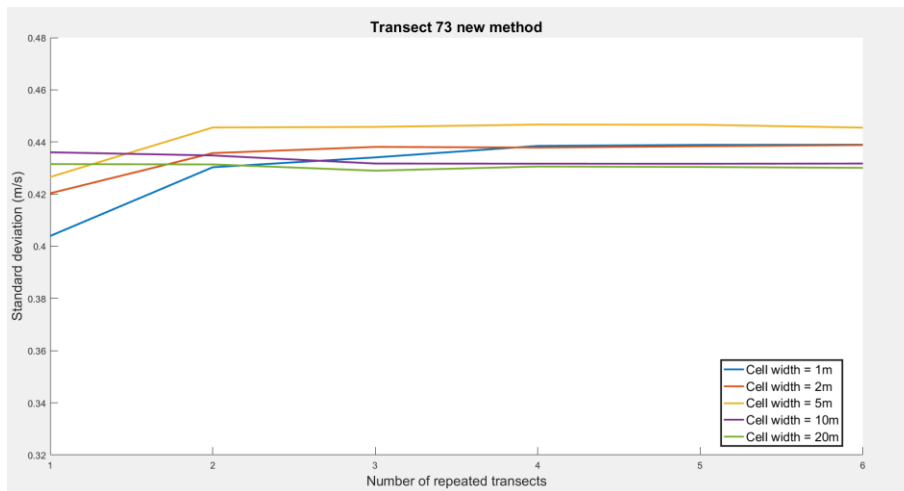


Figure 16 Standard deviation of the mesh for the new method depending on the grid size for transect 73

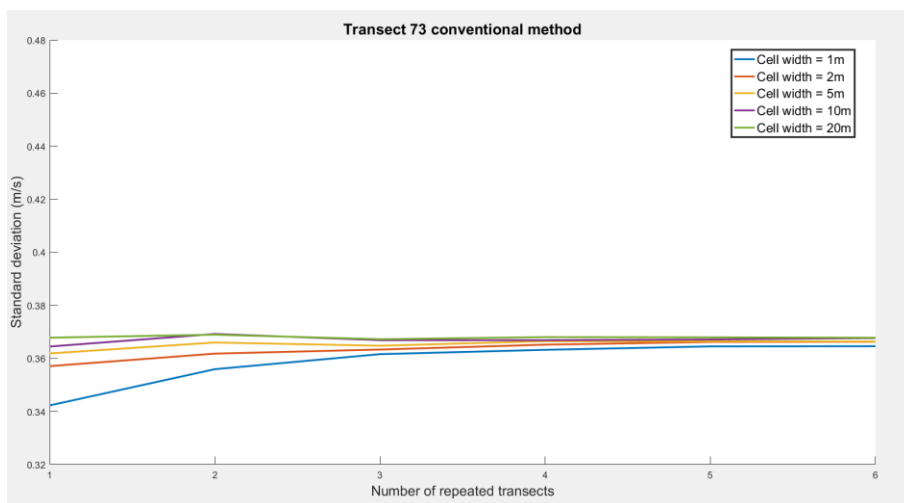


Figure 17 Standard deviation of the mesh for the conventional method depending on the grid size for transect 73

The results tell something about the cell size that should be applied for further analysis. If the cell size is taken too small, then the results obtained in this section imply that turbulence is not captured sufficiently. On the other hand, if the cell sizes are taken to large, then smaller flow patterns will be averaged out of the results and the results will become irrelevant. Consequently, an optimal should be found that on one hand decreases the impact of turbulence as much as possible and on the other hand is detailed enough to distinguish the various flow patterns that are expected to be present.

Based on the results for both methods, the standard deviation seems to be stable for all mesh cell widths when using all the repeated transects that are available. Consequently, the choice of mesh cell width is based on other criteria, which in this case is the visualization of the flow fields. According to the results of the secondary flow velocities, visible for different mesh cell widths in section 3.3.2. and 4.2., a larger mesh width is used in study. The width that is used is 10 meters. This allows for a better visualization of the flow structures. All the repeated transects that are not rejected because they were considered bad (see section 2.1.2.) are used within the study.

### 3.3. Comparison between the methods

#### 3.3.1. Magnitudes

A first step has already been made in the comparison between the two methods in the previous section, but here a more thorough analysis will be done on the difference that arise when the methods

are compared. The transects which will serve as indicator for the comparison are the same as for the noise in the data, i.e. transect 73 and transect 77. These transects are chosen, because they are positioned at the most upstream and downstream part of the measured section downstream of the confluence, respectively. Therefore, it is expected that, if there are differences between the two methods, these will be visible in one of these transects. The three-dimensional flow effects, induced by the confluence, should be more apparent within transect 77, because of this. Hence, the results of the methods are expected to differ the most for this transect, because here the flow is expected to be the least homogeneous. All the plots of transects within this section have been made looking from upstream towards the downstream direction.

Looking at Figure 19 and Figure 18 both methods give comparable results for the flow in the streamwise direction. Both methods show flow patterns with higher streamwise velocities at the surface and lower velocities near the bed and the banks, in concordance with the profiles as described in section 2.5.1. There are also differences in the results of both methods, although they are minor compared to the magnitude of the streamwise velocity. Also, there seems to be no distinct pattern in where the largest differences between the two methods lay. At this point they seem to be randomly distributed and do not give much information on either the flow structure or the performance of the methods.

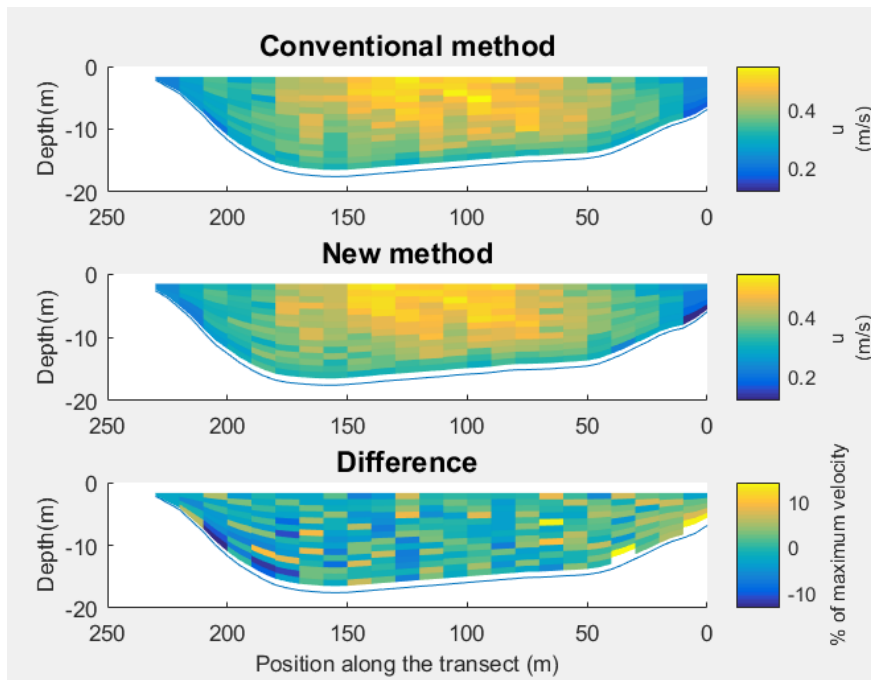


Figure 18 Along stream velocities of transect 77 using the new method and the conventional method together with the difference between the methods as percentage of the maximum streamwise velocity as obtained by the new method

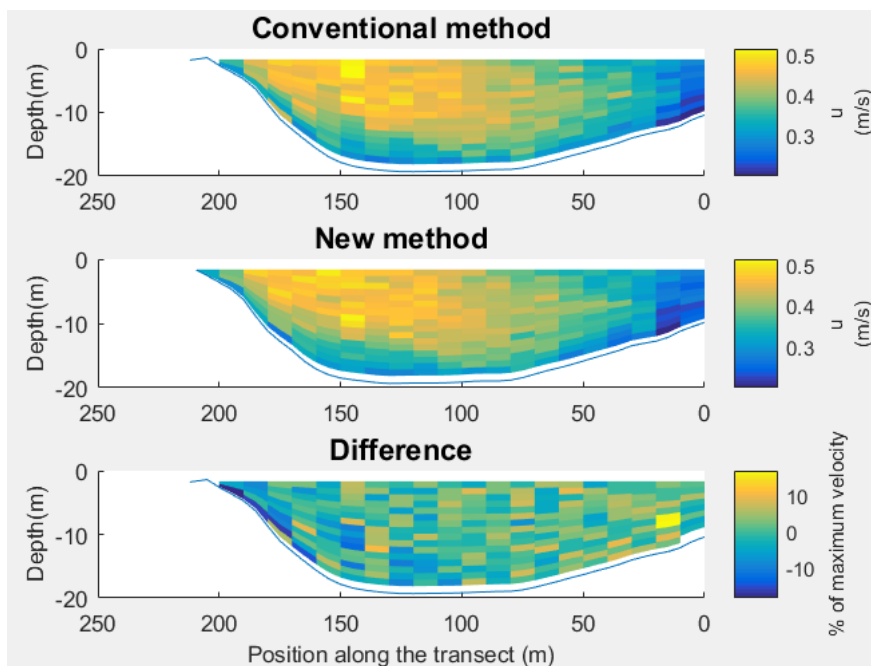


Figure 19 Along stream velocities of transect 73 using the new method and the conventional method together with the difference between the methods as percentage of the maximum streamwise velocity as obtained by the new method

The magnitudes of the differences between the conventional method and new method for the cross-stream and vertical velocities are given in Figure 21, Figure 20, Figure 23 and Figure 22. The results for the velocity magnitudes of both methods for the  $v$  and  $w$  velocity give high differences compared to the velocity magnitudes themselves of up to 50% compared to the maximum velocity. However, the differences do not show clear patterns, but are seemingly distributed randomly. For the cross-stream direction, the largest errors are generated near the bed, which can be caused by the reduced amount

of measurements which are available there, but a similar observation cannot be made for the vertical velocity. Since the comparison of the magnitudes of the secondary velocities does not give clear results, the secondary velocity field of the combined  $v$  and  $w$  velocity is assessed in the next section.

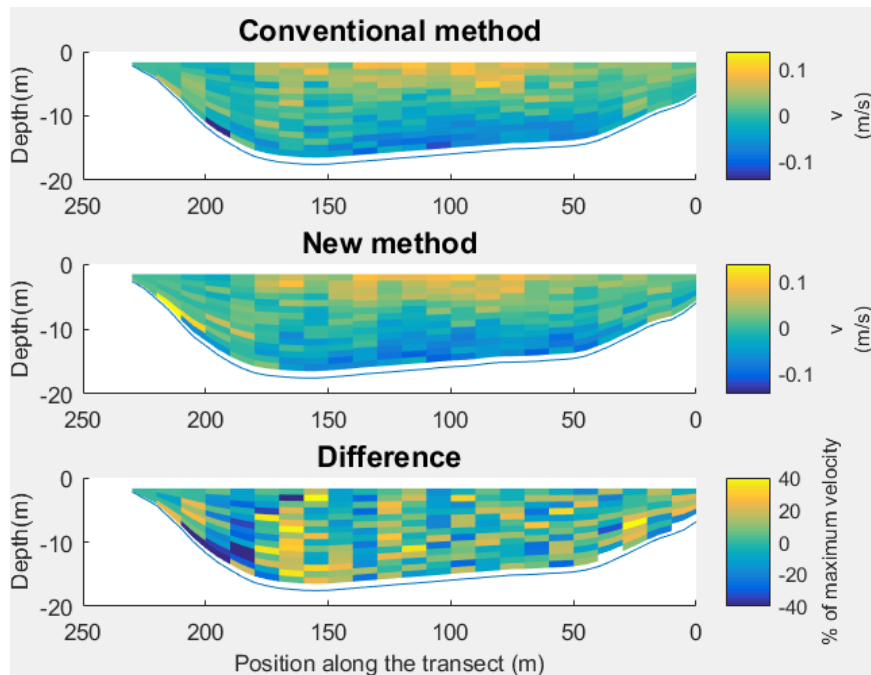


Figure 20 Cross-stream velocities of transect 77 using the new method and the conventional method together with the difference between the methods as percentage of the maximum streamwise velocity magnitude as obtained by the new method. Positive values indicate that the flow is directed left (to the outer bank) and negative values a flow directed to the right (to the inner bank)

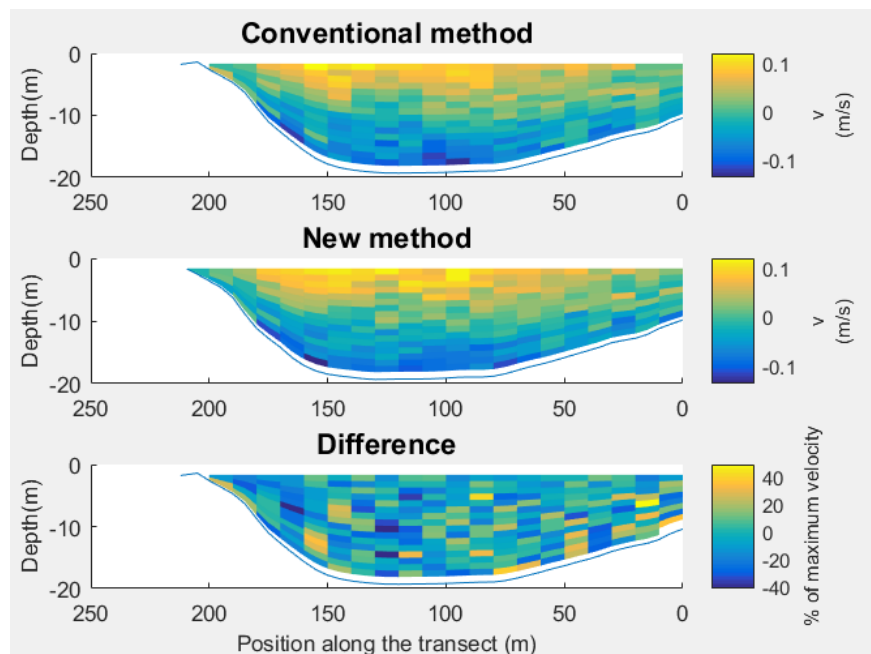


Figure 21 Cross-stream velocities of transect 73 using the new method and the conventional method together with the difference between the methods as percentage of the maximum streamwise velocity magnitude as obtained by the new method. Positive values indicate that the flow is directed left (to the outer bank) and negative values a flow directed to the right (to the inner bank)

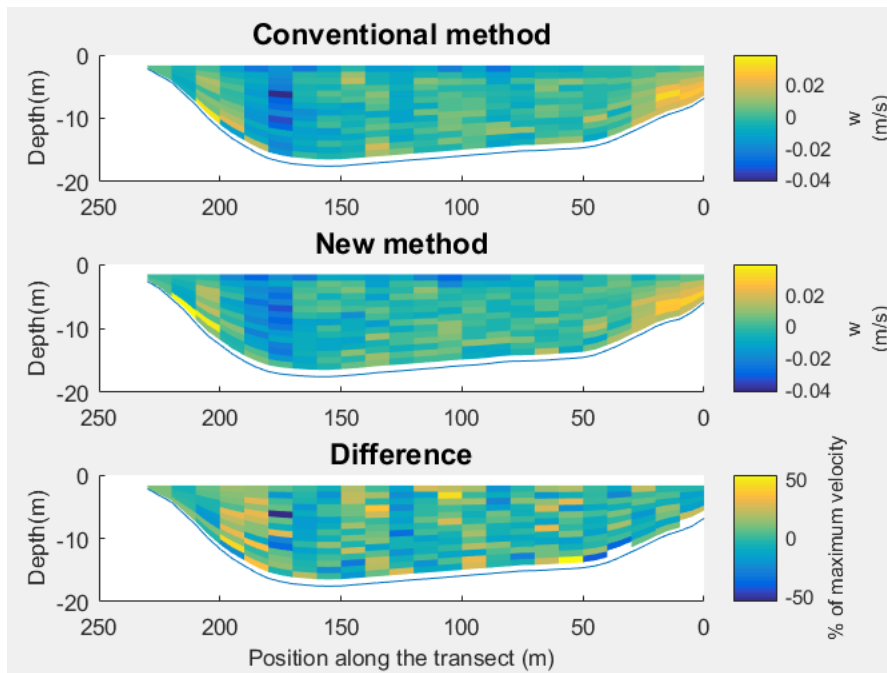


Figure 22 Vertical velocities of transect 77 using the new method and the conventional method together with the difference between the methods as percentage of the maximum streamwise velocity magnitude as obtained by the new method. Positive values indicate upward flow and negative values indicate downward flow

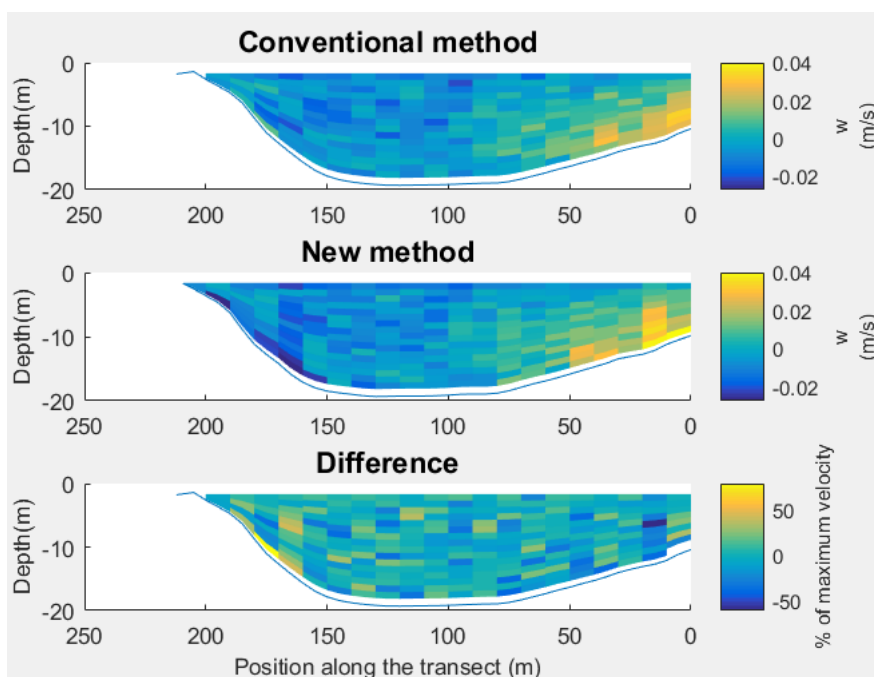


Figure 23 Vertical velocities of transect 73 using the new method and the conventional method together with the difference between the methods as percentage of the maximum streamwise velocity magnitude as obtained by the new method. Positive values indicate upward flow and negative values indicate downward flow

The magnitudes have also been compared in a cross-sectional average way. These averages of the three velocity components for the two different methods are presented in Table 2. Both methods show similar numbers for all three velocity components, where the differences are at least an order of magnitude lower compared to the magnitudes. This reinforces the idea that the differences between the methods are indeed random and that no structural difference is present between the methods.

Interestingly, the numbers do not show a flow acceleration in the streamwise velocity, which is a common feature in confluences. Moreover, the contrary is true when Transect 83 is considered, which is positioned in the main channel upstream of the confluence. When moving downstream, a flow acceleration visible in the cross-sectional averaged cross-stream velocities.

*Table 2 Cross sectional averaged flow velocities (m/s) from both methods, together with the differences between the methods*

Transect	u from conventional method	u from new method	difference in u (%)	v from conventional method	v from new method	difference in v (%)	w from conventional method	w from new method	difference in w (%)
73	0.385	0.379	1.4	0.040	0.0420	-4.9	0.0087	0.0094	-7.7
74	0.368	0.366	0.5	0.044	0.0425	2.5	0.0088	0.0096	-8.6
75	0.370	0.362	2.0	0.034	0.0329	4.6	0.0074	0.0084	-14.3
76	0.368	0.371	-0.9	0.034	0.0353	-4.2	0.0109	0.0113	-3.0
77	0.372	0.370	0.5	0.031	0.0317	-2.5	0.0085	0.0084	1.2
83	0.436	0.430	1.4	0.024	0.0244	3.4	0.0085	0.0082	3.2

### 3.3.2. Flow structure

The data was analyzed by computing secondary flow fields for all transects by using the magnitudes that resulted from the two methods. This secondary flow field is composed out of a combination of the cross-stream and vertical velocity.

For most cross sections, the difference between the secondary circulation fields, using the different methods, is small. When the cross-sections are positioned closer towards the confluence, there is a slight distinction between the methods. To illustrate the difference, the secondary flow fields of cross-section 77 are plotted in Figure 24 and Figure 25. Here the new method shows a little bit clearer patterns compared to the conventional method at. The part of the patterns that shows this marginal difference, is the part of the where the two helical cells meet each other, i.e. the shear layer (visible at 175 meter along the transect in Figure 24 and Figure 25). Significant gradients for the velocities in the horizontal plane exist in this part of the flow. These gradients impact the validness of the assumption of horizontal homogeneous flow. And because the new method is reliable on this assumption to a lesser extent, it can perform better in these locations. Which might be the reason why the new method performs slightly better in this case. This difference is marginal however and might be attributed to a slightly different mesh construction. This difference is not visible in the secondary flow fields for the other transects as well. These are given in Appendix A.

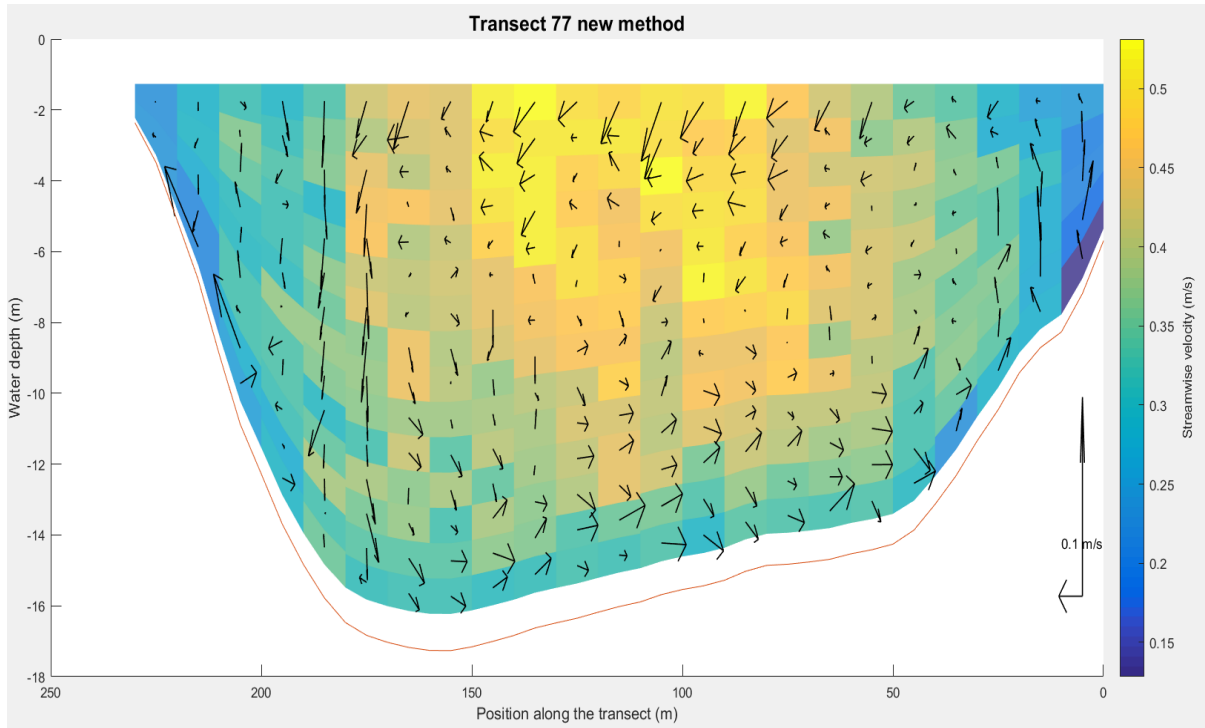


Figure 24 Secondary flow field of transect 77 using the new method

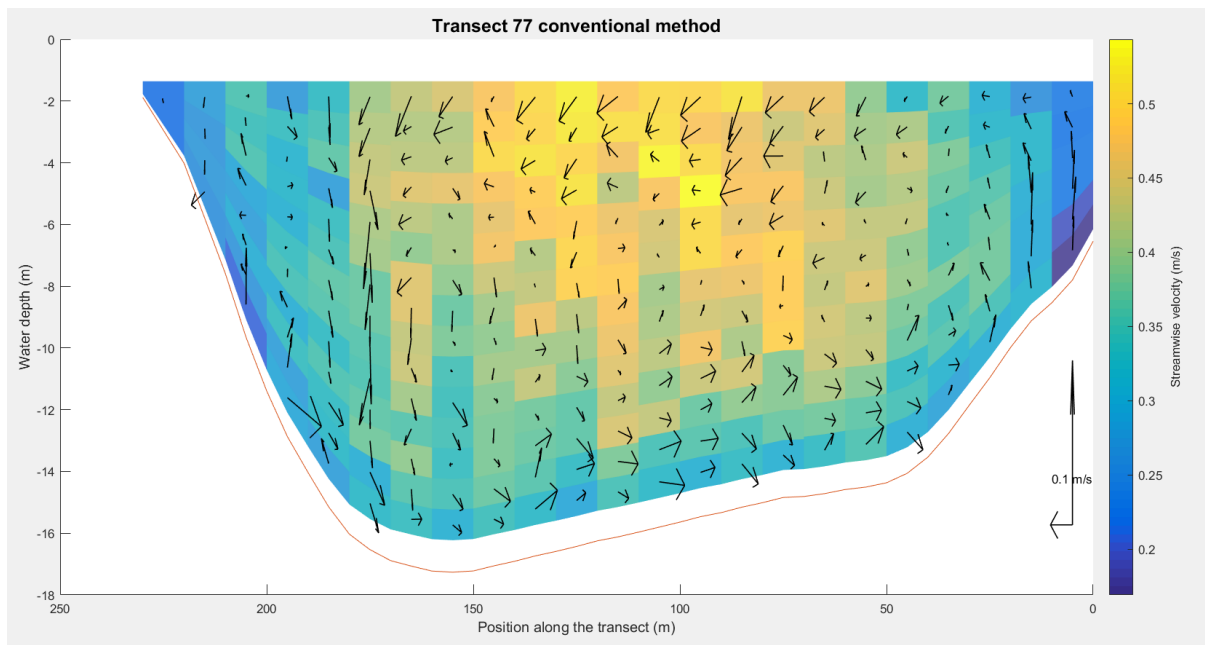


Figure 25 Secondary flow field of transect 77 using the conventional method

### 3.4. Comparison with the model

#### 3.4.1. Flow structures

The first point of comparison is the flow structure of the secondary velocity of both the ADCP data and the numerical model. The flow structures as calculated within the model are presented in Figure 26, where the streamlines of the cross-stream and vertical velocities are plotted. Figure 27 and Figure 28 show the same results for transect 73 and 77, but then obtained by the ADCP data. The secondary flow fields of the other transects, as calculated from the ADCP data, are given in Appendix A.

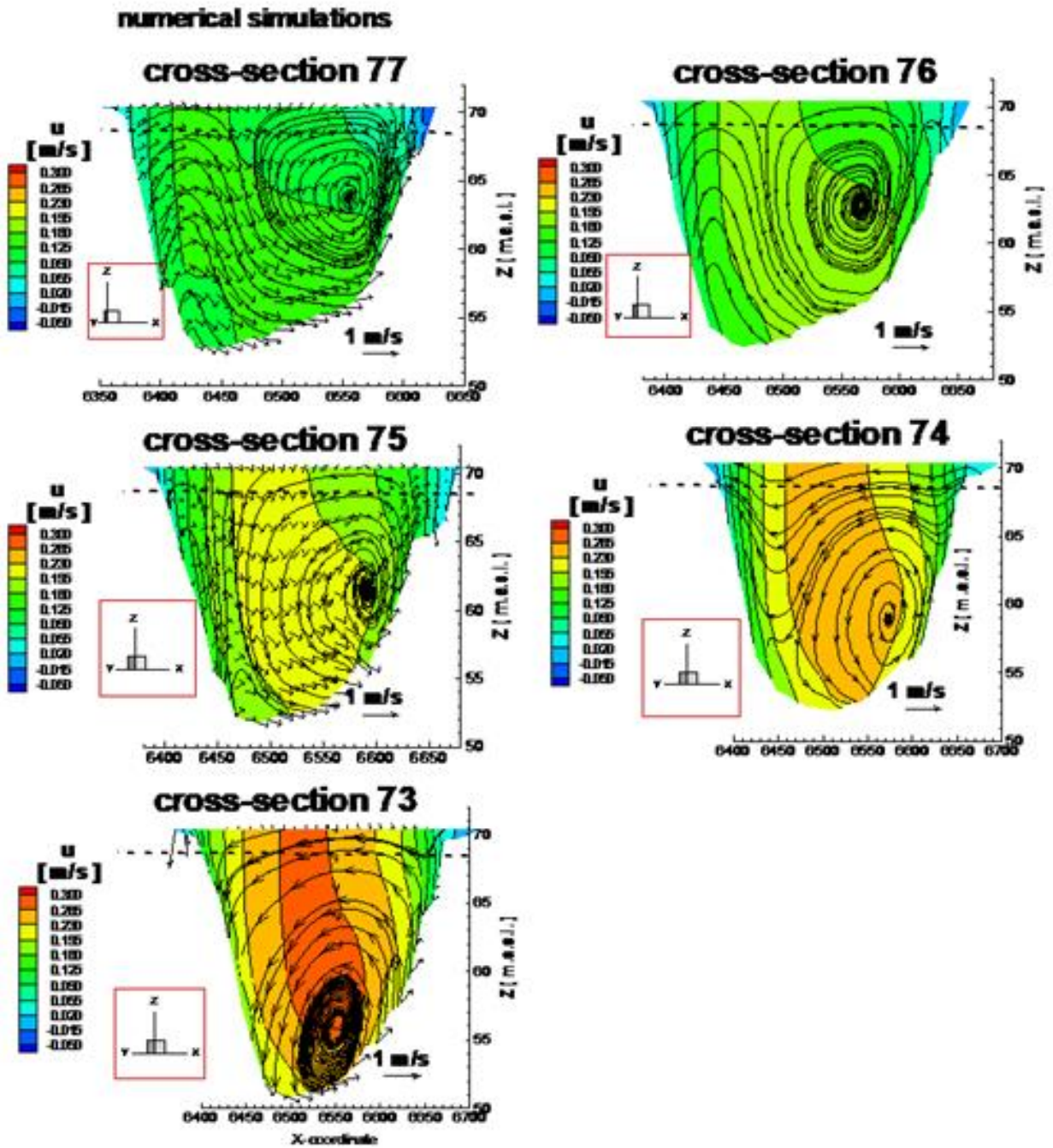


Figure 26 Streamlines of the secondary circulation based on the numerical results

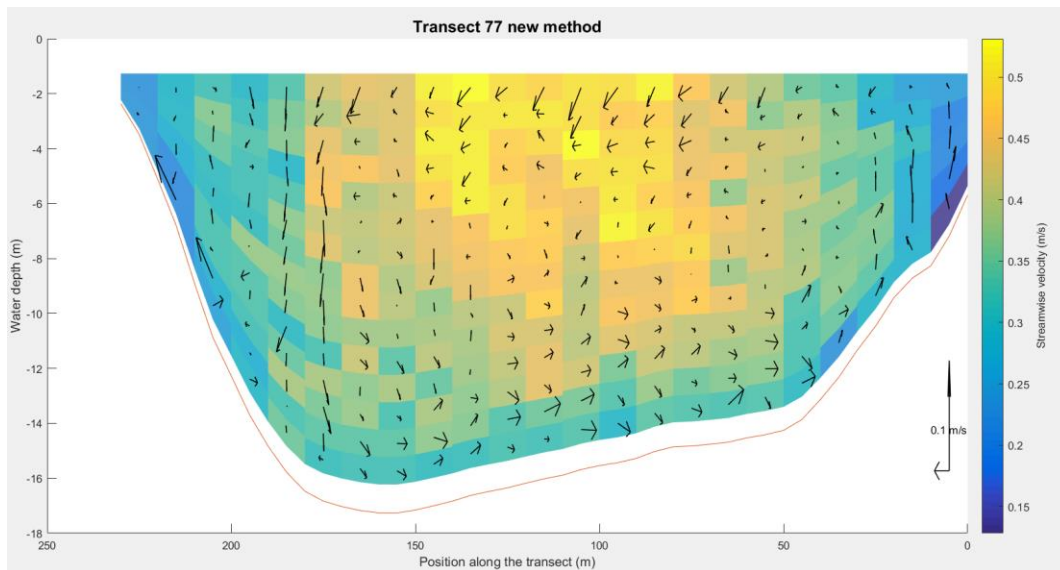


Figure 27 Secondary flow structure of transect 77 obtained by the new method

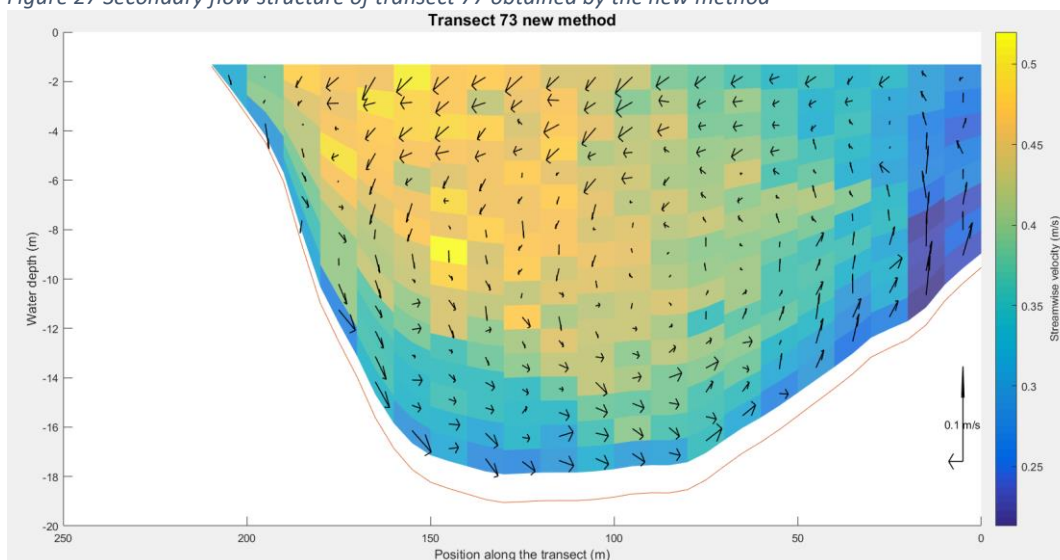


Figure 28 Secondary flow structure of transect 73 obtained by the new method

There is a clear difference within the flow structures that are visible within the ADCP data and those of the numerical model. For most of the transects the ADCP measurements show one secondary cell over the whole width of the channel. Only for transect 76 and 77 a small cell is visible at the outer bend of the flow. For the numerical results, the same helical cell is visible that rotates in the same direction. However, this cell does not extent over the full width of the channel and thus is smaller compared to the cell that is visible in flow structures as obtained from the ADCP data. There is no counter rotating cell present in the flow structures which result from the numerical simulations as well.

### 3.4.2. Velocity magnitudes

In Figure 29, Figure 30 and Figure 31 the velocities in three directions have been plotted for transect 75. These figures show that the numerical data and the model give a similar view of the velocities for the streamwise and cross-stream velocity. However, the comparison is hindered by the fact that the ADCP does not measure the complete flow. Therefore, a smaller part of the flow is visualized for the magnitudes of the ADCP data compared to the results of the numerical model. This can be seen from

the differences in axes in Figure 29, Figure 30 and Figure 31. For the streamwise velocity the magnitudes seem to decrease faster with the depth in the data than for the numerical model. This is further investigated by making a plot of the streamwise velocity as a function of the depth in the center of the transect. For both data sets, the middle 30 meters has been averaged and plotted as function of the depth in Figure 32. These graphs confirm the same observation, despite the difference being small.

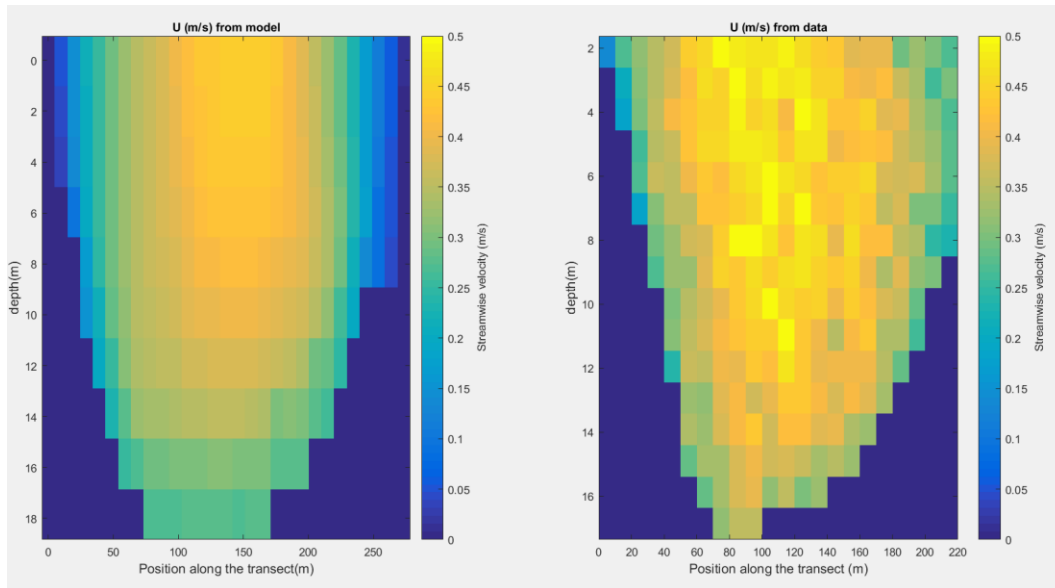


Figure 29 Comparison of the velocities from the numerical model and ADCP data for the stream wise direction

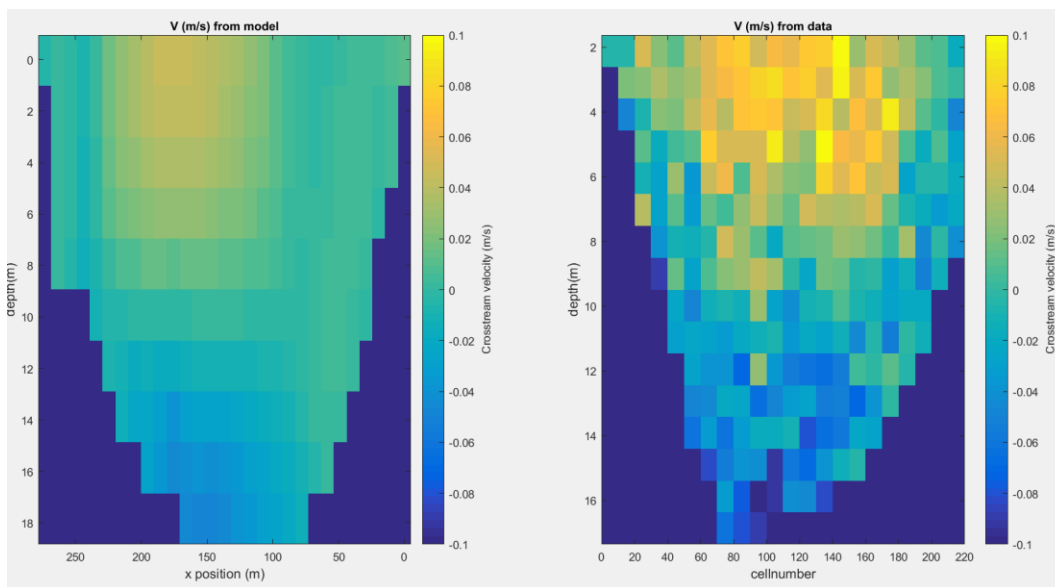


Figure 30 Comparison of the velocities from the numerical model and ADCP data for the cross-stream direction. Positive values indicate that the flow is directed left (to the outer bank) and negative values a flow directed to the right (to the inner bank)

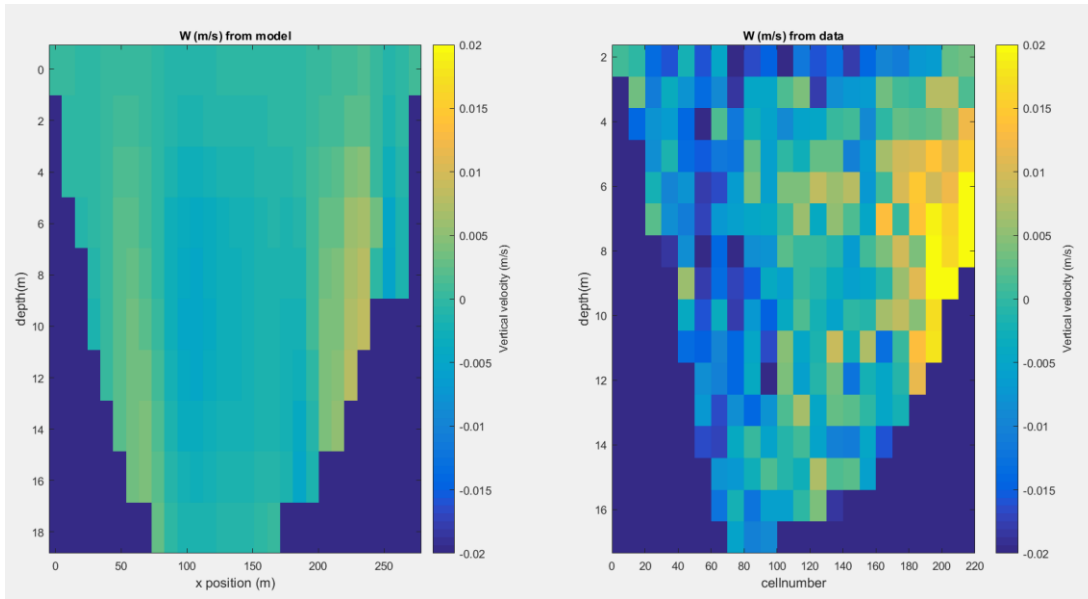


Figure 31 Comparison of the velocities from the numerical model and ADCP data for the vertical direction. Positive values indicate upward flow and negative values indicate downward flow

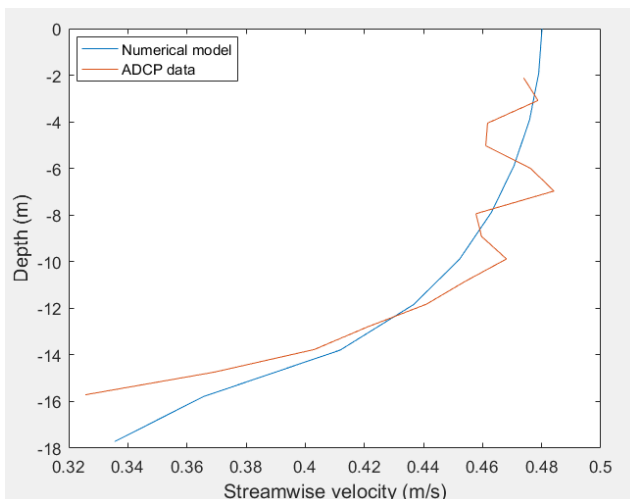


Figure 32 Velocity profiles of the along stream velocity component as function of the depth in the center of transect 73

For the cross-stream and vertical velocities the same graphs have been made in Figure 33 and Figure 34. These show that for the cross-stream direction the patterns are similar in both the ADCP data and the numerical model. However, the velocities observed in the ADCP data seem to be greater in magnitude compared to the numerical model. For the vertical velocities this underestimation by the SSIIM2 model has been observed for other studies as well (Djordjevic, 2012). Also, there is more noise present within the data obtained by the field measurements as can be seen in Figure 33, but that is inherent to obtaining data in the field.

The cross-stream velocities do show large difference in both pattern and magnitude when comparing the ADCP data and the numerical results. This is clearly visible in Figure 31, where the flow distributions in the vertical direction are plotted. There two regions are visible in the numerical model where upward velocities have been predicted, only one such region is present within the ADCP data. This agrees with the earlier observation, with the model showing a helical cell that does not extent over the full width of the channel (see Figure 26). The ADCP did show a helical cell that covered the whole width of transect 75 (see Figure 51 in Appendix A).

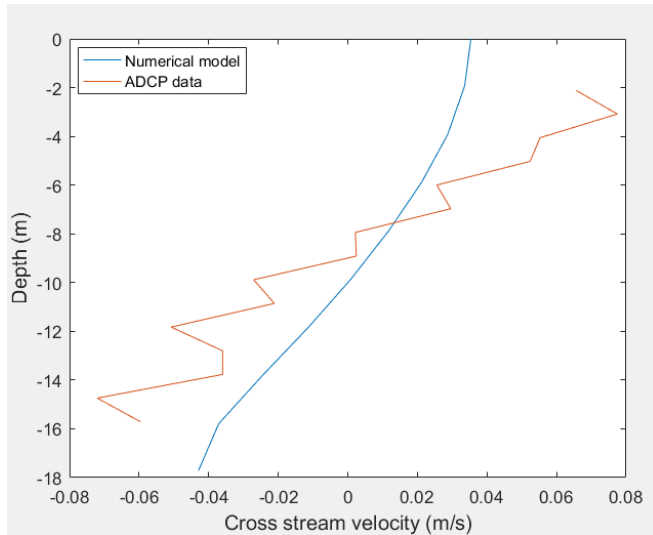


Figure 33 Velocity profiles of the cross-stream velocity component as function of the depth in the center of transect 73

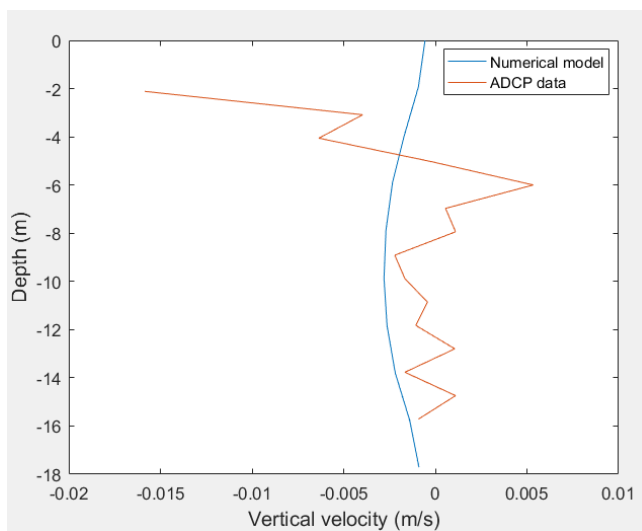


Figure 34 Velocity profiles of the vertical velocity component as function of the depth in the center of transect 73

### 3.5. Bed shear stress

The bed shear stress has been estimated by the application of three methods on the given data, together with the results of the numerical model. These results of these methods are plotted together with the bed level in Figure 36 and Figure 35. Again transect 73 and 77 have been chosen as normative transect. The other three transects are given in Appendix B. The negative values for the position along the transect in the figures is caused by the numerical results being available over large width, compared to the ADCP data. Within this figure a smoothing is applied within the scatter of points, to facilitate the comparison between the different methods. This smoothing is done by calculating the value at a location by using the then values around this value. The weight of these ten values is determined by the distance to the value that is smoothed.

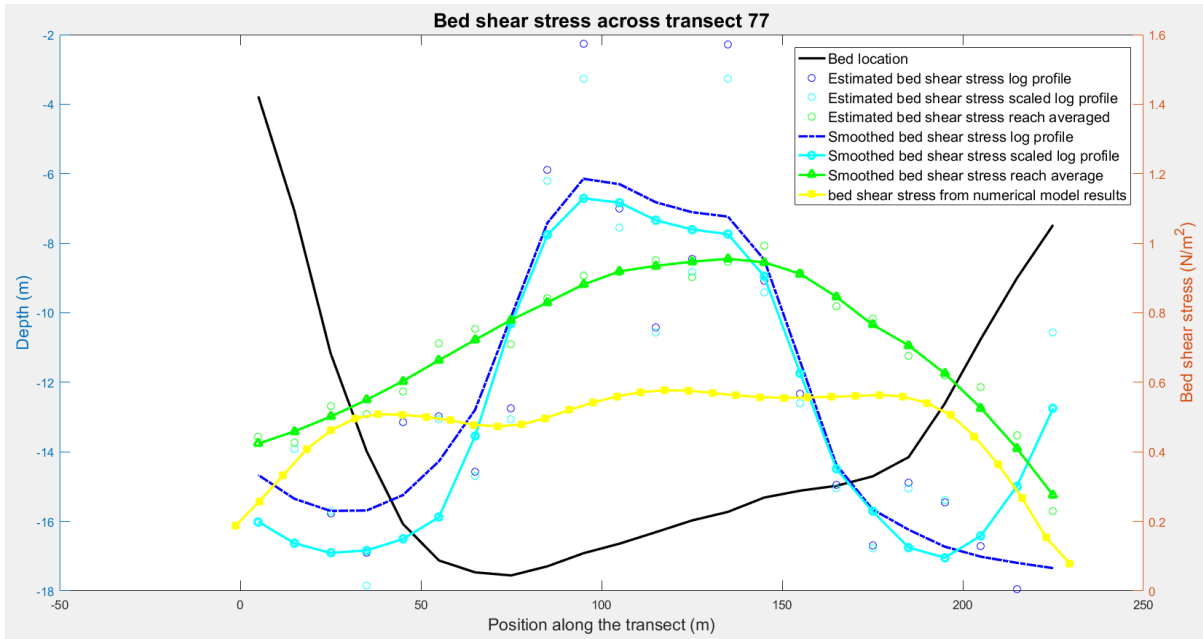


Figure 35 Bed shear stress estimations for transect 77

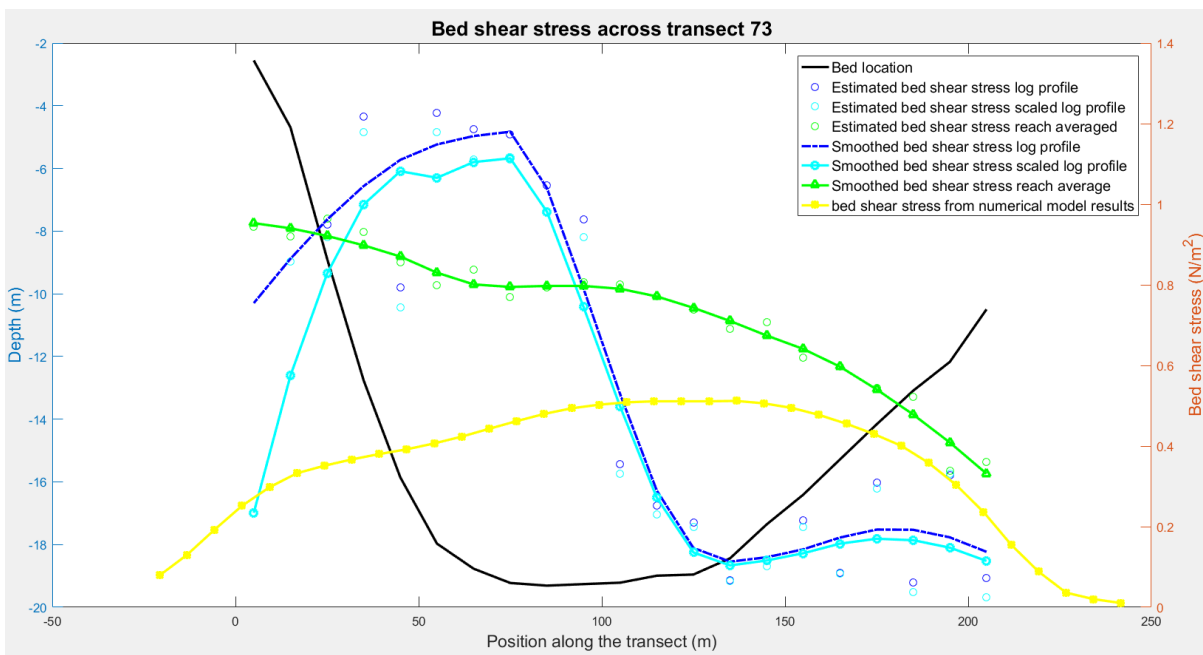


Figure 36 Bed shear stress estimations for transect 73

What is visible from these results is that three methods using ADCP data have their maximum bed shear stress moving from the inner bend towards the outer bend, when moving downstream. Which is similar to where the maximum depth of the channel is positioned. The numerical model does not show the same results. Here a much more constant distribution of the bed shear stress is visible over the course of the river. And even if there is a trend within distribution of the bed shear stress, this seems to move to the inner bend rather than the outer bend as visible in the other method. This is probably related to the underestimated cross-stream velocity in the model, which is was observed in Figure 33. This implies that the model performs worse for the secondary flow compared to the streamwise flow. That the estimates of the bed shear stress from the ADCP show values which follow

the bathymetry better compared to the numerical model, gives confidence that these estimates are indeed better.

The results of the estimated bed shear stresses averaged over the transects are presented in Table 3. From this table it is visible that all the estimations are of the same order of magnitude. Also, it can be stated that the numerical model gives, generally, lower values for the bed shear stress compared to the methods which use the ADCP data. This is in line with the findings of the streamwise velocity profile for the numerical model, as observed in Figure 32. Here the gradients in the streamwise velocity of the ADCP data are larger, i.e. they approach a velocity of zero faster near the bed, then for the results of the numerical model.

Table 3 Results of the cross-sectional averaged bed shear stresses using the different methods and the calculated Manning coefficient based on the logarithmic profile

Transect	Reach averaged (N/m <sup>2</sup> )	Logarithmic profile (N/m <sup>2</sup> )	Logarithmic profile with an averaged velocity (N/m <sup>2</sup> )	Numerical model results (N/m <sup>2</sup> )	Calculated Manning coefficient (N/m <sup>2</sup> )
73	0.73	0.56	0.53	0.35	0.030
74	0.68	0.94	0.91	0.38	0.032
75	0.63	0.47	0.42	0.39	0.026
76	0.69	0.51	0.47	0.42	0.027
77	0.70	0.60	0.57	0.47	0.024

For the difference between the three methods that use the ADCP data it can be said that the two methods that fit a logarithmic profile perform similar, where the logarithmic profile scaled by the mean velocity gives lower values throughout the confluence. This difference is marginal however. When these values are compared to the reach-averaged bed shear stress, large deviations between the methods are present. Still the order of magnitude is similar, but the shape of the reach-averaged bed shear stress gives a more constant value over the width of the transects. Also reach average method gives higher values for all the transects. An explanation for this is an overestimation of the Manning coefficient that is used for these transects.

It is visible that for all the transects the Manning coefficient is lower compared to the default value of 0.035 s/m<sup>1/3</sup>. This implies that the channel is smoother than what is expected in the literature for major streams. Consequently, the bed shear stress estimated with the new Manning value is also lower. This causes the estimated bed shear stresses to also decrease, when the value that estimated based on the logarithmic profile is used. However, it is questionable to which extent this indicates a better estimation of the absolute bed shear stress, since the values are based on a fitting which showed a lot of uncertainty. Also, the distribution over the transect will remain the same, which differs significantly from the distribution obtained by the fits of the logarithmic profile.

An indication of the uncertainty of the fitting of the logarithmic method is given by the results of the bed roughness that resulted from fitting Eq. (7) and combining this with Eq. (12) and Eq. (13). These resulted in roughness heights  $k_s$  between 4 and 10 centimetres. Since both the beds of the Sava and Danube Rivers are reported to consist out of sand, these values are unrealistic. This can be caused by the quality of the fit, or because the assumption  $k_s \approx \text{grain diameter}$  is not valid in this case. The latter can be caused by other forms of roughness within the channel.

The difference in the uncertainty of the fits between the logarithmic profile and the scaled logarithmic profile is given in Table 4, where the average  $R^2$  values for the transects are given. The fitting of the logarithmic profile gives higher average values compared to the values of the fit of the logarithmic profile with the average velocity. Also, the distribution of these values has been studied, for which the results are given for transect 75 in Figure 37 and Figure 38. The other transects are given in Appendix C. From these figures it is visible that the  $R^2$  values in general follow the values of the bed shear stress itself.

Table 4 Cross-sectional averaged  $R^2$  values for the fits of the logarithmic profile and the logarithmic profile scaled with the average velocity

Transect	Logarithmic profile	Scaled logarithmic profile
73	0.81	0.61
74	0.80	0.62
75	0.82	0.62
76	0.78	0.50
77	0.82	0.58

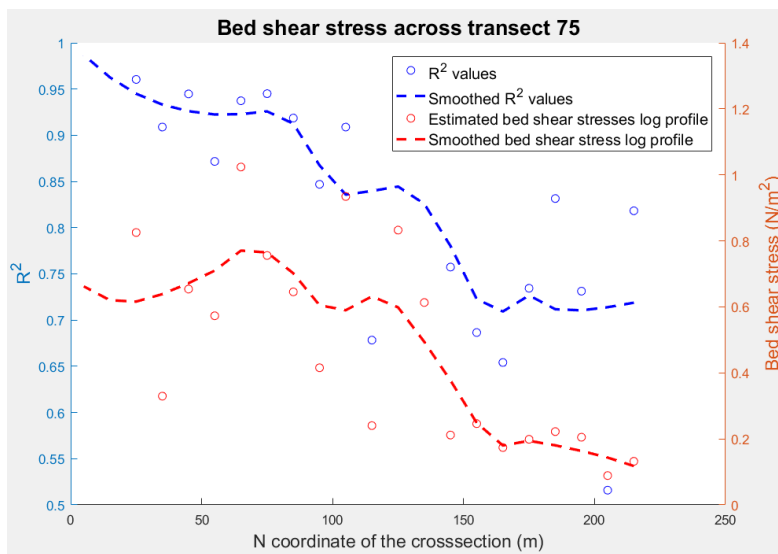


Figure 37 Distribution of the  $R^2$  values and the bed shear stress values for the fitting of the logarithmic profile

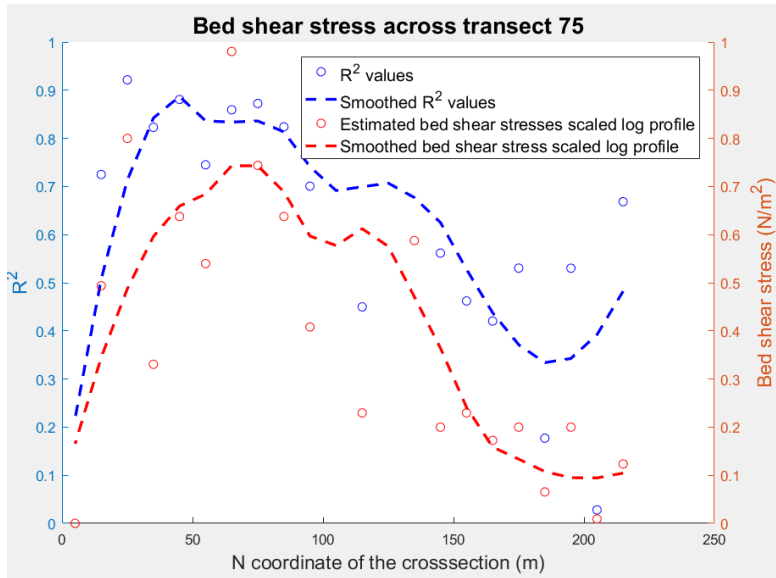


Figure 38 Distribution of the  $R^2$  values and the bed shear stress values for the fitting of the logarithmic profile  $w$

## 4. Discussion

This chapter will deal with the interpretation of the results that are obtained in this study. This includes a reflection on the assumptions that has been made and the uncertainties that lay in the used methods. Also results obtained that have been obtained for the Sava River and Danube River confluence and will be compared to other confluences that are studied in the literature.

### 4.1. Comparison of the methods

The first point that is assessed is whether the newly proposed method can give additional insights in the flow, despite the inaccuracies that are present within the data. This analysis indicates that the assessed inaccuracies, which include the inaccuracy of the device and the inaccuracy caused by the separate ADCP and GPS measurements, are lower with an estimated accuracy of 0.56 meter compared to the distance between the beams, which can go up to 10 meters in region near the bed of the channel. Therefore, also the assumption of homogeneous flow should be valid for this distance when using the new method, thus the conventional method could give better results in this study. However, the method still assumes homogeneity over all the values within a cell. Since a mesh cell width of 10 meters is used within this study, the new method requires homogeneity in the flow region near the bed. Moreover, the new method requires this homogeneity over ten meters throughout the whole transect. This implicates that the conventional method assumes horizontal homogeneity over a smaller distance compared to the conventional method for most of the area of the flow, where the distance between the ADCP beams is smaller than the 10 meters used as mesh cell width.

Since the methods work in a different way, from combining the 4 four beams of a single ADCP measurements for the conventional method to combining all measurement within a predefined mesh cell for the new method, differences can also be observed which are not related to the horizontal homogeneity of the flow.

One way to assess the differences between the methods has been the investigation of how the methods deal with noise in the data, caused by turbulence among others. This is done by assessing the standard deviation. The average standard deviation or different cell widths in the mesh has been calculated, for increasing numbers of repeated transects. This value of the standard deviation should become stable after a certain number of repeated transects if the flow is steady (Soulsby, 1980). The

results indicated that this value indeed approaches a stable value when more repeated transects were used, but the signal cannot be called unambiguous, especially for the new method. This can be caused by not having enough repeated transects to completely incorporate the turbulence in the flow, but this seems unlikely because the wider cells show the same pattern. For these larger cells it is expected that the turbulence is captured more easily because more measurements are available within these larger cells. Therefore, this unstable signal in the standard deviation is more likely caused by other sources of noise within the data, caused by for example by the fact that the measurements were taken using a moving boat, instead of a fixed position. And although the ADCP does compensate for this, there can be inaccuracies in the measurements in the roll, pitch and heading for example. The track of the ship is also not exactly the same for each repeated transect, which can also introduce noise. The last explanation is that the flow is unsteady. However, the measurements have been done within a relative short time period (the data of a single transect have been obtained in between 15 and 60 minutes) and no information is available that points towards special events that might have caused this.

There is also a difference between the methods when it comes to the absolute values of the standard deviation. The reason for this is that the variance of the new method is based on the radial velocities and the variance of the conventional methods is based on the estimated velocity vectors (Vermeulen *et al.*, 2014). Since there are four times more radial velocities than estimated vectors, the conventional method will show lower values of the standard deviation.

For the analysis that has been done between the two methods, no clear differences were found in the results of both methods. A reason for this might be the part of the confluence where the measurements are done. These measurements were taken downstream of the confluence, where the data shows that the mixing between the flows is almost completed. This is visible in both the figures of the secondary flow structure (see for example Appendix A) and Figure 1, where the mixing is roughly indicated by color of the flows. Therefore, downstream of the confluence no large deviations of the horizontal homogeneity of the flow are expected, hence this might explain why the two methods do not show significant differences. However, the resulting secondary flow structures (Appendix A) show that the flow is not completely homogeneous. Especially at the point where the helical cells meet each other the flow changes significantly in the horizontal direction (see Figure 24). Still, this inhomogeneity is still expected to be minor compared to inhomogeneity expected at the location of the bed discordancy. Even jet-like characteristics have been observed for confluences with bed discordancy (Sukhodolov *et al.*, 2017) Therefore it might be more interesting to do the same kind of measurements this part of the flow. These measurements are already underway and should give insight in whether the methods do give significant differences at the flow itself.

Another way to see the impact of the new method, is to use smaller width for the mesh cell sizes. However, taking smaller mesh cell sizes showed a lot of noise in the results. This might be induced by the uncertainty within the determination of the location of the ADCP measurements. The inaccuracy herein was estimated to be 56 centimeters (see section 3.1.), which becomes more significant when smaller mesh cell sizes are taken. Consequently, the general flow patterns were hardly visible anymore in the visualization of the secondary flow. This is illustrated in Figure 39, which depicts the transect and flow as in Figure 24, except the mesh cell width is now reduced to 5 meters compared to the 10 meters which is used throughout this report. From Figure 24 clearer patterns are visible compared to Figure 39. Therefore, the width of 10 meters is used for this study. The same observation can be made by comparing Figure 25 to Figure 40. Combining the smaller cell sizes with a more quantitative approach could provide a solution to get insight into the effects of the new method. This approach should quantify per mesh cell what the difference per cell is and in what part of the flow the largest

difference is apparent between the methods. However, since the results cannot be visualized anymore it might be difficult to convert such results into conclusion on flow structures or other physical processes. Therefore, the value of such an approach might be questionable.

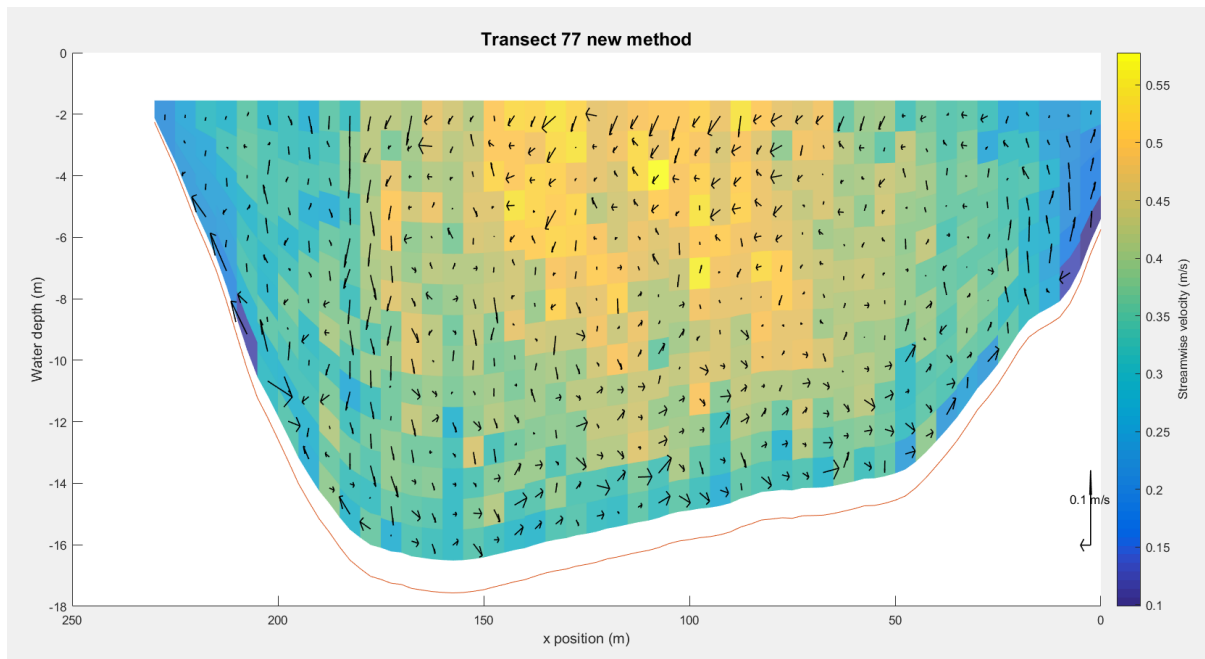


Figure 39 Secondary flow field of transect 77, which displays the same flow structure as Figure 24 but then calculated with a mesh cell width of 5 meters instead of 10 meters

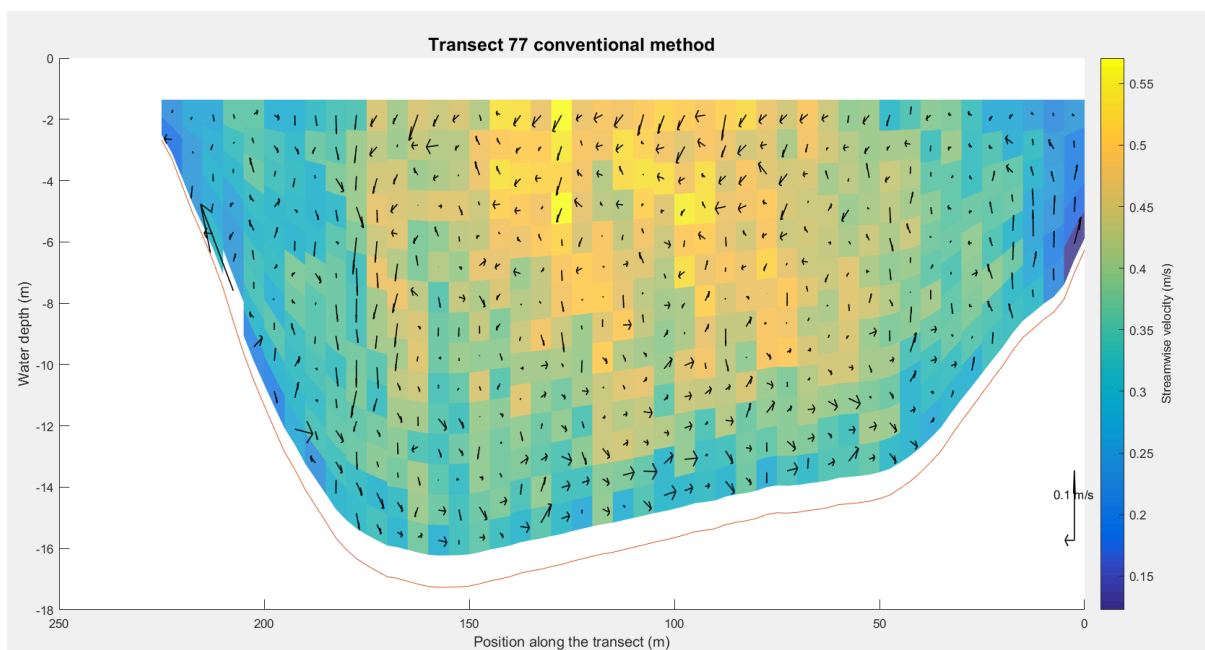


Figure 40 Secondary flow field of transect 77, which displays the same flow structure as Figure 25 but then calculated with a mesh cell width of 5 meters instead of 10 meters

#### 4.2. Comparison of the ADCP data and numerical model

Several large differences between the processed ADCP data and the numerical model were found within the study. Firstly, differences were observed in the vertical profiles of the streamwise velocities. The velocity magnitudes were available for one transect within the model, which makes it harder to

draw general conclusions from the differences. However, the results are in concordance with the other data that is available from the results of the model, i.e. the bed shear stress and the visualizations of the secondary flow. The vertical profiles of the streamwise velocity are comparable when averaged, but the ADCP data showed velocities which approached zero when moving to the bed earlier than the numerical model results, as visible in Figure 32. This implies a lower roughness in the model input, compared to what it should be to approach the velocity values in the ADCP data. This is something to research further with the numerical model, to see whether the ADCP data can be better mimicked by changing this input. Secondly, the model shows smaller cross-stream and vertical velocities. This is in accordance with other studies done with the SSIIM2, where vertical velocities were predicted up to 45 percent lower than measurements showed (Djordjevic, 2012). However, in this study the shape is captured well by the model, which cannot be said for the vertical velocities in Figure 34. That the secondary velocities are larger than expected by the model might be caused by the bed discordancy, which can enhance the secondary flow by increasing the lateral pressure gradients at the bed of the confluence (Bradbrook *et al.*, 2001). However, this should be included within the model, since it uses a three-dimensional approach.

Thirdly, the structures in the secondary flow from both the numerical model and the ADCP data are different in the sense that the large secondary cell occupies a larger portion of the transect, compared to what the results of the numerical model indicate. This can be seen by comparing Figure 27 and Figure 28, for the secondary flow structure as found by the ADCP data, and Figure 26, which indicates the same flow patterns, but then as output of the numerical model. This might be caused by the underestimation of the cross-stream currents in the numerical model, which are already addressed in this section.

#### 4.3. Bed shear stress estimations

Within this study, the data has been used to get an estimation of the bed shear stress. As described before, different methods have been applied to calculate the bed shear stress. However, these methods only give an estimate of the bed shear stress, since it is hard to calculate it accurately (Biron *et al.*, 2004). Especially the two methods that involve fitting, show that there is a lot of uncertainty within the estimations. This is illustrated in Figure 41, where an arbitrary example is shown of the fit of the logarithmic profile for streamwise velocities in a vertical. Especially near the banks of the channel the correlation coefficient  $R^2$  value, which has been chosen to estimate the goodness of fit of the method, shows lower values compared to the rest of channel. Apart from being indicative of the goodness of fit of the methods, the  $R^2$  value is also used to select the part of the flow which is used to make the fit between the logarithmic profile and the streamwise velocities in the vertical. This value is set to 0.5 in this study, but this value is chosen arbitrary. Changing this value showed that the bed shear stress values can increase significantly when required  $R^2$  values approach 1 (see Figure 42). However, for smaller for smaller values the difference in bed shear stress is not significant. From Figure 42 it is visible that a higher required  $R^2$  always causes a higher cross-sectional averaged bed shear stress. The reason for this is that requiring a higher  $R^2$  value means that values in the upper part of the flow are omitted. In this region the gradient in streamwise velocity has flattened out (see e.g. Figure 32). Therefore, the fit without with the values of these region will that of a steeper profile and therefore result in a higher bed shear stress. Another thing that is shown by Figure 42 is that using a threshold for  $R^2$  does not give significantly different value compared to using all the values in the vertical, which would be the same as requiring a  $R^2$  value of 0.

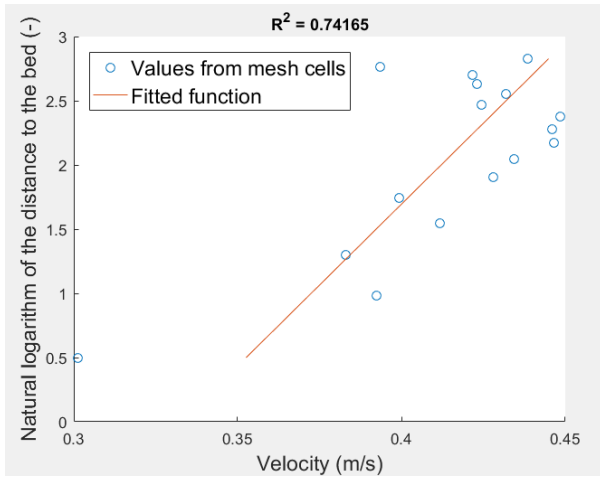


Figure 41 Fit of the logarithmic function for the velocities in a vertical in the center of transect 73

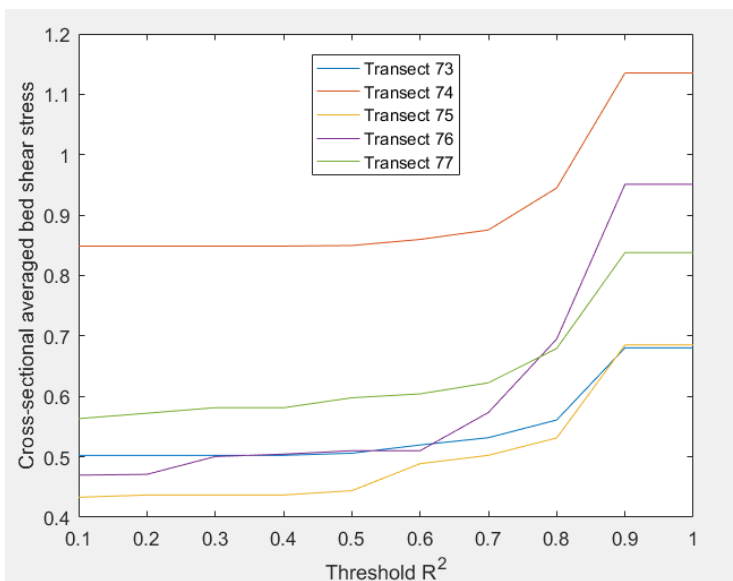


Figure 42 Sensitivity of the bed shear stress as estimated using the logarithmic fit as function of the threshold for  $R^2$

Another important assumption that is made within the bed shear stress estimations is the assumption of a wide channel. This seems contradictory to the statement the channel is relatively deep for a large-scale confluence. This assumption has been investigated by calculating the hydraulic radius and depth for all transects. This is based on the bed profiles that resulted from the ADCP measurements (see Appendix B). The results are given in Table 5. From this table it is visible that the assumption  $R \approx h$  is not valid for this channel, at least for the section that is measured by the ADCP. When the profile is extrapolated to the full width, the average depth of the channel reduces to around 11 and the hydraulic radius will only drop by a few decimeters. Thus, this will make the assumption better. The hydraulic radius in Eq. (10) and (11) will still be overestimated, however. This is an explanation why the reach average method gives higher values compared to the logarithmic fits. The extent of this could be investigated in further research.

Table 5 Hydraulic radius and average depths of the 5 transects based on the ADCP measurements.

Transect	Hydraulic radius (m)	Average depth (m)
73	8.23	14.95
74	8.23	14.76
75	8.07	14.01
76	7.97	14.41
77	8.08	13.79

The results of these estimations of the bed shear stress give a general picture of how the bed shear stress behaves over the width of the channel, by comparing the different methods. Also, the estimation is used to make a comparison with the numerical model, for which the bed shear stress is also available for the five transects.

A study of the Danube River upstream in Hungary has shown some comparable bed shear stresses (Baranya, et al. 2012). For sections with average streamwise velocities of around 1 m/s, shear velocities have been fitted around 0.06 m/s. These were also obtained by fitting a logarithmic profile, which is also done in this study. The ratio between the bed shear velocity and streamwise velocity is comparable to the Sava River-Danube River case where the streamwise velocities are around 0.37 m/s and estimated shear velocities, averaged over the width of the channel, between 0.02 and 0.03 m/s.

It must be kept in mind that the six percent of the flow that is positioned closest to bed does not give usable results from the ADCP. Therefore, all the bed shear stress estimations that used the ADCP data miss the information about the flow velocities of the bottom six percent of the water column. The flow near the bed is the most indicative for the bed shear stress, so the lack of near-bed velocity data reduces the accuracy of these methods.

#### 4.4. Flow structures

The back-to-back helical cells that are generally absent within the flow structure is an important result of this study. This flow pattern is only visible in transect 77 in a restricted part of the flow which can be seen in Figure 24 and is still notable in transect 76 plotted in appendix A. The helical cell near the outer bank of transect 77, that rotates in the opposite direction of the main helical cell in that transect, seems to be an example of back-to-back helical flow. Which implies that it is caused by the tributary channel. However, a secondary helical cell can also be caused by the curvature within the flow (Blanckaert *et al.*, 2001). In this study it is shown that also in river bends a second helical cell can arise, which is indicated in Figure 43. This outer-bank cell is caused by a combination of the centrifugal force and cross-stream turbulent stresses (Blanckaert *et al.*, 2005). This could be an alternative explanation for the flow structure in transect 77. However, given that it is only visible in the transects closest to the confluence, the cell seems more likely to be caused by the tributary channel.

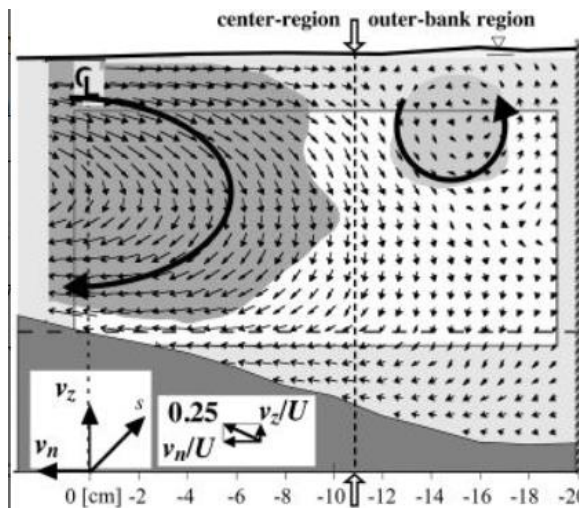


Figure 43 Example of an outer bank cell in a river bend (Blanckaert *et al.*, 2001)

An important result that was found within the data, is the absence of back-to-back helical flows in a large part of the confluence. In general, it is thought that the flow in a confluence should consist out of two counter rotating cells. For example, this is found in a study of the Kaskaskia River and Copper Slough. For these small flows, with discharges below  $2 \text{ m}^3/\text{s}$ , the two helical cells are visible. However, these results were obtained at a lower discharge ratio of approximately one (Rhoads *et al.*, 1995), compared to the discharge ratio of the Danube and Sava Rivers of 2.9. The back-to-back helical cells were mainly visible when the discharge ratio dropped below one, which could be a reason why they are not visible in this study.

The reason why these features are not visible in this case can be caused by multiple reasons. As said, it could be that the Sava and Danube Rivers confluence is incomparable with the studies in laboratories, because of the different parameters are used there. The discharge ratio in the Danube River-Sava River confluence is high compared to the beforementioned studies. However, this parameter is not unusually high and also the junction angle, which is mentioned as an important parameter in the confluence literature (Riley *et al.*, 2012), is, with a junction angle of 78 degrees, similar to other confluences and lab experiments, which often use a 90 degrees angle (Djordjevic *et al.*, 2006).

Another reason why the results may differ from the research on small confluences and laboratory researches might be the bed discordancy that is present within the confluence. This feature has also been identified as one of the key indicators of the flow structure within a confluence (Biron *et al.*, 1996). The shear layer between the two flows can be distorted towards the tributary channel by the bed discordancy. This is also visible within the data that is available for the Danube River-Sava River confluence. In a study on a small confluence with discordant bed, it has also been found that the helical flow can be absent in such a case (De Serres *et al.*, 1999). This was also found in a numerical study on discordant confluences where the bed discordancy is larger than half of the main river depth (Djordjevic, 2013a). Here it is found that that the discordancy can distort the shear layer. This can cause the helical flows not to form. Another indication that the bed morphology has an important impact on is a numerical study on the Danube River and Sava River confluence (Djordjevic *et al.*, 2006). This study modelled the Danube River and Sava River confluence without detailed knowledge of the bathymetry. The results showed clear back-to-back helical flows, in contrary to the numerical model results that are shown in this study.

A third possible reason why the back-to-back helical flow structures are not visible in the ADCP data, is the scale of the confluence that is assessed. Most of the research that is done on confluences, focuses on small scale confluences or laboratory experiments (Biron & Lane, 2008). For large scale confluences, usually defined as confluences with a width of more than 100 meters (Parsons *et al.*, 2008), there are other factors that impact the flow. Therefore, these larger confluences usually are not simply scaled versions of the smaller counterparts, which are studied more extensively (Parsons *et al.*, 2007). One of these is the absence of the helical flow within the confluence.

There are several potential causes for this. One is that for larger rivers the width increases more than the depth, and therefore the results obtained on smaller confluences might not be applicable on larger confluences (Parsons *et al.*, 2008). However, this statement is often made about confluences with width to depth ratios of over 100, whereas the width to depth ratio of the Danube River-Sava River confluence lies around 20. Other factors in larger confluences include the increasing role of form roughness, the lesser importance of secondary flows driven by gradients in water-surface elevation and spatial differences in the bed morphology (Parsons *et al.*, 2008).

One study of two large river confluences in the Amazon found that the secondary circulation caused by the confluence only were visible in a small portion of the channel width (Szupiany *et al.*, 2009). These sections expanded up to 20 percent of the channel width, where the two counter rotating cells were visible. Here the vertical velocities ranged between 0.02 m/s and -0.02 m/s. However, also this confluence has characteristics, that differ from the characteristics of the Danube River and Sava River confluence, especially the lower discharge ratio around 1.

#### 4.5. Data set

The unique part about the data set is that it is about a large river confluence, which has a case of large bed discordancy and an unusually small river width to depth ratio for a confluence of this scale. Large confluences typically have width to depth ratios of over 100 (Parsons *et al.*, 2008), whereas the assessed confluence of the Sava and Danube Rivers has a width to depth ratio of around 15 to 20.

The first reason why this is important, is that this data set allows the identification of unmarked territory in confluence research. The second point why this is such an important data set, is closely related to the first, and has to do with the hypotheses that are made about the scaling effects of large confluences. One of the ideas why large confluences are thought to have different flow characteristics compared to smaller confluences, is because of the larger width to depth ratios. This is thought to hinder the development of back-to-back helical flows, due to the form roughness that dominates the flow (Parsons *et al.*, 2008). This study however shows that for this confluence with a low width to depth ratio the helical flows are not developed as well. This shows that the width to depth ratio might not be the most important factor in why differences exist between large and small confluences.

However, there are different reasons why the back-to-back helical cells did not develop in this confluence. These are mentioned in the previous section. It is likely that the presence of the large bed discordancy and the different characteristics, like the discharge ratio, of this confluence are the driving factor in the absence of the helical flow, instead of the width to depth ratio.

Despite this data set showing a lot of potential to study a confluence with characteristic that have not been observed in other studies, there are some points which require attention when assessing the results of the data. The available data is all collected at the same day, which has some advantages and disadvantages. An advantage of the almost simultaneous measurements is that all the data can be compared to each other. The different cross-sections can be compared to each other, because the conditions are expected to remain similar. A disadvantage is that it is more difficult to link observed

flow patterns to the morphology of the confluence. Since the morphology might be caused by different flow conditions than those observed within the data, one can be tempted into making false claims about connections between flow patterns and the morphology that do not exist. In this case the flow conditions were a low discharge compared to the average. These flow under these conditions might have a low impact on the morphology of the confluence, due the lower flow velocities, compared to conditions with high discharges and flow velocities. On the other hand, parameters like discharge and momentum ratio might be more important parameters, compared to the absolute discharges, giving a better indication of the confluence characteristics (Riley *et al.*, 2012).

#### 4.6. Bed load transport

The structural differences between the position as determined by the ADCP data and by the bottom tracking (see Figure 12 and Figure 13) can be related to a bed load transport. As said before, bottom tracking assumes that the bed is fixed. If it is assumed that there are no further errors in the methods, then the difference between the two methods of determining the position is mostly likely be caused by a moving bed. This idea is further confirmed by the difference being almost constant for all the measurements.

By assuming that indeed the observed difference is caused by the moving bed, this can be used to estimate the velocity of the bed. First the difference in the x and y-direction need to be combined. Knowing this difference in meters between the two methods of determining the location and the time that elapses between the measurements, a velocity of the bed can be estimated. Research has been done into converting this velocity to a bed load transport. From this research the following equation has been developed (Rennie *et al.*, 2002):

$$g_b = \frac{4}{3} \rho_s r v_p \quad (9)$$

Where  $g_b$  is the bedload transport rate per unit width,  $\rho_s$  is the density of the sediments in the river,  $r$  the radius of the particles and  $v_p$  is the bed load velocity. This approach assumes uniform sized, spherical sediment particles. This method is thought to work for bed velocities up to 0.6 m/s (Jamieson *et al.*, 2011). However, since there are no measurements of the particle sizes in the channel and the application of Eq. (7) gave unrealistic values (see section 3.5.) this method is not applicable in this case. This is something which could be further investigated by taking samples of the bed material in the confluence. Information about the bed load transport could give an indication on how the morphology of the river evolves.

## 5. Conclusions

In this thesis the confluence of the Danube River and Sava Rivers has been studied with the help of ADCP measurements and the results of a numerical simulation. Two methods have been used that process the obtained data in more manageable meshes. One conventional method, which uses the four beams of an ADCP at a point in time to combine them to a velocity vector. The other method is a newly proposed method, which combines measurement based on location rather than time. The numerical model results have been compared to the flow structures of the ADCP data as well.

This research follows up on a PhD thesis (Djordjevic, 2010), which studied this confluence which has characteristics that have, to the extent of the knowledge of the author, not been studied before. Having a bed discordancy, a relatively large depth and being of a large scale are an uncommon set of characteristics within confluences. Especially the latter two are a combination which are not observed regularly. For this study, four research questions have been formulated which will be answered here.

1. *To what extent do the conventional method and new method of processing the ADCP data differ in results for the available data set?*

From the data set that is used within this study, the inaccuracies have been determined. The accuracy of the data was found to be larger than the distance between the beams of the ADCP, for a large part of the flow. Hence, it can be concluded that the newly proposed method of processing ADCP data could give improved results for this study. However, when the width of the mesh cells is considered, the methods require horizontal homogeneity to a similar extent in the region of the flow near the bed. The conventional method even depends less on the assumption of horizontal homogeneity in most of the flow. The results of the comparison of the two methods are in line with this statement. The results indicate that both methods need the same amount of data to capture the turbulence. Both in the flow structure of the secondary circulation and in the magnitude of the velocities in the stream wise, cross-stream and vertical direction, no significant differences have been found between the two methods as well.

2. *What does the flow structure of the confluence look like according to the ADCP data?*

The first observation that can be made from the data is that there is no clear sign of flow acceleration present within the flow. The secondary flow structure that is visible from both methods, is a single helical flow over the full width of the channel for the largest part of the measured section. Only in the section that is the closest to the confluence, there is a small cell visible, near the outer bank, which rotates in the opposite direction of the large cell. The large cell suggests that the secondary flow in the confluence is caused by the curvature rather than by the confluence.

3. *How does the numerical model compare to the data obtained for the confluence, with respect to the secondary flow structure and bed shear stress?*

The structure of the secondary flow derived from ADCP data is different from the structures that are produced by numerical model, in which the confluence has been modelled by the application of the Reynolds averaged Navier-Stokes equations and a  $\kappa - \epsilon$  turbulence model. Compared the results from the ADCP data, the main helical cell occupies a smaller part of the channel. The numerical model shows similar results to the data that has been obtained for the stream wise and cross-stream direction. However, there are differences within vertical gradients of the streamwise velocity. Here the streamwise velocities seem to approach a velocity of zero faster near the bed for ADCP data, compared to the numerical model results. This indicates that the roughness height in the model is underestimated. This is further confirmed by the underestimation of the bed shear in the model,

compared to the estimations based on the available ADCP data. However, this should be further confirmed by near bed velocity measurements, which the ADCP is not able to collect.

4. *How does the flow structure of the Sava River-Danube River confluence compare to other confluences?*

Confluences have been subject of many scientific studies. However, a study on a similar case of a large confluence with large bed discordancy and relatively large depth has not been found. Within the studies that have been done on confluences, back-to-back helical cells are observed within smaller confluences and laboratory studies. However, the literature also suggests that these cells can be absent in case of discordant beds and in larger confluence in general. For the latter this is mostly thought to be caused by the larger width to depth ratio of large rivers. Due to relative deep channel in this case, the absence of back-to-back helical cells is thought not to be linked to the large scale of the confluence. In this case, the discordancy is thought to be the driving factor behind this absence of the back-to-back helical flows.

### 5.1. Recommendations

This study pointed out that in the region of the flow that is measured by the ADCP no significant difference has been found between the two methods. Also, the back-to-back helical cells have been found to a very limited extent. It could be that the data that is measured is just not accurate enough to display these features. However, it could also be that these features are only present within the region close to the confluence itself. New measurements have recently been done in this part of the confluence, where the hypothesis is that the new method should give a better view of the flow, due to the large horizontal inhomogeneities that are expected to be present near the bed step. So, the new method could be applied to the new data to investigate the flow near the confluence. This also will show whether the back-to-back helical cells are indeed absent within the confluence, or whether they are present at the confluence itself.

The morpho dynamics of the confluence could be studied as well. For example, the new ADCP measurements that have been done on the confluence could provide some insight in the morphology of the system. Since there is a gap of about 11 years between the measurement, it would be interesting to see how the system has changed over that period. It would be good to know whether the bed step increases and how the depth of the side channel of the Danube River evolves. This could help in the choices that have to be made about the developing the area around the confluence.

## References

- Ashmore, P. E. (1982) 'Laboratory modelling of gravel braided stream morphology', *Earth Surface Processes and Landforms*, 7(3), pp. 201–225. doi: 10.1002/esp.3290070301.
- Babaeyan-Koopaei, K., Ervine, D., Carling, P. and Cao, Z. (2002) 'Velocity and turbulence measurements for two overbank flow events in River Severn', *Journal of Hydraulic Engineering-Asce*, 128(10), pp. 891–900. doi: 10.1061/(asce)0733-9429(2002)128:10(891).
- Best, J. L. (1987) 'Flow Dynamics At River Channel Confluences: Implications for Sediment Transport and Bed Morphology', in *Recent Developments in Fluvial Sedimentology*. SEPM (Society for Sedimentary Geology), pp. 27–35. doi: 10.2110/pec.87.39.0027.
- Biron, P., Best, J. L. and Roy, A. G. (1996) 'Effects of Bed Discordance on Flow Dynamics at Open Channel Confluences', *Journal of Hydraulic Engineering*, 122(12), pp. 676–682. doi: 10.1061/(ASCE)0733-9429(1996)122:12(676).
- Biron, P. M. and Lane, S. N. (2008) 'Modelling Hydraulics and Sediment Transport at River Confluences', in *River Confluences, Tributaries and the Fluvial Network*. Chichester, UK: John Wiley & Sons, Ltd, pp. 17–43. doi: 10.1002/9780470760383.ch3.
- Biron, P. M., Robson, C., Lapointe, M. F. and Gaskin, S. J. (2004) 'Comparing different methods of bed shear stress estimates in simple and complex flow fields', *Earth Surface Processes and Landforms*. Wiley-Blackwell, 29(11), pp. 1403–1415. doi: 10.1002/esp.1111.
- Blanckaert, K. and Graf, W. H. (2001) *Mean Flow and Turbulence in Open-Channel Bend*, *Journal of Hydraulic Engineering*. doi: 10.1061/(ASCE)0733-9429(2001)127:10(835).
- Blanckaert, K. and de Vriend, H. J. (2005) 'Turbulence structure in sharp open-channel bends', *Journal of Fluid Mechanics*. Cambridge University Press, 536, pp. 27–48. doi: 10.1017/S0022112005004787.
- Bradbrook, K. F., Lane, S. N. and Richards, K. S. (2000) 'Numerical simulation of three-dimensional, time-averaged flow structure at river channel confluences', *Water Resources Research*, 36(9), pp. 2731–2746. doi: 10.1029/2000WR900011.
- Bradbrook, K. F., Lane, S. N., Richards, K. S., Biron, P. M. and Roy, A. G. (2001) 'Role of Bed Discordance at Asymmetrical River Confluences', *Journal of Hydraulic Engineering*, 127(5), pp. 351–368. doi: 10.1061/(ASCE)0733-9429(2001)127:5(351).
- Chow, V. Te (1959) *Open-channel hydraulics*, McGraw-Hill Book Company. New York: McGraw-Hill. doi: ISBN 07-010776-9.
- Constantinescu, G., Miyawaki, S., Rhoads, B., Sukhodolov, A. and Kirkil, G. (2011) 'Structure of turbulent flow at a river confluence with momentum and velocity ratios close to 1: Insight provided by an eddy-resolving numerical simulation', *Water Resources Research*, 47(5). doi: 10.1029/2010WR010018.
- Dietrich, W. E. and Whiting, P. (1989) 'Boundary shear stress and sediment transport in river meanders of sand and gravel', in American Geophysical Union (AGU), pp. 1–50. doi: 10.1029/WM012p0001.
- Dinehart, R. L. and Burau, J. R. (2005) 'Averaged indicators of secondary flow in repeated acoustic Doppler current profiler crossings of bends', *Water Resources Research*. Wiley-Blackwell, 41(9), pp. 1–18. doi: 10.1029/2005WR004050.
- Djordjevic, D. (2010) *Numerical investigation of the river confluence hydrodynamics*. Belgrade: PhD dissertation, University of Belgrade, Faculty of Civil Engineering.

Djordjevic, D. (2012) 'Application of 3D Numerical Models in Confluence Hydrodynamics Modelling', in *XIX International Conference on Water Resources*. Available at: [http://cmwr2012.cee.illinois.edu/Papers/Special Sessions/High-Dimensional Computational Modeling of Rivers and Streams/Dordevic.Dejana.pdf](http://cmwr2012.cee.illinois.edu/Papers/Special%20Sessions/High-Dimensional%20Computational%20Modeling%20of%20Rivers%20and%20Streams/Dordevic.Dejana.pdf).

Djordjevic, D. (2013a) *Controls of three-dimensional flow at river confluences*. Belgrade: Zadužbina Andrejević.

Djordjevic, D. (2013b) 'Numerical study of 3D flow at right-angled confluences with and without upstream planform curvature', *Journal of Hydroinformatics*, 15(4), pp. 1073–1088. doi: 10.2166/hydro.2012.150.

Djordjevic, D. and Jovanovic, M. (2006) 'On the effect of the bed morphology on the river confluence hydrodynamics', in *River Flow 2006, Vols 1 and 2*, pp. 1165–1174.

Doppler, J. (1842) *Über das farbige Licht der Dopplersterne und einiger anderer Gestirne des Himmels, Abhandlungen der Königlichen Böhmischen Gesellschaft der Wissenschaften*1. doi: 10.1007/s13398-014-0173-7.2.

Jamieson, E. C., Rennie, C. D., Jacobson, R. B. and Townsend, R. D. (2011) 'Evaluation of ADCP Apparent Bed Load Velocity in a Large Sand-Bed River: Moving versus Stationary Boat Conditions', *Journal of Hydraulic Engineering*, 137(9), pp. 1064–1071. doi: 10.1061/(ASCE)HY.1943-7900.0000373.

von Karman, T. (1931) 'Mechanical Similitude and Turbulence'. Available at: <https://ntrs.nasa.gov/search.jsp?R=19930094805> (Accessed: 30 July 2018).

Manning, R. (1891) 'On the flow of open channels and pipes', *Transactions of the Institution of Civil Engineers of Ireland*, 20, pp. 161–207.

Marriott, M. J. and Jayaratne, R. (2010) *Hydraulic roughness – links between Manning's coefficient, Nikuradse's equivalent sand roughness and bed grain size*, *Advances in Computing and Technology*.

Muste, M., Kim, D. and González-Castro, J. a. (2010) 'Near-Transducer Errors in ADCP Measurements: Experimental Findings', *Journal of Hydraulic Engineering*, 136(5), pp. 275–289. doi: 10.1061/(ASCE)HY.1943-7900.0000173.

Muste, M., Yu, K. and Spasojevic, M. (2004) 'Practical aspects of ADCP data use for quantification of mean river flow characteristics; Part I: Moving-vessel measurements', *Flow Measurement and Instrumentation*. Elsevier, 15(1), pp. 1–16. doi: 10.1016/j.flowmeasinst.2003.09.001.

Nikolaos, T. and Kiyoshi, T. (2010) 'QR-code calibration for mobile augmented reality applications', in *ACM SIGGRAPH 2010 Posters on - SIGGRAPH '10*. New York, New York, USA: ACM Press, p. 1. doi: 10.1145/1836845.1836999.

Nikora, V. I. and Smart, G. M. (1997) 'Turbulence characteristics of New Zealand gravel-bed rivers', *Journal of Hydraulic Engineering*, 123(9), pp. 764–773. doi: 10.1061/(ASCE)0733-9429(1997)123:9(764).

Parsons, D. R., Best, J. L., Lane, S. N., Kostaschuk, R. A., Hardy, R. J., Orfeo, O., Amsler, M. L. and Szupiany, R. N. (2008) 'Large River Channel Confluences', in *River Confluences, Tributaries and the Fluvial Network*. Chichester, UK: John Wiley & Sons, Ltd, pp. 73–91. doi: 10.1002/9780470760383.ch5.

Parsons, D. R., Best, J. L., Lane, S. N., Orfeo, O., Hardy, R. J. and Kostaschuk, R. (2007) 'Form roughness and the absence of secondary flow in a large confluence-diffuence, Rio Paraná, Argentina', *Earth Surface Processes and Landforms*. Wiley-Blackwell, 32(1), pp. 155–162. doi:

10.1002/esp.1457.

Parsons, D. R., Jackson, P. R., Czuba, J. A., Engel, F. L., Rhoads, B. L., Oberg, K. A., Best, J. L., Mueller, D. S., Johnson, K. K. and Riley, J. D. (2013) 'Velocity Mapping Toolbox (VMT): A processing and visualization suite for moving-vessel ADCP measurements', *Earth Surface Processes and Landforms*, 38(11), pp. 1244–1260. doi: 10.1002/esp.3367.

Rennie, C. D. (2008) *Uncertainty of ADCP spatial velocity distributions, 6th International Symposium on Ultrasonic Doppler Methods for Fluid Mechanics and Fluid Engineering*. Available at: [http://www.isud-conference.org/proc/split/ISUD-06\\_147\\_Rennie.pdf](http://www.isud-conference.org/proc/split/ISUD-06_147_Rennie.pdf) (Accessed: 12 October 2018).

Rennie, C. D., Millar, R. G. and Church, M. A. (2002) 'Measurement of Bed Load Velocity using an Acoustic Doppler Current Profiler', *Journal of Hydraulic Engineering*, 128(5), pp. 473–483. doi: 10.1061/(ASCE)0733-9429(2002)128:5(473).

Rhoads, B. L. and Kenworthy, S. T. (1995) 'Flow structure at an asymmetrical stream confluence', *Geomorphology*. Elsevier, 11(4), pp. 273–293. doi: 10.1016/0169-555X(94)00069-4.

Rhoads, B. L., Riley, J. D. and Mayer, D. R. (2009) 'Response of bed morphology and bed material texture to hydrological conditions at an asymmetrical stream confluence', *Geomorphology*. Elsevier, 109(3–4), pp. 161–173. doi: 10.1016/j.geomorph.2009.02.029.

Rhoads, B. L. and Sukhodolov, A. N. (2001) 'Field investigation of three-dimensional flow structure at stream confluences: 1. Thermal mixing and time-averaged velocities', *Water Resources Research*, 37(9), pp. 2393–2410. doi: 10.1029/2001WR000316.

Ribberink, J. S., de Vriend, H. J., Hulscher, S. J. M. H., Souren, A. W. M. G. and Vermeulen, B. (2016) *River dynamics –Shallow water flows*. Enschede.

Riley, J. D. and Rhoads, B. L. (2012) 'Flow structure and channel morphology at a natural confluent meander bend', *Geomorphology*. Elsevier, 163–164, pp. 84–98. doi: 10.1016/j.geomorph.2011.06.011.

Sassi, M. G., Hoitink, A. J. F., Vermeulen, B. and Hidayat (2011) 'Discharge estimation from H-ADCP measurements in a tidal river subject to sidewall effects and a mobile bed', *Water Resources Research*. Wiley-Blackwell, 47(6). doi: 10.1029/2010WR009972.

De Serres, B., Roy, A. G., Biron, P. M. and Best, J. L. (1999) 'Three-dimensional structure of flow at a confluence of river channels with discordant beds', *Geomorphology*. Elsevier, 26(4), pp. 313–335. doi: 10.1016/S0169-555X(98)00064-6.

Soulsby, R. L. (1980) 'Selecting Record Length and Digitization Rate for Near-Bed Turbulence Measurements', *Journal of Physical Oceanography*, 10(2), pp. 208–219. doi: 10.1175/1520-0485(1980)010<0208:SRLADR>2.0.CO;2.

Sukhodolov, A. N., Krick, J., Sukhodolova, T. A., Cheng, Z., Rhoads, B. L. and Constantinescu, G. S. (2017) 'Turbulent flow structure at a discordant river confluence: Asymmetric jet dynamics with implications for channel morphology', *Journal of Geophysical Research: Earth Surface*. Wiley-Blackwell, 122(6), pp. 1278–1293. doi: 10.1002/2016JF004126.

Szupiany, R. N., Amsler, M. L., Parsons, D. R. and Best, J. L. (2009) 'Morphology, flow structure, and suspended bed sediment transport at two large braid-bar confluences', *Water Resources Research*, 45(5). doi: 10.1029/2008WR007428.

Teledyne RD Instruments, I. (2007) *WorkHorse Rio Grande*. Available at: [www.rdinstruments.com](http://www.rdinstruments.com) (Accessed: 16 October 2018).

Teledyne RD Instruments, I. (2011) *Acoustic Doppler Current Profiler Principles of Operation A*

*Practical Primer*. Available at: <http://www.rdinstruments.com> (Accessed: 30 July 2018).

Vermeulen, B., Hoitink, A. J. F., Kastner, K., Niesten, I. and Verbeek, M. (2015) 'Including generic models in repeat-transect ADCP data processing', *IAHR2015 World Congress*, p. 21.

Vermeulen, B., Sassi, M. G. and Hoitink, A. J. F. (2014) 'Improved flow velocity estimates from moving-boat ADCP measurements', *Water Resources Research*. Wiley-Blackwell, 50(5), pp. 4186–4196. doi: 10.1002/2013WR015152.

Williams, J. J. (1995) 'Drag and Sediment Dispersion Over Sand Waves', *Estuarine, Coastal and Shelf Science*. Academic Press, 41(6), pp. 659–687. doi: 10.1006/ecss.1995.0083.

## Appendix A Secondary velocity structures in the five transects

### A.1. Secondary flow structures obtained by the conventional method

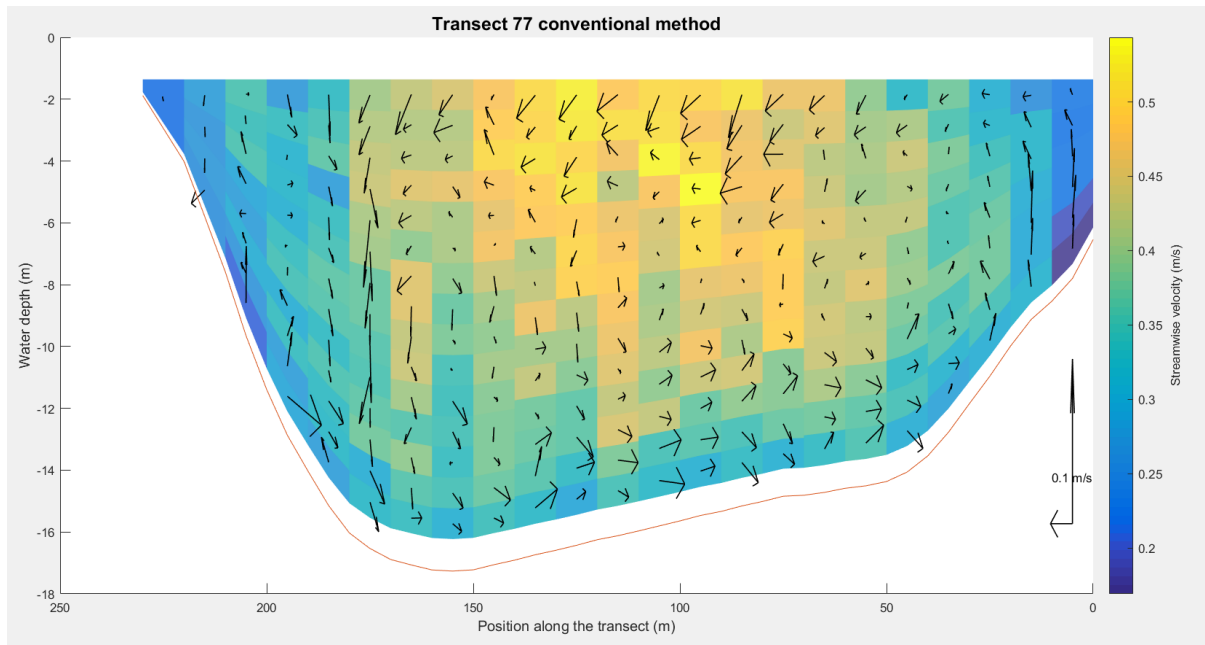


Figure 44 Secondary flow structure of transect 77 obtained by the conventional method

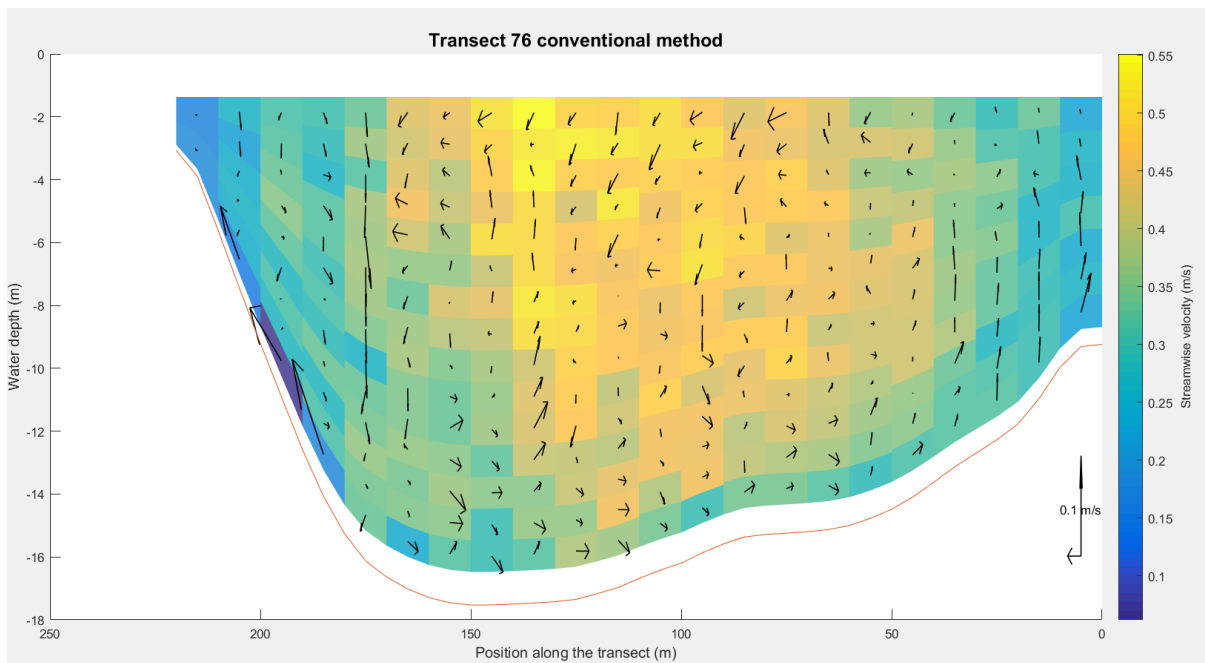


Figure 45 Secondary flow structure of transect 76 obtained by the conventional method

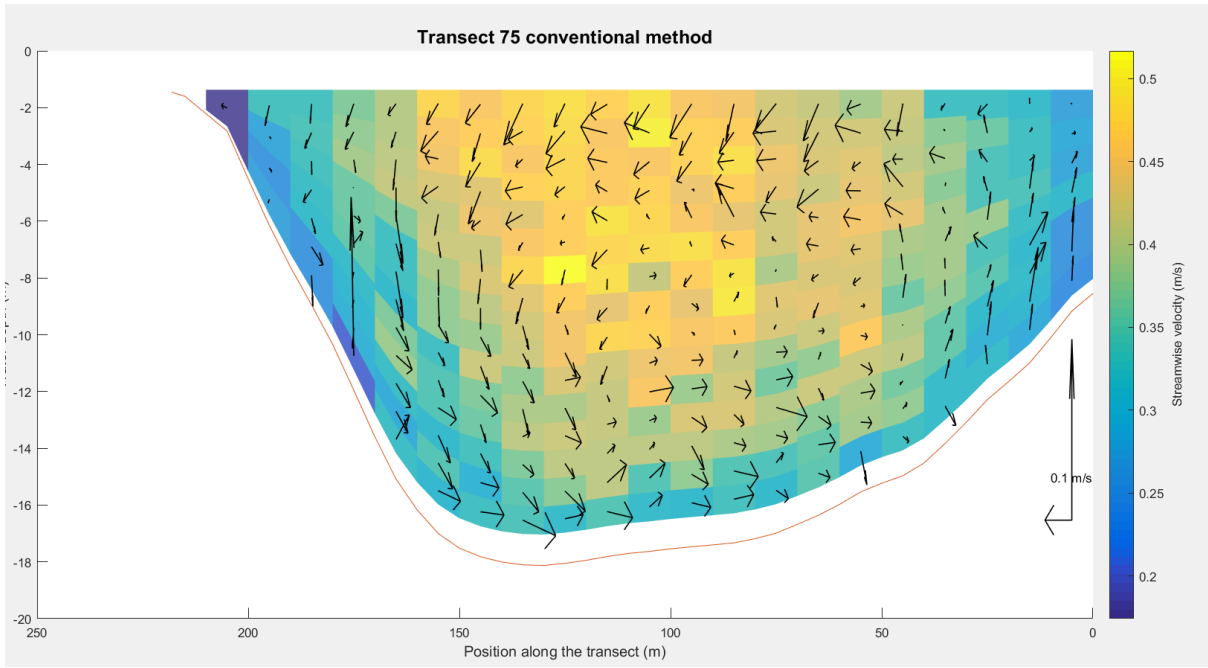


Figure 46 Secondary flow structure of transect 75 obtained by the conventional method

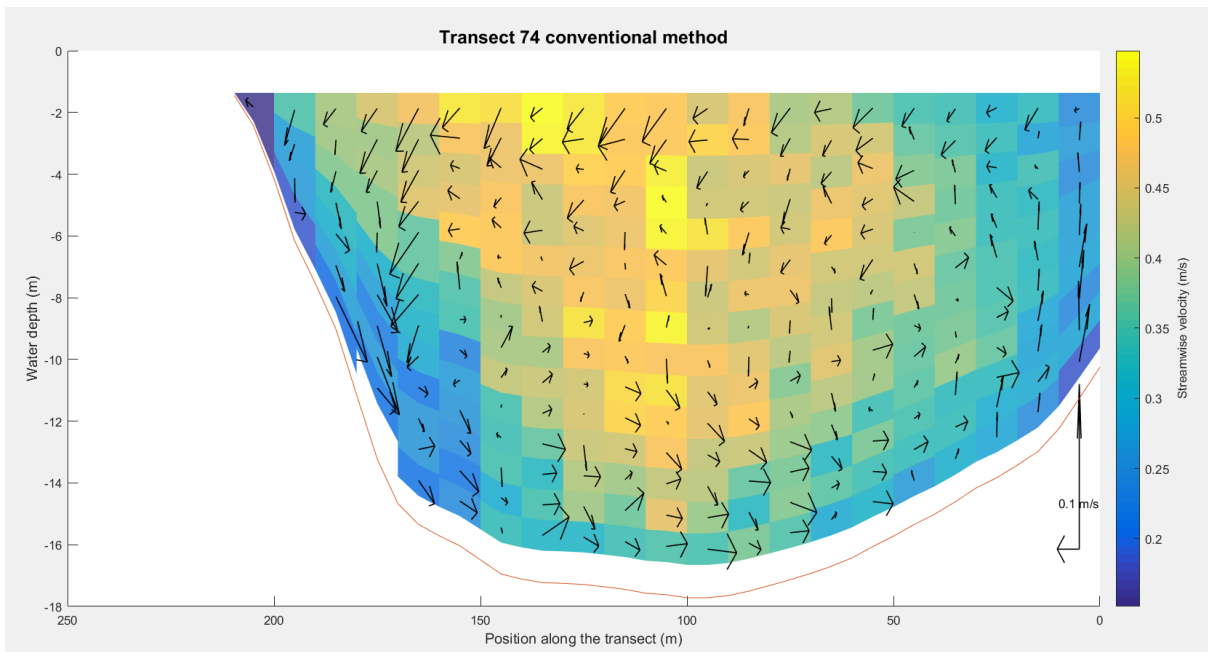


Figure 47 Secondary flow structure of transect 74 obtained by the conventional method

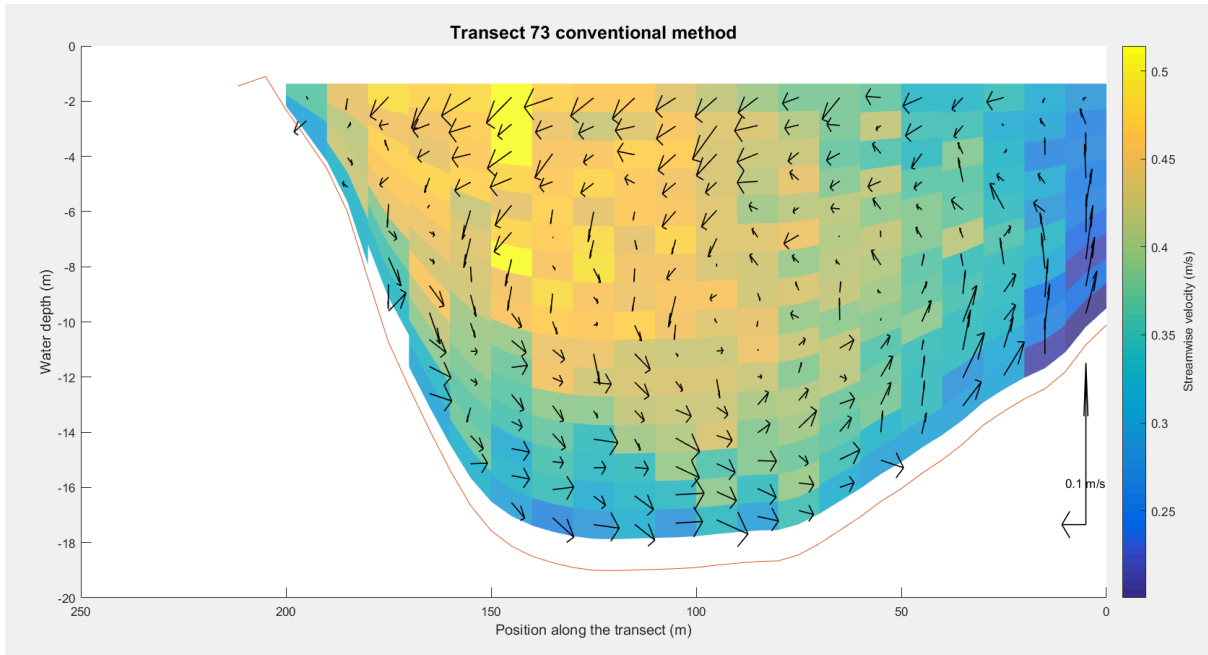


Figure 48 Secondary flow structure of transect 73 obtained by the conventional method

## A.2. Secondary flow structures obtained by the new method

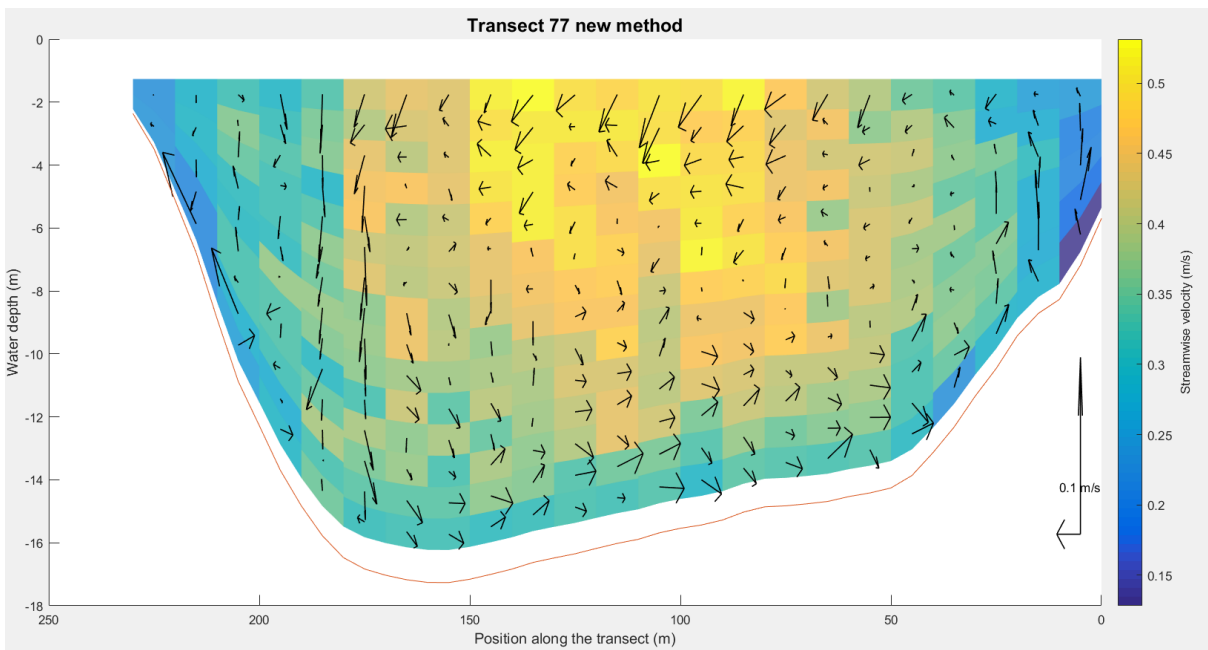


Figure 49 Secondary flow structure of transect 77 obtained by the new method

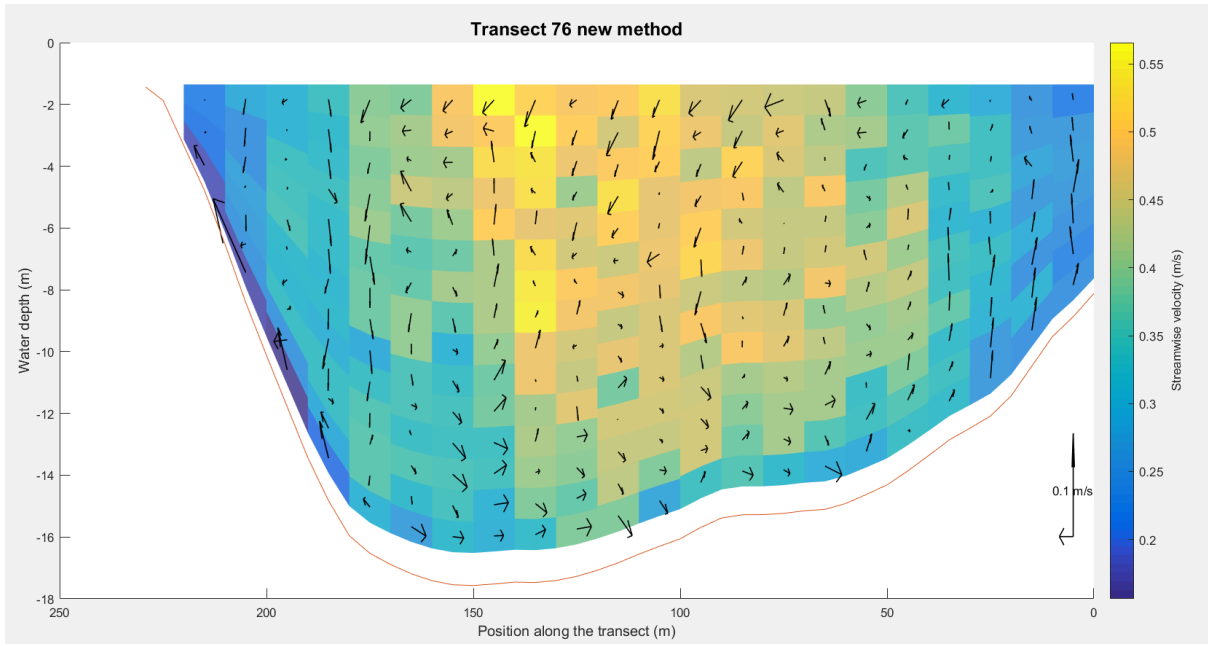


Figure 50 Secondary flow structure of transect 76 obtained by the new method

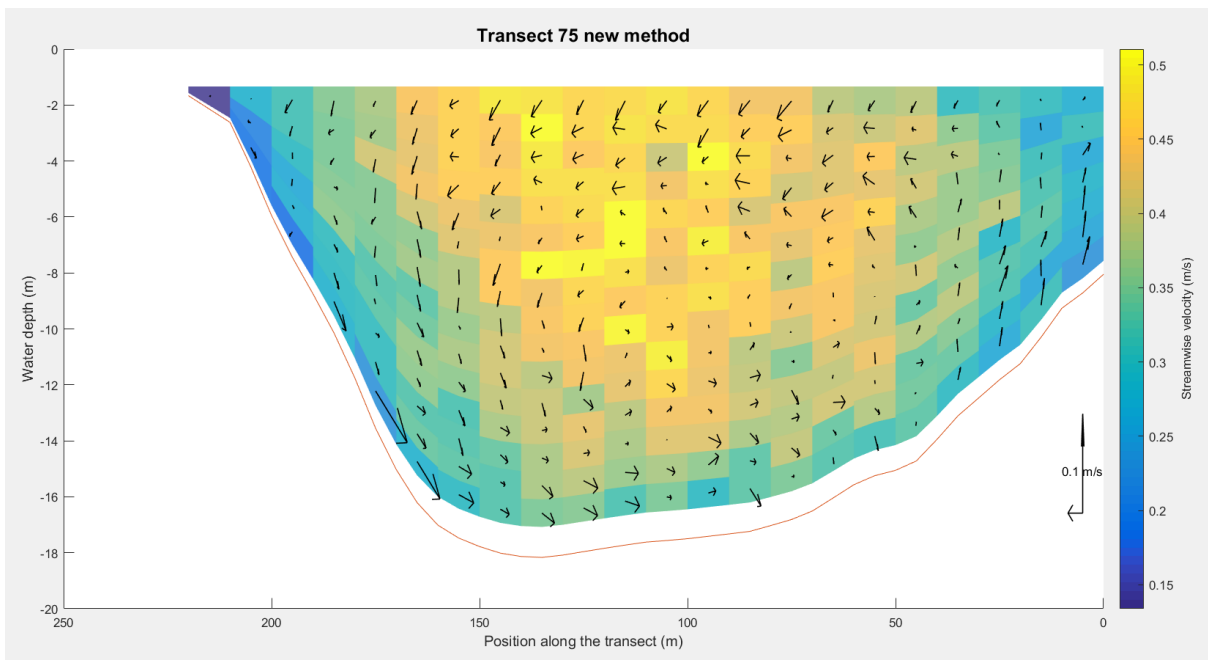


Figure 51 Secondary flow structure of transect 75 obtained by the new method

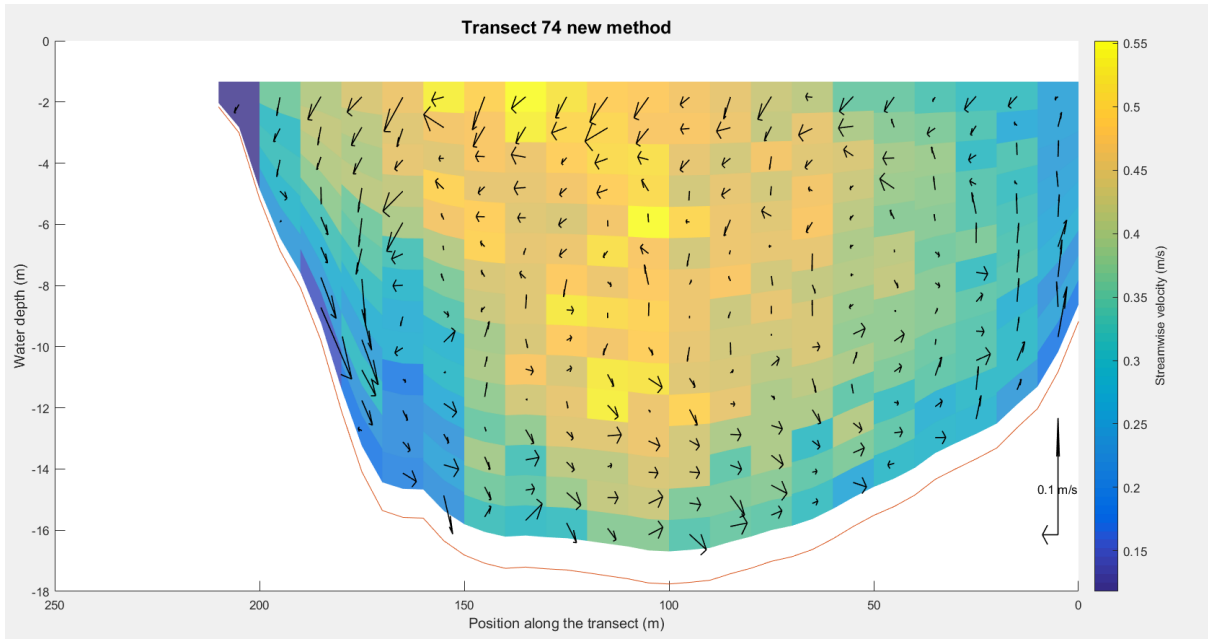


Figure 52 Secondary flow structure of transect 74 obtained by the new method

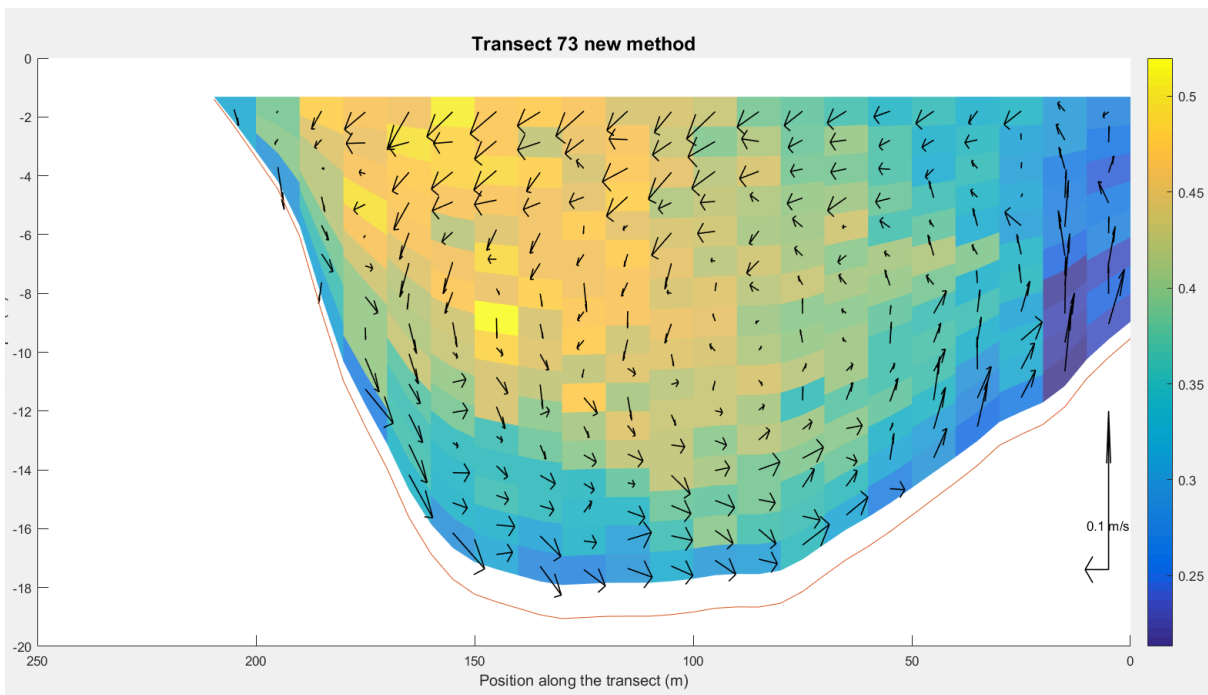


Figure 53 Secondary flow structure of transect 73 obtained by the new method

## Appendix B bed shear stress distributions

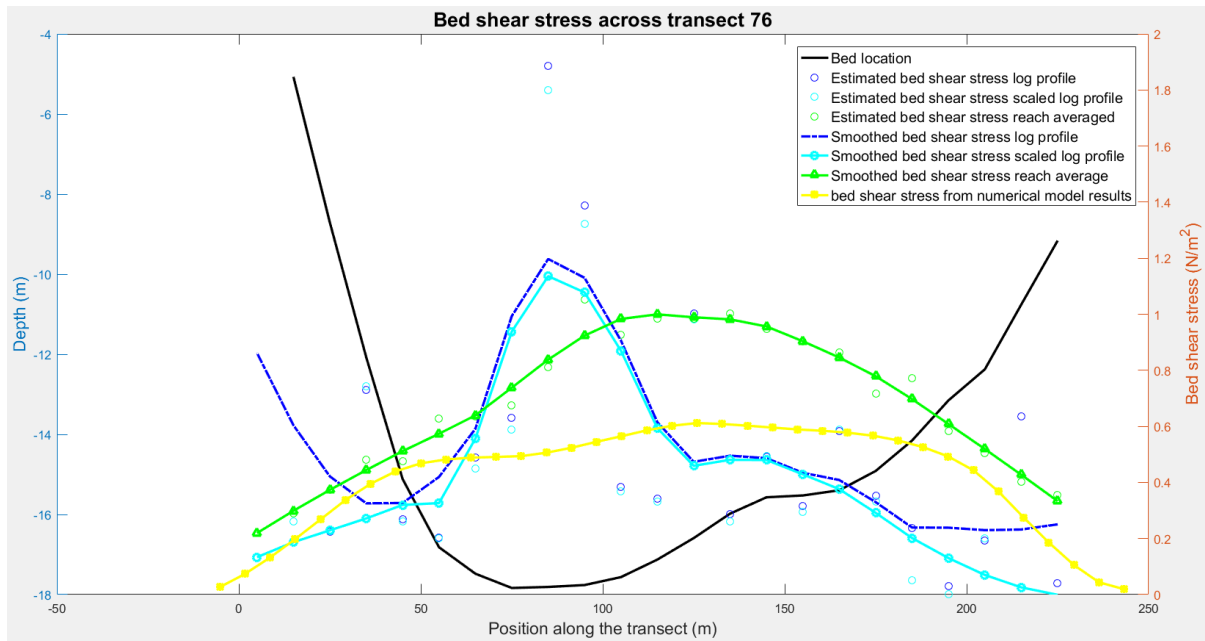


Figure 54 Bed shear stress estimations for transect 76

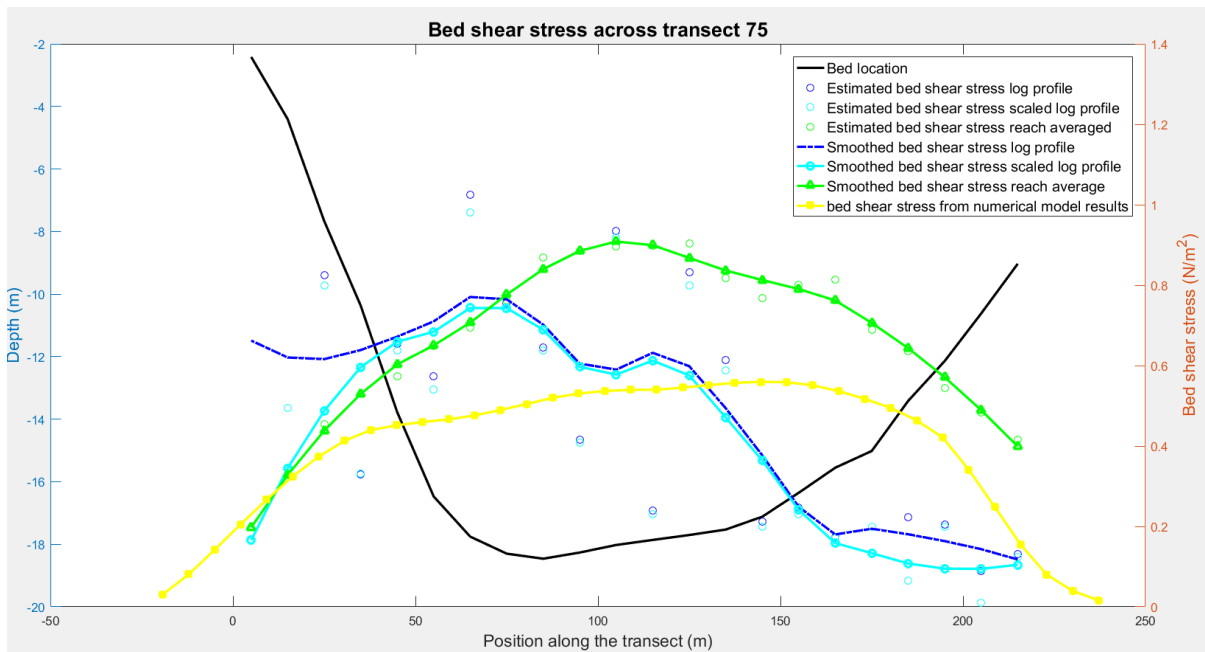


Figure 55 Bed shear stress estimations for transect 75

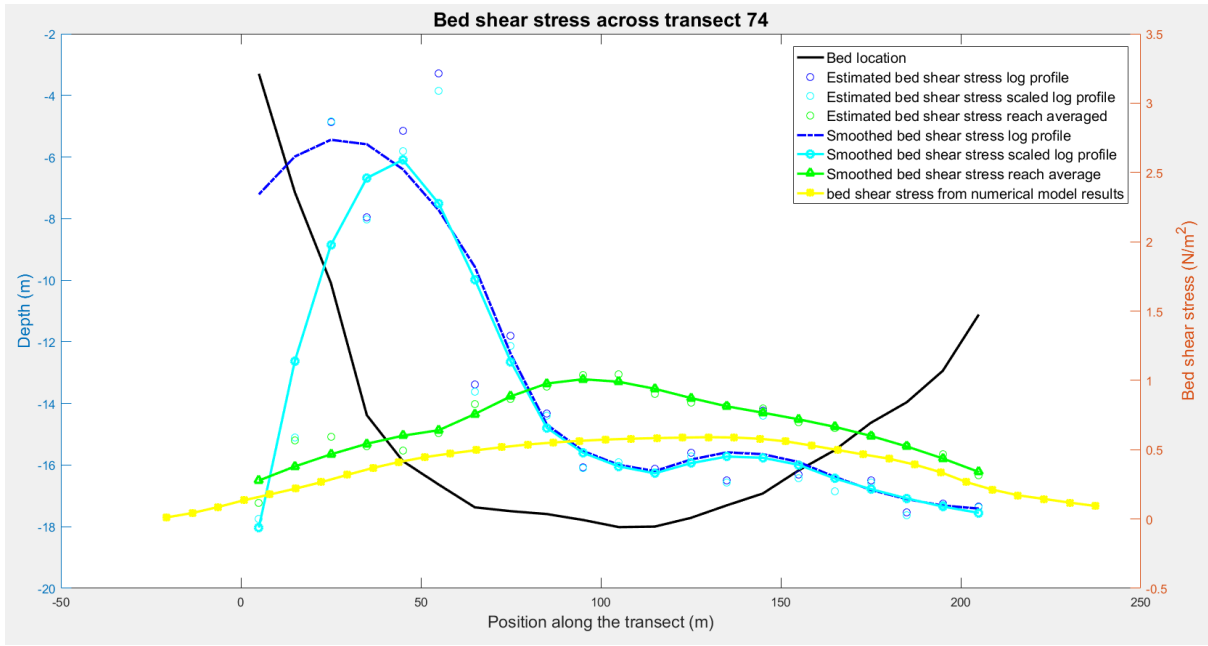


Figure 56 Bed shear stress estimations for transect 74

## Appendix C Distribution of the $R^2$ values

### C.1. Distributions of the $R^2$ values based on the fits of the logarithmic profile

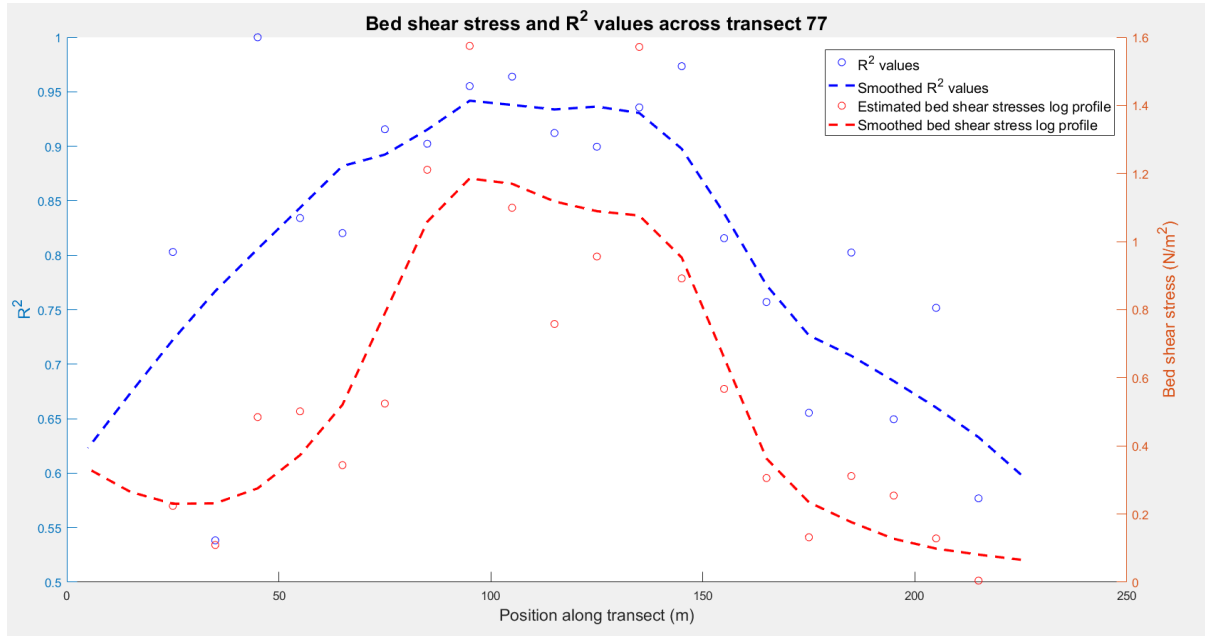


Figure 57 Distribution over transect 77 of the  $R^2$  values and the bed shear stress values for the fitting of the logarithmic profile

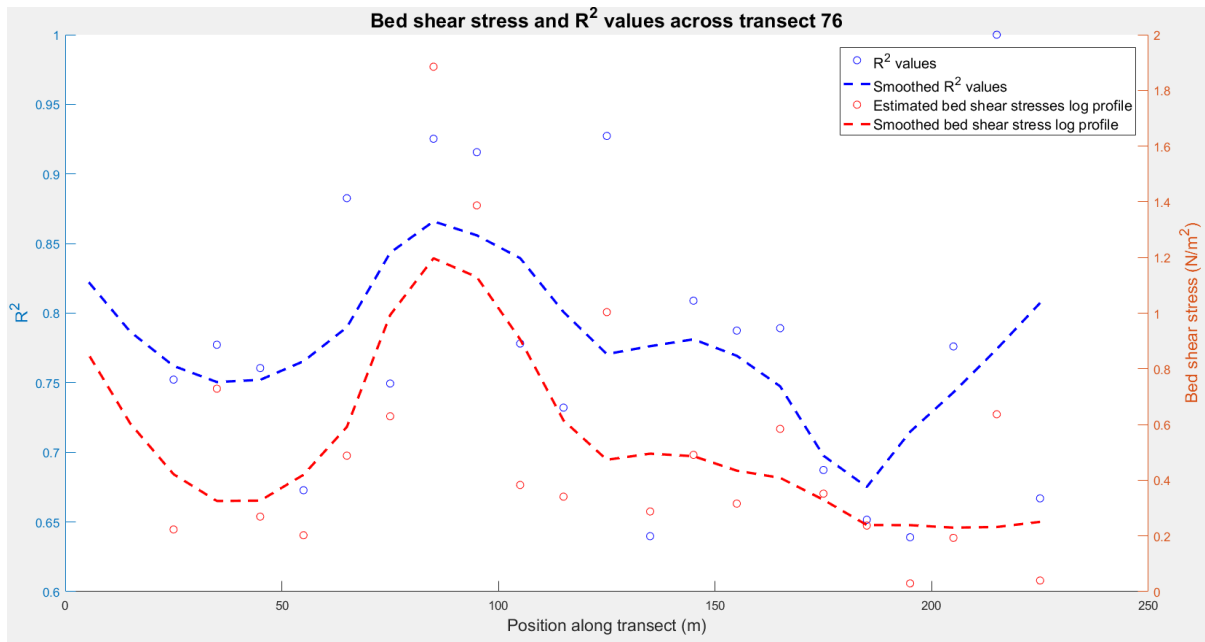


Figure 58 Distribution over transect 76 of the  $R^2$  values and the bed shear stress values for the fitting of the logarithmic profile

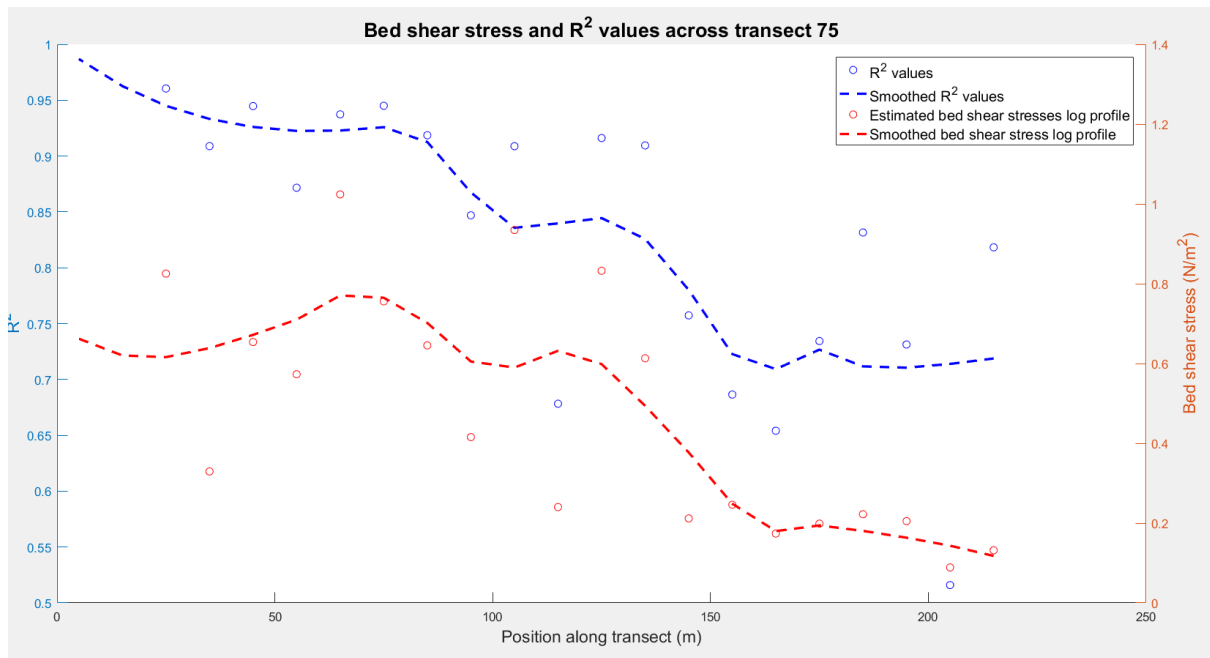


Figure 59 Distribution over transect 75 of the  $R^2$  values and the bed shear stress values for the fitting of the logarithmic profile

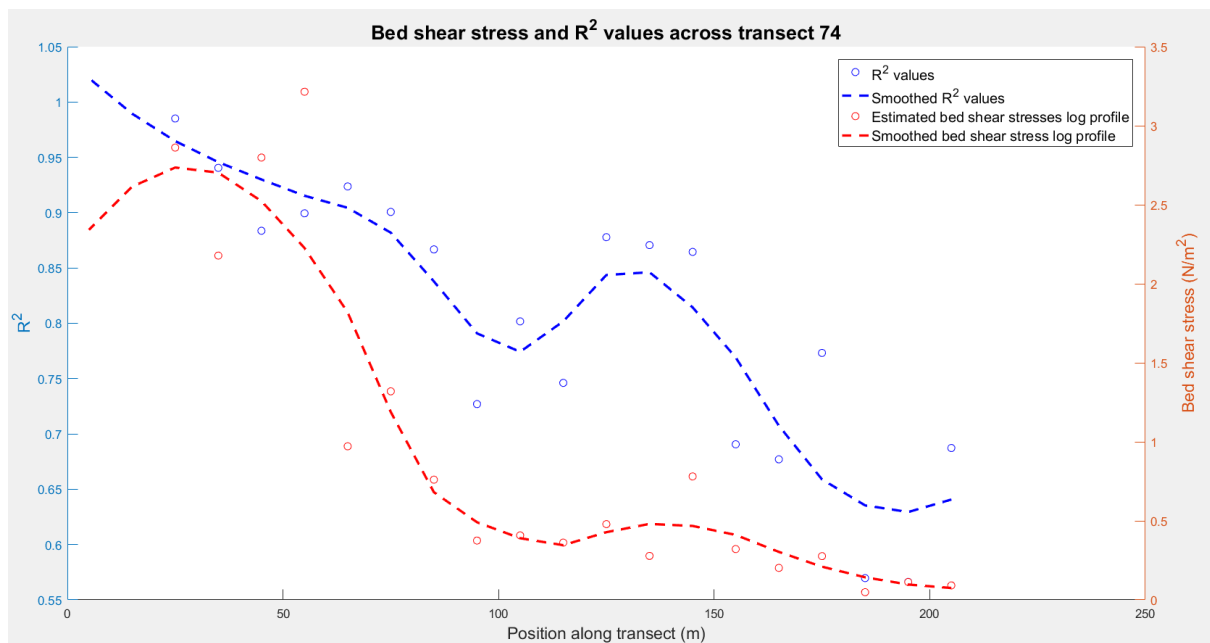


Figure 60 Distribution over transect 74 of the  $R^2$  values and the bed shear stress values for the fitting of the logarithmic profile

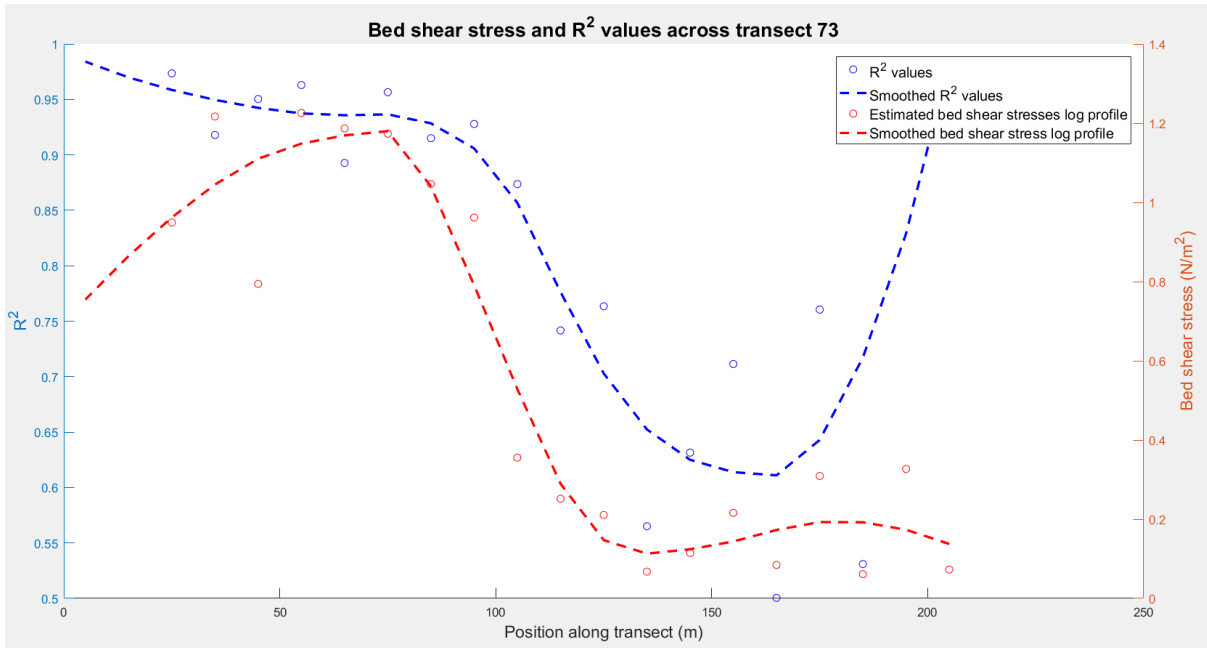


Figure 61 Distribution over transect 73 of the  $R^2$  values and the bed shear stress values for the fitting of the logarithmic profile

### C.2. Distributions of the $R^2$ values based on the fits of the scaled logarithmic profile

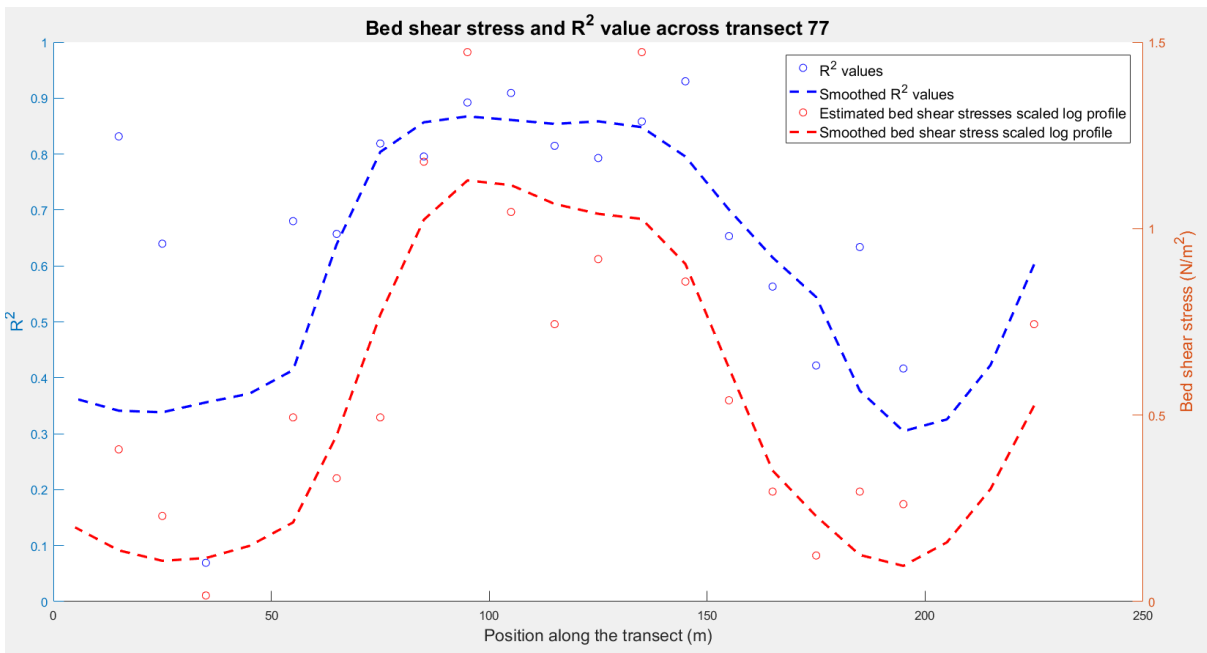


Figure 62 Distribution over transect 77 of the  $R^2$  values and the bed shear stress values for the fitting of the logarithmic profile scaled with the average velocity

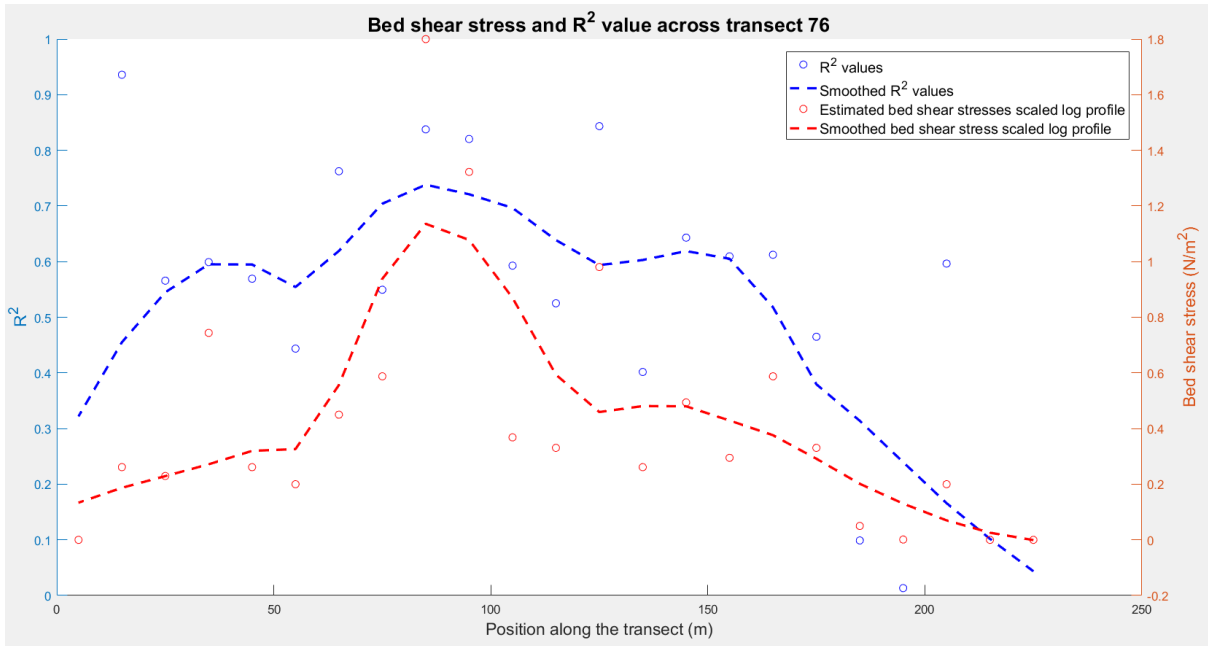


Figure 63 Distribution over transect 76 of the R<sup>2</sup> values and the bed shear stress values for the fitting of the logarithmic profile scaled with the average velocity

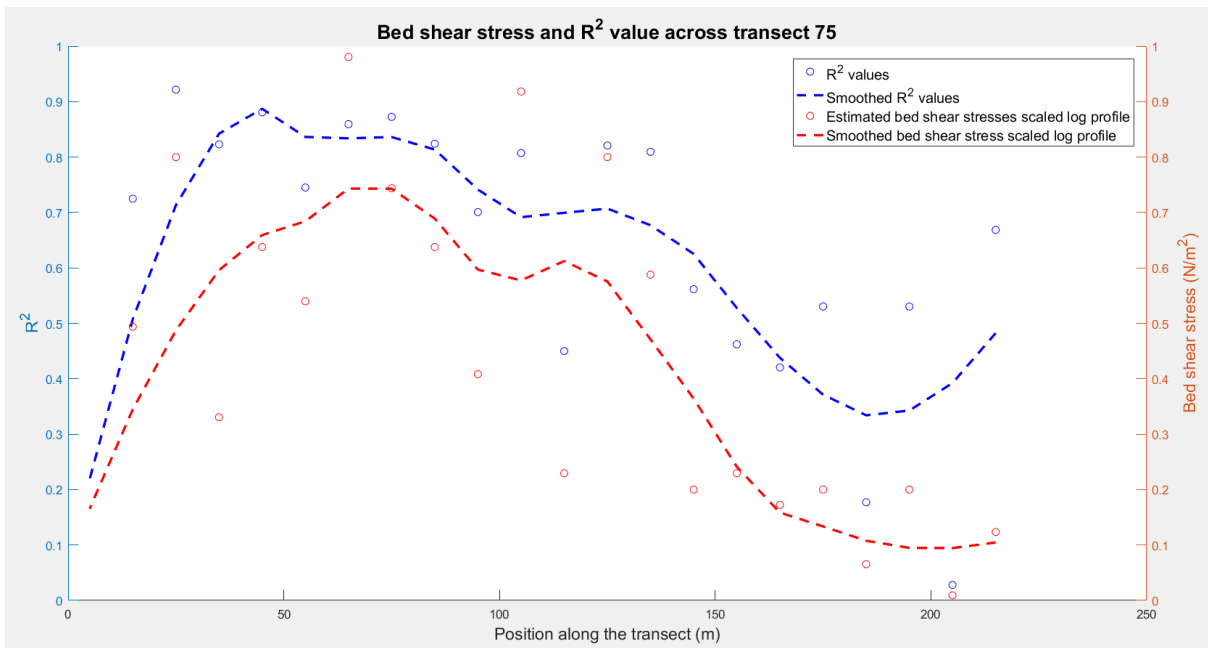


Figure 64 Distribution over transect 75 of the R<sup>2</sup> values and the bed shear stress values for the fitting of the logarithmic profile scaled with the average velocity

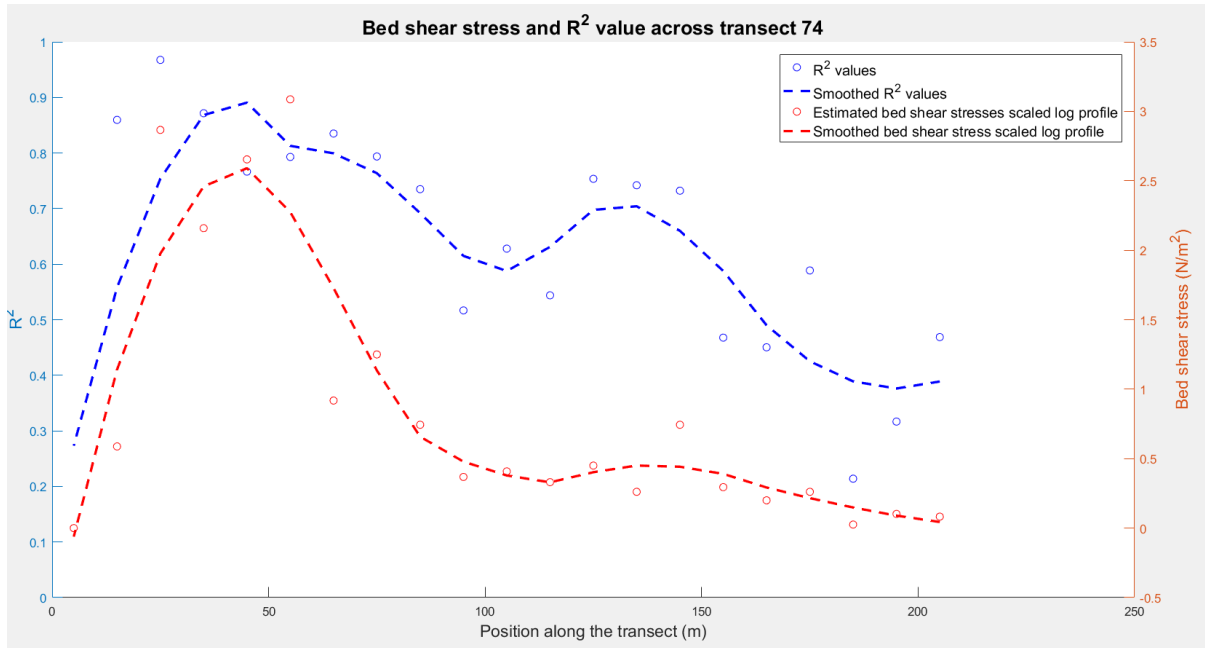


Figure 65 Distribution over transect 74 of the  $R^2$  values and the bed shear stress values for the fitting of the logarithmic profile scaled with the average velocity

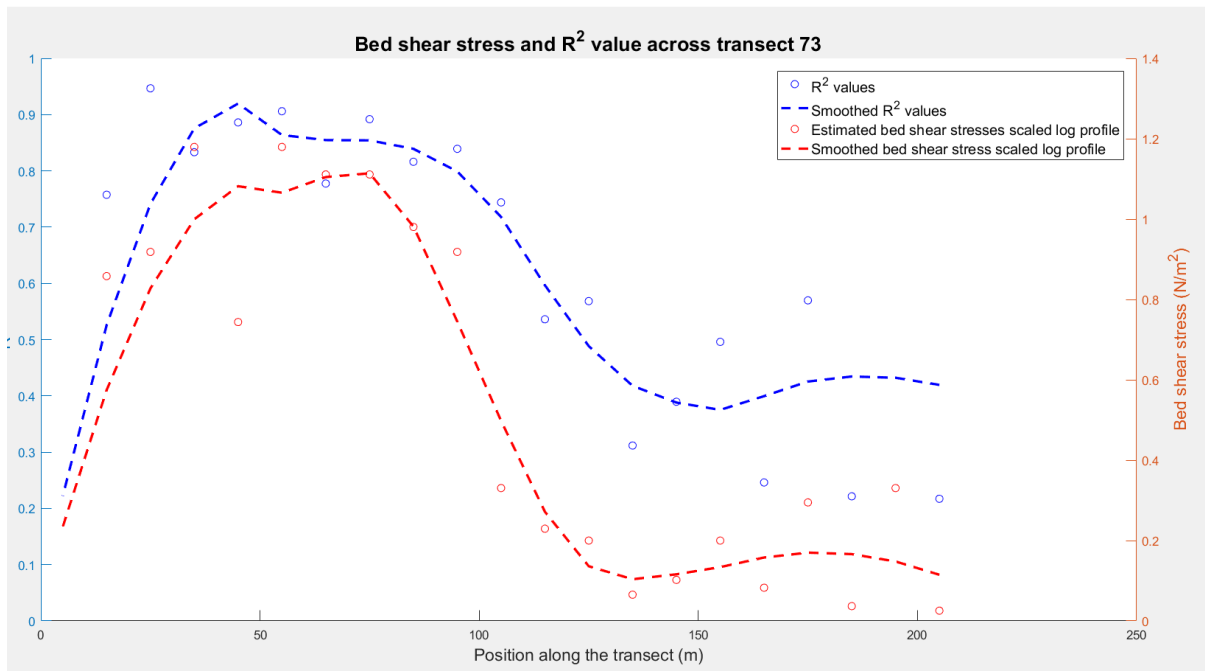


Figure 66 Distribution over transect 73 of the  $R^2$  values and the bed shear stress values for the fitting of the logarithmic profile scaled with the average velocity